

Stellar obliquities in exoplanetary systems

SIMON H. ALBRECHT,¹ REBEKAH I. DAWSON,² AND JOSHUA N. WINN³

¹*Stellar Astrophysics Centre, Department of Physics and Astronomy, Aarhus University, Ny Munkegade 120, 8000 Aarhus C, Denmark*

²*Department of Astronomy & Astrophysics, Center for Exoplanets and Habitable Worlds, The Pennsylvania State University, University Park, PA 16802, USA*

³*Department of Astrophysical Sciences, Princeton University, Princeton, NJ 08544, USA*

ABSTRACT

The rotation of a star and the revolutions of its planets are not necessarily aligned. This article reviews the measurement techniques, key findings, and theoretical interpretations related to the obliquities (spin-orbit angles) of planet-hosting stars. The best measurements are for stars with short-period giant planets, which have been found on prograde, polar, and retrograde orbits. It seems likely that dynamical processes such as planet-planet scattering and secular perturbations are responsible for tilting the orbits of close-in giant planets, just as those processes are implicated in exciting orbital eccentricities. The observed dependence of the obliquity on orbital separation, planet mass, and stellar structure suggests that in some cases, tidal dissipation damps a star’s obliquity within its main-sequence lifetime. The situation is not as clear for stars with smaller or wider-orbiting planets. Although the earliest measurements of such systems tended to find low obliquities, some glaring exceptions are now known in which the star’s rotation is misaligned with respect to the coplanar orbits of multiple planets. In addition, statistical analyses based on projected rotation velocities and photometric variability have found a broad range of obliquities for F-type stars hosting compact multiple-planet systems. The results suggest it is unsafe to assume that stars and their protoplanetary disks are aligned. Primordial misalignments might be produced by neighboring stars or more complex events that occur during the epoch of planet formation.

Keywords: Planet hosting stars (1242) — Stellar rotation (1629) — Tidal interaction (1699) — Exoplanet dynamics (490) — Exoplanet formation (492) — Exoplanet migration (2205)

1. INTRODUCTION

Soon after the earliest observations of sunspots by Galileo, Scheiner, Harriot, and Fabricius, it became clear that the Sun’s equator is nearly aligned with the ecliptic (Casanovas 1997). A modern value for the Sun’s obliquity, based on helioseismology, is $7.155 \pm 0.002^\circ$ (Beck & Giles 2005). This relatively low solar obliquity was part of the body of evidence that led Laplace to his “nebuluar theory” for the formation of the Solar System, which was incorrect but is remembered for the theoretical debut of the protoplanetary disk. Another fact that has inspired theorists is that the Sun’s obliquity seems significantly higher than the root-mean-squared mutual inclination of 1.9° between the orbits of the Sun’s eight planets. Among the proffered explanations are a close encounter

with another star (Heller 1993), a torque resulting from the motion of the protoplanetary disk through the interstellar medium (Wijnen et al. 2017), spin-axis precession driven by an undiscovered outer planet (Bailey et al. 2016; Lai 2016; Gomes et al. 2017), an asymmetry of the solar wind (Spalding 2019), and the imprint of a nearby supernova (Portegies Zwart et al. 2018).

Exoplanetary systems show a wider range of orbital characteristics than had been expected based on observations and interpretations of the properties of the Solar System (see, e.g., Winn & Fabrycky 2015; Zhu & Dong 2021, for reviews). One of the goals of exoplanetary science is to understand the physical processes responsible for this architectural diversity. Some examples of surprising systems are those with close-orbiting giant planets (Mayor & Queloz 1995), planets on highly eccentric orbits (Latham et al. 1989; Marcy & Butler 1996), miniature systems of multiple planets on tightly packed orbits (Lissauer et al. 2011; Fabrycky et al. 2014) and,

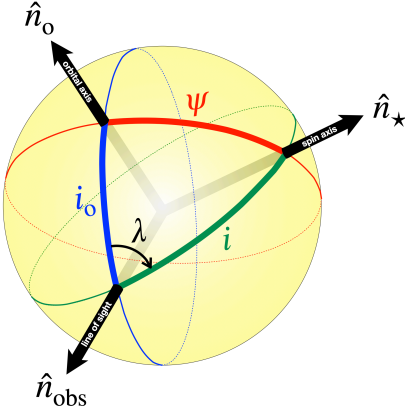


Figure 1. Angles that specify the orientation of the spin and orbital angular momentum vectors. The obliquity is ψ , the orbital inclination is i_o , and the inclination of the stellar rotation axis is i . Many authors define a Cartesian coordinate system with $\hat{z} = \hat{n}_{\text{obs}}$ and \hat{y} aligned with the sky projection of \hat{n}_o , although it is sometimes more convenient to align \hat{y} with the sky projection of \hat{n}_* .

the subject of this review, stars with large obliquities (Hébrard et al. 2008; Winn et al. 2009b).

Measuring a star’s obliquity is challenging because ordinary observations lack the angular resolution to discern any details on the spatial scale of the stellar surface. Nevertheless, using an array of techniques, obliquity measurements are available for $\sim 10^2$ stars, and statistical inferences about obliquity distributions have been drawn from samples of $\sim 10^3$ stars. Prograde, polar, and retrograde orbits have been found, and a few patterns have emerged relating obliquities to stellar mass, planetary mass, orbital distance, and transit multiplicity. There is unlikely to be a simple explanation for all the results. Misalignments might occur before, during, or after the epoch of planet formation. They might be linked to specific dynamical events in a planet’s history, such as planet–planet scattering or high-eccentricity migration, or they might be the outcome of general processes affecting stars and protoplanetary disks irrespective of the planets that eventually form.

This article reviews the current status of the observations and theories regarding the obliquities of stars with planets. Section 2 introduces the relevant geometry and terminology. Section 3 describes the measurement techniques and key findings. Section 4 discusses the proposed physical mechanisms that can excite and damp obliquities, and their success or failure in matching the observations. Section 5 summarizes the main observational findings and their relationships to theories and gives some recommendations for future work in this area.

Contents

1. Introduction	1
2. Geometry	3
3. Methods and Key Findings	4
3.1. The Rossiter-McLaughlin effect	6
3.1.1. The RM geometry	7
3.1.2. The Doppler Shadow	7
3.1.3. The anomalous radial velocity	8
3.1.4. The photometric RM effect	10
3.1.5. Hot stars with hot Jupiters have high obliquities	10
3.1.6. Stars with especially massive planets have lower obliquities	12
3.1.7. Cool stars with warm Jupiters have high obliquities	12
3.1.8. Some cool stars with HJs are very well aligned	12
3.1.9. Obliquities and stellar age	13
3.1.10. Are very young giant-planet hosts well-aligned?	13
3.1.11. Obliquity & eccentricity	14
3.1.12. Interlude: Mutual orbital inclinations	16
3.1.13. Compact multi-transiting systems: aligned with notable exceptions	17
3.2. Asteroseismology	17
3.3. Spectro-interferometry	19
3.4. The projected rotation velocity technique	20
3.5. Starspots	22
3.5.1. Quasi-Periodic Variation	22
3.5.2. Starspot-tracking method	23
3.6. Gravity darkening, fast rotators	24
3.7. A Preponderance of Perpendicular Planets?	24
3.8. Interlude: Planetary obliquities	25
4. Processes that influence obliquities	25
4.1. Tidal realignment	26
4.1.1. Simplified tidal friction model	28
4.1.2. More realistic tidal models	28
4.2. Primordial misalignment	30
4.3. Post-formation misalignment	32
4.4. Altering the stellar spin vector	36
5. Summary and discussion	36
A. Population synthesis simulations	39
B. Histogram plot	40
C. Systems	40

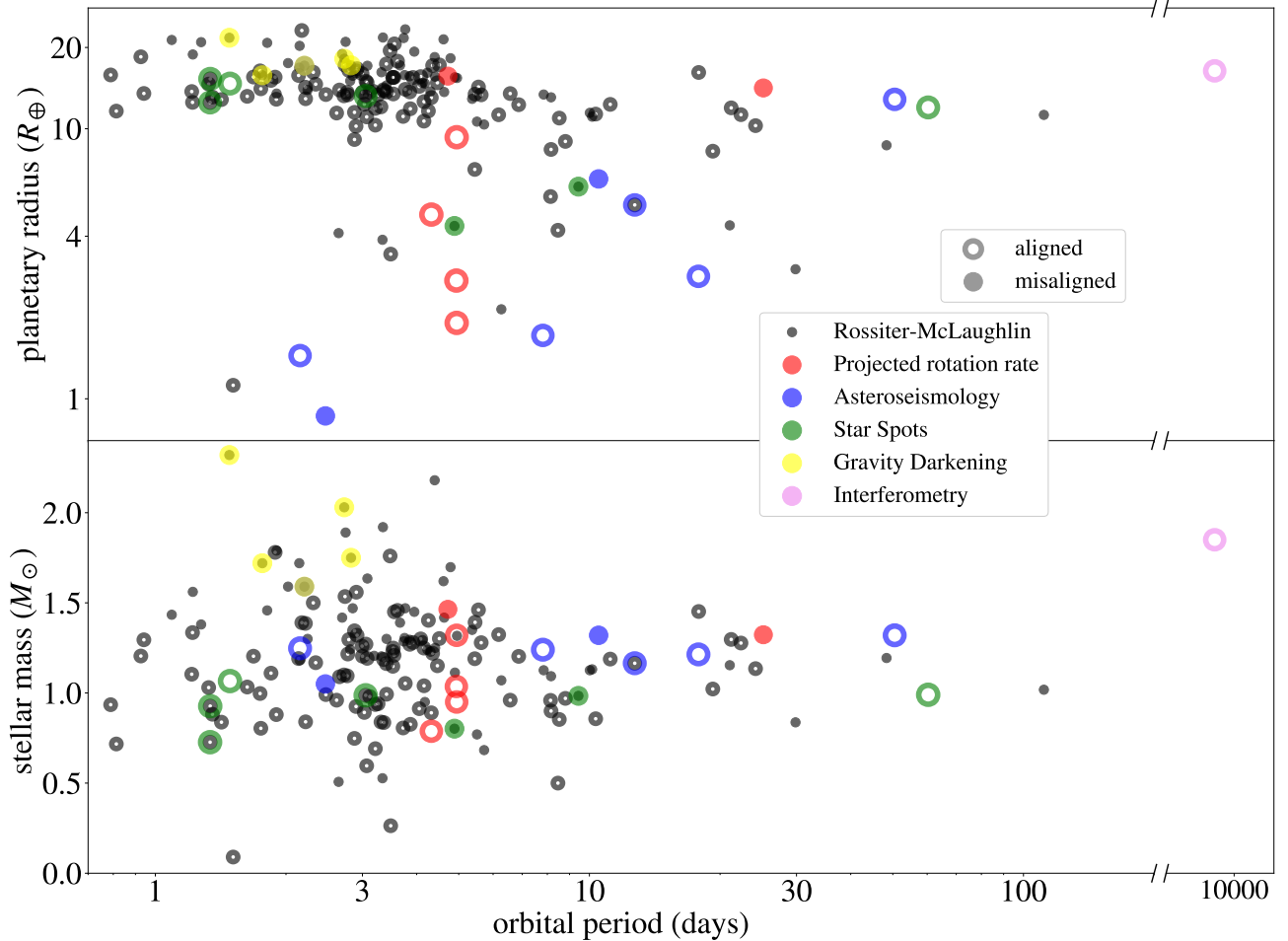


Figure 2. Parameter space of obliquity measurement methods. Each point represents an obliquity measurement, with a location that specifies the orbital period and either the planet’s radius (top panel) or the star’s mass (bottom panel). The points are color-coded by method. Solid symbols are for misaligned stars (by more than 10° with a $>3\sigma$ departure from zero); open symbols are for well-aligned stars or ambiguous cases. The RM, starspot, and gravity-darkening methods require observations during transits, making them less applicable to systems with smaller planets or longer periods. The gravity-darkening method requires fast rotators, i.e., high-mass stars, while the starspot method is most applicable to low-mass stars with large and long-lived starspots. The asteroseismic and projected rotation velocity methods require a transiting planet but do not require intensive observations conducted during transits, making them applicable to planets of all types. The asteroseismic method requires moderately rapid rotation and long-lived pulsation modes, which generally occur for stars somewhat more massive than the Sun. Similarly, the projected rotation velocity method requires moderately rapid rotation, which is associated with more massive stars. The interferometric method requires very bright and rapidly rotating stars, as well as a constraint on the planetary orbital inclination. Also important, though not conveyed in this diagram, is that the methods differ in the achievable precision and the severity of parameter degeneracies.

2. GEOMETRY

Figure 1 illustrates the unit vectors \hat{n}_* , \hat{n}_o , and \hat{n}_{obs} that specify the directions of the stellar angular momentum, the orbital angular momentum, and the line of sight to the observer, respectively. The obliquity ψ is the angle between \hat{n}_* and \hat{n}_o . The angles i and i_o are the line-of-sight inclinations of the stellar and orbital angular momentum vectors, and λ is the position angle between the sky projections of those two vectors, mea-

sured clockwise from \hat{n}_o to \hat{n}_* . With these definitions,¹

$$\hat{n}_* \cdot \hat{n}_o = \cos \psi = \cos i \cos i_o + \sin i \sin i_o \cos \lambda, \quad (1)$$

$$(\hat{n}_* \times \hat{n}_o) \cdot \hat{n}_{\text{obs}} = \sin i \sin i_o \sin \lambda. \quad (2)$$

As explained in Section 3, some techniques are capable of measuring $\sin i$ and $\sin i_o$ but provide no information

¹ Some authors use the opposite sign convention, measuring the position angle *councclockwise* from \hat{n}_o to \hat{n}_* and denoting the angle β instead of λ .

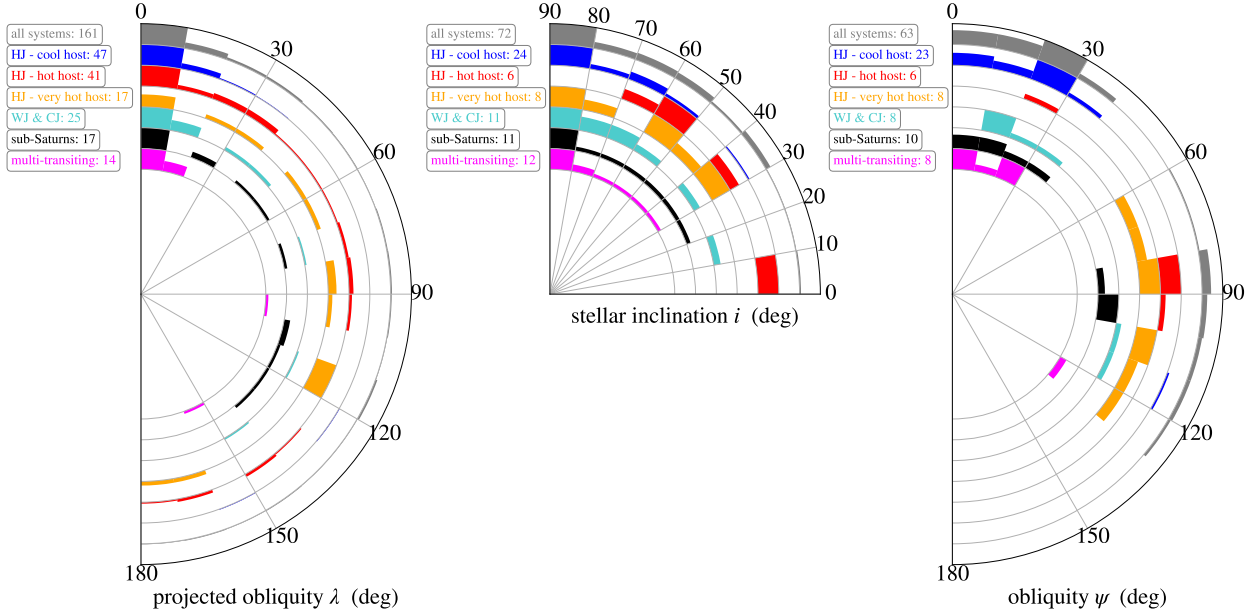


Figure 3. Histograms of host star obliquities. *Left:* Projected obliquities (λ), folded onto the range $[0, 180^\circ]$. *Middle:* Stellar inclination measurements (i), folded onto the range $[0, 90^\circ]$. *Right:* Three-dimensional obliquities (ψ), for the cases in which λ and i have both been measured. The histograms are color-coded according to the system’s characteristics. Stars are designated as cool, hot, or very hot, using effective temperature boundaries of 6250 K and 7000 K. Planets with masses exceeding $0.3 M_{\text{Jup}}$ are designated hot Jupiters (HJ) if $a/R < 10$, and warm/cold Jupiters (WJ/CJ) if $a/R > 10$. Planets with masses $\lesssim 0.3 M_{\text{Jup}}$ are designated sub-Saturns. Readers preferring more traditional histograms are directed to Appendix B.

about λ . Some other techniques are mainly sensitive to λ . Thus, to determine ψ for an individual system, it is usually necessary to combine the results from more than one measurement technique. On the other hand, to study the obliquity distribution of a population of stars, it suffices to obtain information about either λ or i for each star. Current statistical studies rely on stars with transiting planets, for which $i_o \approx 90^\circ$ is guaranteed. If a population of transit-hosting stars were randomly oriented, then λ and $\cos i$ would be uniformly distributed. If, instead, the stars had low obliquities, then only low values of λ and $\cos i$ would be observed. In between these two extremes, the measured width of the distribution of either λ or $\cos i$ can be used to determine the width of the obliquity distribution.

For statistical analyses, two useful references are Fabrycky & Winn (2009) and Muñoz & Perets (2018). The former authors provided analytic formulas for the conditional probability densities $p(\psi|\lambda)$ and $p(\lambda|\psi)$ under the assumption of random orientations. They also showed how to use measurements of λ to model the obliquity distribution of a population of stars as a von Mises-Fisher (vMF) distribution,

$$p(\hat{n}_*) \propto \exp(\kappa \hat{n}_* \cdot \hat{n}_o) \quad (3)$$

$$\frac{dp}{d\psi} = \frac{\kappa}{2 \sinh \kappa} \exp(\kappa \cos \psi) \sin \psi. \quad (4)$$

This is a widely used model in directional statistics, which resembles a two-dimensional Gaussian distribution wrapped around a sphere. For small values of the concentration parameter κ , the distribution approaches an isotropic distribution. For large values of κ , the distribution of ψ approaches a Rayleigh function with a width of $\sigma = \kappa^{-1/2}$. Muñoz & Perets (2018) extended this framework to include information about i in addition to λ .

3. METHODS AND KEY FINDINGS

The main challenge in measuring any of the angles in Figure 1 is that stars are almost always spatially unresolved. We can only observe a star’s flux and spectrum integrated over its entire visible hemisphere. Fortunately, some characteristics of the disk-integrated flux and spectrum depend on the star’s orientation in space. One such characteristic is the **rotational Doppler broadening** of its spectral absorption lines, which is quantified by $v \sin i$, the projected equatorial rotation velocity (§ 3.4). Another observable that is related to a star’s orientation is the **amplitude of photometric variability** due to rotating starspots, which is expected to vary roughly in proportion to $\sin i$ (§ 3.5.1). A third type of data that bears information about a star’s orientation is the fine structure in its **asteroseismic oscillation spectrum**. The inclination i affects the relative

Table 1. Key results and systems of special interest. The first column describes an observational finding, and the second column indicates the main measurement technique. The third column specifies the section of this article in which the trend is discussed, and the fourth column provides the key citations to the literature.

Result	Method	Section	Ref.
Hot stars with hot Jupiters have high obliquities.	RM, VSI, QPV	3.1.5	1,2
The highest-mass hot Jupiters have lower obliquities.	RM	3.1.6	3
Cool stars with Neptunes or warm Jupiters have high obliquities.	RM	3.1.7	4
Cool stars with hot Jupiters are sometimes aligned within 1° .	RM	3.1.8	
Tidal effects appear to damp obliquities.	RM	4.1	1,4
Stars younger than 100 Myr tend to be well-aligned?	RM/VSI/INT	3.1.10	
Cool stars with compact multi-planet systems have $\psi \lesssim 30^\circ$	RM/SC/AS/QPV/VSI	3.1.13	5–11
Hot stars with compact multi-planet systems have high obliquities	QPV/VSI	3.4	12
A preponderance of perpendicular planets?	RM/VSI/QPV/GD/AS	3.7	13
HD 80606: A high obliquity from Kozai-Lidov cycles and tidal friction?	RM	4.3	14,15
Kepler-56: A high obliquity from precession induced by an outer planet?	AS	3.2	16
K2-290: A high obliquity from primordial disk misalignment?	RM/VSI	4.2	17

NOTE—**Techniques:** RM, Rossiter-McLaughlin effect. VSI, $v \sin i$ (projected rotation velocity). QPV, quasiperiodic photometric variability. AS, asteroseismology. SC, spot crossings. GD, gravity darkening. INT, interferometry.

References— 1. Winn et al. (2010a), 2. Schlaufman (2010), 3. Hébrard et al. (2011a), 4. Albrecht et al. (2012b), 5. Albrecht et al. (2013), 6. Morton & Winn (2014), 7. Campante et al. (2016), 8. Mazeh et al. (2015b), 9. Li & Winn (2016), 10. Winn et al. (2017), 11. Muñoz & Perets (2018), 12. Louden et al. (2021), 13. Albrecht et al. (2021), 14. Wu & Murray (2003), 15. Hébrard et al. (2010), 16. Huber et al. (2013), 17. Hjorth et al. (2021)

amplitudes of the modes within each rotationally split multiplet (§ 3.2). When we also have knowledge of i_o (based on transit observations, direct images, or astrometric measurements), then the constraints on i from any of the three techniques described above allow us to place constraints on the stellar obliquity.

These **inclination-based methods** for obliquity determination have important limitations. Because of the north/south symmetry of the star, they cannot distinguish between i and $180^\circ - i$, leading to a twofold degeneracy in the star’s orientation. In particular, we cannot tell whether a star has prograde or retrograde rotation with respect to the line of sight or with respect to the planetary orbit.² Another limitation is that the inclination-based methods tend to give weak constraints at high inclinations, because of flattening of the sine function as $i \rightarrow 90^\circ$. Even if $\sin i$ is constrained to be in the narrow range from 0.9 to 1, the inclination can be any value between 64 and 116° . This problem arises often, because high inclinations are common. In a sample of randomly oriented stars, we expect 44% of the stars to have $\sin i > 0.9$.

² For transiting planets, a similar degeneracy afflicts measurements of i_o , although this is usually a minor concern because the geometrical requirement for transits implies that i_o is never far from 90° .

The other main class of methods for measuring the obliquity relies on a transiting planet to provide spatially resolved information, as its shadow scans across the stellar disk. The intensity and emergent spectrum vary across the star’s photosphere in a manner that depends on the star’s orientation. For example, stellar rotation causes the radial velocity of its photosphere to exhibit a gradient from the approaching side to the receding side. When a transiting planet hides a portion of the stellar disk, the corresponding radial-velocity component is diminished in the disk-integrated stellar spectrum, leading to line-profile distortions known as the **Rossiter-McLaughlin effect** (§ 3.1). Another technique is based on detecting the glitches in the light curve whenever a transiting planet occults a starspot (or any kind of inhomogeneity) on the stellar disk. Observations of these **starspot anomalies** can sometimes be used to constrain the stellar obliquity (§ 3.5.2). A third technique is based on **gravity darkening**. The equatorial zone of a rapidly rotating star is centrifugally lifted to higher elevation, lowering its temperature and intensity relative to the polar regions. This effect breaks the usual circular symmetry of the intensity profile across the stellar disk, which in turn causes a distortion of the transit light curve (§ 3.6). The circular symmetry is also broken by relativistic effects known as **rotational Doppler boosting** (§ 3.1.4).

These **transit-based methods** are usually more sensitive to λ than they are to i .³ Indeed, in the best cases, λ can be measured with a precision on the order of 1° . The disadvantages of these methods are that they require time-critical observations of transits, and the signals are generally proportional to the area of the planet’s silhouette divided by the area of the stellar disk. In practice, it has proven to be very challenging to deploy these methods on planets smaller than Neptune around Sun-like stars.

Finally, there is a technique that is mainly sensitive to λ and does *not* require a transiting planet: **spectro-interferometry**. For nearby bright stars, optical interferometric observations with high spatial and spectral resolution can partially resolve the stellar disk and reveal the displacement on the sky between the redshifted and blueshifted sides of the rotating star (§ 3.3). This is still a highly specialized technique, though, and must be combined with other data that specify the orientation of the planet’s orbit.

Each technique works best in certain circumstances. Figure 2 illustrates the applicability of these different techniques to systems with different planet sizes, stellar masses, and orbital periods. Below, we describe these techniques in more detail, although not in the geometry-based order described here. Instead, we devote the most attention to the techniques that have delivered the most information.

3.1. The Rossiter-McLaughlin effect

In a letter to the editor of the *Sidereal Messenger*, Holt (1893) pointed out that a star’s rotation rate could be measured by observing the time-variable distortions of its absorption spectrum during an eclipse. We have not been able to learn anything more about this insightful correspondent, nor have we found any earlier reference to what is now called the Rossiter-McLaughlin (RM) effect. The name honors the work of Rossiter (1924) and McLaughlin (1924), who observed the effect in the β Lyrae and Algol systems, respectively.⁴

Due to rotation, light from the approaching half of the stellar disk is blueshifted, light from the receding half is redshifted, and the disk-integrated spectrum shows a

³ To be more precise, the transit-based techniques are sensitive to $|\lambda|$, rather than λ . This is because with transit data alone, we cannot distinguish a system with $\lambda = a$ and $i_o = b$ from an otherwise identical system with $\lambda = -a$ and $i_o = 180^\circ - b$. Most authors arbitrarily assume $i_o < 90^\circ$ and report λ in the range from -180 to $+180^\circ$, or from 0 to 360° . We also note that when $i_o \approx 90^\circ$, as is the case for transiting planets, then $\psi > |\lambda|$ when $|\lambda| < 90^\circ$, and $\psi < |\lambda|$ when $|\lambda| > 90^\circ$.

⁴ An earlier and less convincing detection was reported by Schlesinger (1910) for the δ Librae system.

spread in Doppler shifts. During an eclipse or transit, a portion of the stellar disk is hidden from view, weakening the corresponding radial-velocity components in the disk-integrated spectral absorption lines. The character and time-evolution of the spectral distortions depend on $v \sin i$ and λ , in addition to the usual eclipse parameters.

Observers have detected and modeled the RM effect in several ways. When the spectral lines are not well resolved, the line-profile distortions are manifested as shifts in the apparent central wavelength of the line. When the blueshifted half of the star is eclipsed, the lines exhibit an anomalous redshift, and vice versa. This is the manner in which Rossiter (1924) and McLaughlin (1924) displayed their data, as well as Queloz et al. (2000), who first observed the RM effect for an exoplanet-hosting star. Parametric models for the “anomalous radial velocity” and its relation to the positions and attributes of the two bodies have been developed by many authors (e.g. Hosokawa 1953; Kopal 1959; Sato 1974; Ohta et al. 2005; Giménez 2006; Hirano et al. 2011c; Shporer & Brown 2011).

Alternatively, the line-profile distortions can be detected and modeled directly without the intermediate step of computing an anomalous radial velocity. Models for the line-profile distortions have been extensively developed, starting with a beautiful exposition by Struve & Elvey (1931) for the Algol system and continuing to the present (Albrecht et al. 2007; Collier Cameron et al. 2010a; Albrecht et al. 2013; Johnson et al. 2014; Cegla et al. 2016; Zhou et al. 2016a; Johnson et al. 2017). This method is sometimes referred to as Doppler tomography, although we prefer the terms Doppler transit or Doppler shadow.⁵

The RM effect has been the basis of most of the obliquity measurements of individual planet-hosting stars, as reviewed by Triaud (2018). Below, we describe the geometry of the RM effect (§ 3.1.1) and the results from the two main methods for analyzing the RM effect: as a line-profile distortion (§ 3.1.2) and as an anomalous radial velocity (§ 3.1.3). Then, we review the key findings that have emerged from RM observations (§ 3.1.5–3.1.13). Table 1 gives an overview of these trends and highlights some systems of particular interest. Appendix C describes the compilation of data that was

⁵ Tomography is the reconstruction of a 3-d structure based on 2-d observations obtained over a wide range of viewing angles. In astrophysics, the term “Doppler tomography” was introduced in the 1980s to describe the reconstruction of a star’s surface features or a binary’s accretion geometry based on spatially unresolved observations spanning an entire rotational or orbital cycle. In the case of a planetary transit, though, the range of viewing angles is so narrow that there is no tomographic quality to the analysis.

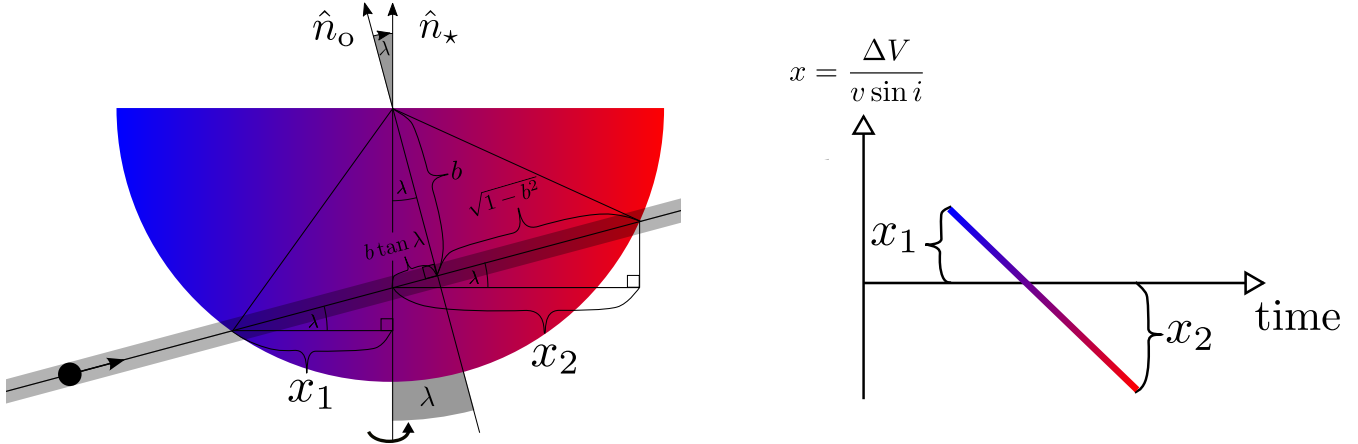


Figure 4. Geometry of the Rossiter-McLaughlin effect. The left panel illustrates a transit with $i_o < 90^\circ$. The planet crosses from left to right. Due to stellar rotation, the left side of the star is approaching the observer, and the right side is receding. Expressing distance in units of the stellar radius with the x -axis parallel to the stellar equator, and neglecting differential rotation, the sub-planet radial velocity is $(v \sin i)x$ and the extrema of the RM signal occur at ingress (x_1) and egress (x_2). The relations between x_1 , x_2 , λ and the impact parameter b are indicated. The right panel shows the corresponding velocity of the planet’s “Doppler shadow.” Adapted from Albrecht et al. (2011).

used to make the charts in this article and an overview of λ , i , and ψ measurements is shown in figure 3.⁶

3.1.1. The RM geometry

Consider a transit of a planet of radius r across a uniformly rotating star of radius R , equatorial rotation velocity v , and line-of-sight inclination i . During the transit, the stellar absorption lines suffer a fractional loss of light on the order of $(r/R)^2$ associated with the velocity component

$$\Delta V(t) = (v \sin i)x(t), \quad (5)$$

which is the rotational radial velocity of the point on the star directly behind the planet. Sometimes, this “sub-planet velocity” is denoted by v_p . Here, $x(t)$ is the planet’s position in units of the stellar radius along the coordinate axis running perpendicular to the star’s projected rotation axis, as in Figure 4.

If the radius ratio r/R and transit impact parameter b are known, then observations of the time series $\Delta V(t)$ can be used to determine λ and $v \sin i$. In practice, one fits a parameterized model to the time series, but it is useful to understand which aspects of the signal provide the information. Figure 4 illustrates the transit geometry and the corresponding $\Delta V(t)$. The extremes of the signal occur at ingress (x_1) and egress (x_2), with amplitudes

$$\Delta V_1 = (v \sin i)x_1, \quad \Delta V_2 = (v \sin i)x_2. \quad (6)$$

⁶ The data will be made available via the [NASA Exoplanet Archive](#) and can also be obtained from [phys.au.dk/exoplanets](#).

Based on the transit geometry,

$$\begin{aligned} x_1 &= \sqrt{1 - b^2} \cos \lambda - b \sin \lambda, \quad \text{and} \\ x_2 &= \sqrt{1 - b^2} \cos \lambda + b \sin \lambda, \end{aligned} \quad (7)$$

allowing us to write

$$\Delta V_2 + \Delta V_1 = 2v \sin i \cos \lambda \times \sqrt{1 - b^2}, \quad (8)$$

$$\Delta V_2 - \Delta V_1 = 2v \sin i \sin \lambda \times b. \quad (9)$$

This system of equations makes clear that the *amplitude* depends on $\cos \lambda$ (Eq. 8), while the *asymmetry* of the signal depends on $\sin \lambda$ (Eq. 9). It also indicates that measurements of the amplitude and asymmetry are sufficient to determine $v \sin i$ and λ , as long as b is not too close to 0 or 1 (Albrecht et al. 2011).

3.1.2. The Doppler Shadow

The line-profile distortions due to the RM effect can also be analyzed directly. For simplicity, consider an idealized spectral line broadened only by rotation. When the planet is at position x_p , the range of velocity components partially blocked by the planet is $(v \sin i)(x_p \pm r/R)$. Within this velocity range, the fractional loss of light is equal to the area of the planet’s silhouette divided by the area of the strip of the star within $x_p \pm r/R$,

$$\Delta L_{\text{RM}}(t) \approx -\frac{\pi}{4} \frac{r}{R} \frac{1}{\sqrt{1 - x(t)^2}}. \quad (10)$$

This equation gives the intensity contrast of the “Doppler shadow”—the bump that appears in the line profile. Because ΔL_{RM} is proportional to r instead of

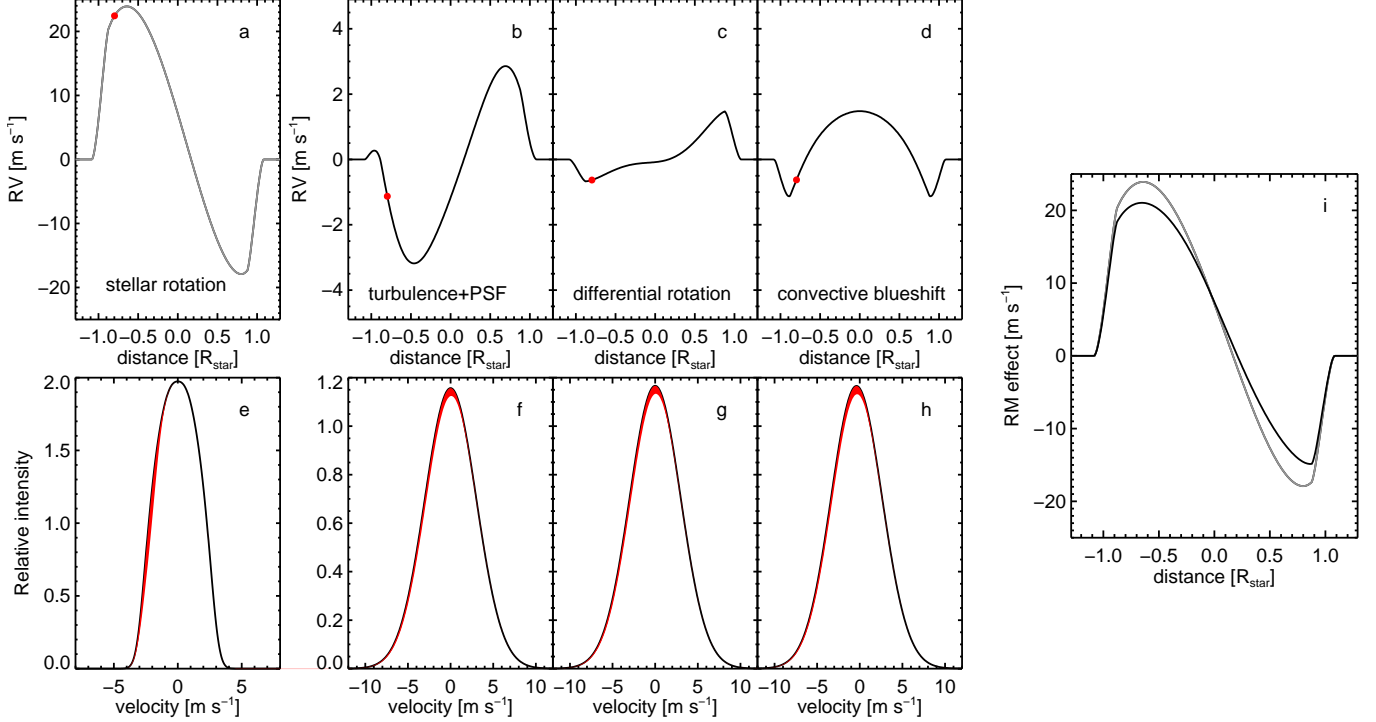


Figure 5. Higher-order effects in the anomalous radial velocity, illustrated for a Sun-like star with $v \sin i = 3 \text{ km s}^{-1}$ and a transiting planet with $\lambda = 40^\circ$, $r/R = 0.12$, and $b = 0.2$. (a) Limb darkening causes the maxima and minima to be rounded, rather than sharp as in Figure 4. (b) Instrumental broadening (taken to be 2.2 km s^{-1}) and macroturbulence ($\zeta_{\text{RT}} = 3 \text{ km s}^{-1}$) act oppositely to the rotational effect. (c) Differential rotation introduces a dependence on the range of stellar latitudes crossed by the planet. (d) The convective blueshift produces an anomalous velocity depending on the planet’s distance from the center of the stellar disk. (e-h) The corresponding models for the stellar absorption lines. The red region identifies the RM distortion at the phase of the transit that is indicated by a red dot in the corresponding upper panel. For the lower panels, the radius of the planet was doubled, to allow improved visibility of the missing velocity components. (i) The combined model including all aforementioned effects. The gray line is the model from panel (a). From Albrecht et al. (2012b).

r^2 , this technique is, in principle, more sensitive to small planets than the anomalous-RV technique. In practice, though, unless the star is rotating very rapidly, the contrast of the bump is reduced by other line-broadening mechanisms, which at least partially negates this advantage. See Fig. 7 for an illustration.

Albrecht et al. (2007) applied this technique to the eclipsing binary V1143 Cyg. They created synthetic line profiles by numerically integrating over a 2-d pixelated stellar disk, after assigning intensities and velocities to each pixel due to rotation, limb darkening, velocity fields, etc. The pixels hidden by the planet were assigned zero intensity. Collier Cameron et al. (2010a) used a simpler approach in which the stellar line profile and planetary disturbance were modeled with 1-d functions. In a variation of this technique dubbed “RM Reloaded,” Cegla et al. (2016) replaced the synthetic line profiles that had been used in previous studies with an empirical model based on the spectra obtained outside of transits. They used a parametric model only for

the portion of the photosphere covered by the planet, a method developed further by Bourrier et al. (2021).

3.1.3. The anomalous radial velocity

The effect on a spectral line is a distortion, not an overall Doppler shift. Nevertheless, a radial-velocity (RV) extraction algorithm will respond to the distortion by reporting an anomalous velocity,

$$RV_{\text{RM}}(t) \approx -\left(\frac{r}{R}\right)^2 \Delta V(t). \quad (11)$$

A decent approximation for the maximum amplitude of the anomalous RV is

$$RV_{\text{RM(max)}} \approx 0.7\sqrt{1-b^2} \left(\frac{r}{R}\right)^2 v \sin i. \quad (12)$$

The factor of 0.7 accounts for limb darkening. There are other corrections of order unity due to the effects of turbulent and instrumental broadening, and the details of the RV-extraction algorithm. For the case of a cross-correlation algorithm, a more accurate formula

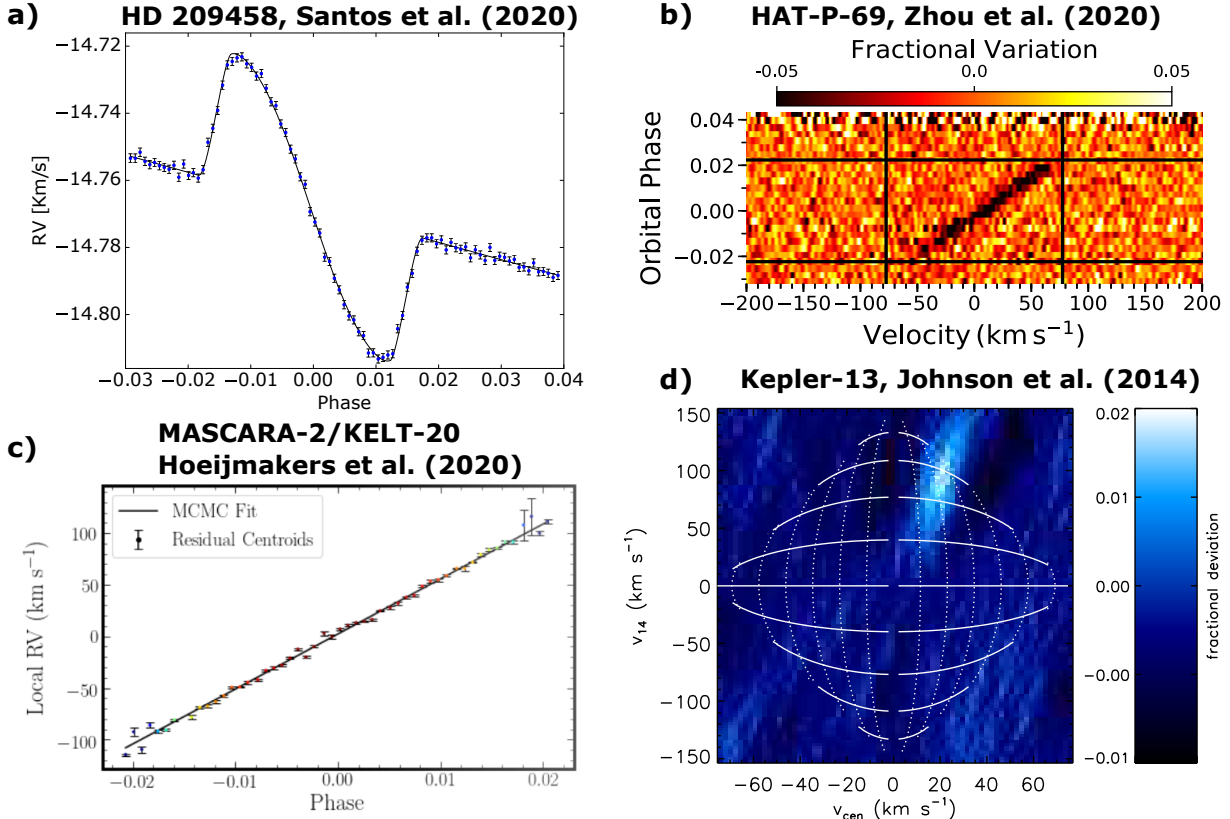


Figure 6. Different visualizations of the RM effect. Top left: Time series of anomalous RVs observed during a transit of HD 209458 (Santos et al. 2020). Top right: Time series of cross-correlation functions (CCFs) during a transit of HAT-P-69, after subtracting a model with no RM effect (Zhou et al. 2019a). The dark stripe is the planet’s Doppler shadow. Lower left: Time series of the sub-planet velocity during a transit of MASCARA-2, inferred from the absorption line profiles using the “RM Reloaded” technique (Hoeijmakers et al. 2020). Lower right: Stacked CCF residuals based on a spectroscopic time series obtained during a transit of Kepler-13 (Johnson et al. 2014). The residuals were shifted and binned for various choices of two parameters that control the calculated trajectory of the planet. The first parameter, v_{14} , controls the amplitude of the RM effect and the second parameter, v_{cen} , controls the asymmetry. Curves of constant λ are solid white, and curves of constant impact parameter are dotted white. The bright area is the region of parameter space preferred by the data.

was derived by Hirano et al. (2011c), building on work by Ohta et al. (2005).

Gaudi & Winn (2007) exposed the information content of the RM signal in more detail. They derived an approximate formula⁷ to estimate the achievable precision in a measurement of λ ,

$$\sigma_\lambda = \frac{\sigma_v/\sqrt{N}}{v \sin i} \left(\frac{r}{R} \right)^{-2} \left[\frac{(1-b^2) \cos^2 \lambda + 3b^2 \sin^2 \lambda}{b^2(1-b^2)} \right]^{1/2}, \quad (13)$$

assuming the transit is well-sampled with N uniformly spaced data points, each with an uncertainty σ_v in the radial velocity. The formula was derived assuming that λ and $v \sin i$ are the only two free parameters, and that

limb darkening can be neglected. The uncertainty diverges as $b \rightarrow 0$, when the asymmetry vanishes regardless of obliquity (Eqn. 9), and as $b \rightarrow 1$, when the transit/RM signal itself vanishes (Eqn. 8).

Figure 5 shows some higher-order effects that were neglected in the preceding discussion. Limb darkening weakens the RM effect near the ingress and egress phases. Differential stellar surface rotation causes ΔV to depend on both x and y , which makes the RM effect sensitive to i in addition to λ (Gaudi & Winn 2007; Cegla et al. 2016). Turbulence on the stellar surface also affects ΔV , as does the “convective blueshift” — the higher intensity of the hot, upwelling material compared to the cooler, sinking material (Shporer & Brown 2011; Cegla et al. 2016). Some other effects that are usually neglected, but that may be important in special cases, are the tidal and rotational deformations of the star, the saturation or pressure-broadening of some

⁷ Equations 16 and 17 of Gaudi & Winn (2007) contain errors; the sine and cosine functions should be swapped in both cases. The formula given here, as Equation 13, is correct.

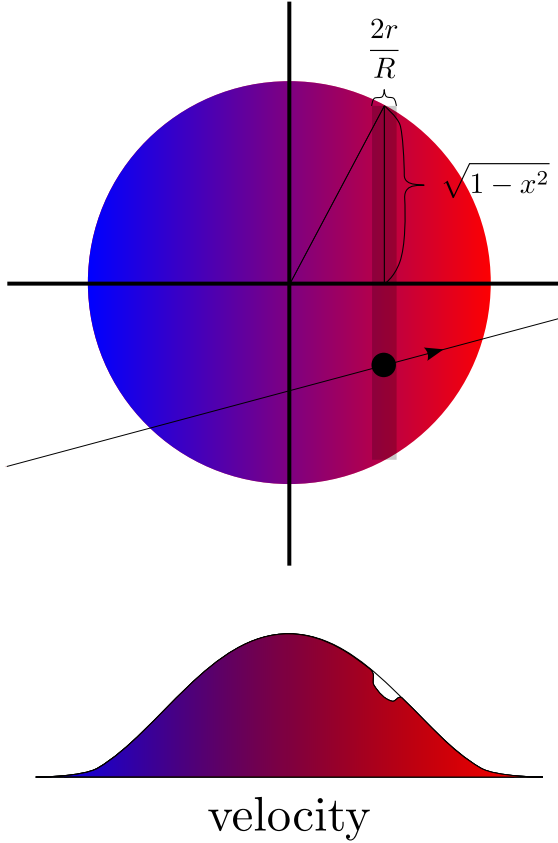


Figure 7. Stellar line deformation for a rapidly rotating star. For this illustration, rotation was assumed to be the dominant broadening mechanism, leading to a deformation that is well-localized in wavelength.

absorption lines, and the influence of star spots and pulsations.

Whether to analyze the data in terms of the anomalous RV or the line-profile variations, or both, depends on the instrument and the system parameters. Roughly speaking, the larger the ratio

$$\alpha = \frac{(v \sin i)(r/R)}{\sqrt{\sigma_{\text{inst}}^2 + \sigma_{\text{mic}}^2 + \sigma_{\text{mac}}^2}}, \quad (14)$$

the easier it will be to resolve the planet’s Doppler shadow in the line profiles. Here, σ_{inst} is the instrumental broadening of the spectrograph, and σ_{mic} and σ_{mac} are the magnitudes of micro- and macroturbulence (Gray 2005). Those are the most important terms which determine the shapes and widths of unsaturated absorption lines, besides rotation. For rapidly rotating stars, precise RV determination is difficult but the RM anomalies in the line profiles can reach depths of several percent of the overall line depth (e.g. Talens et al. 2018), making them relatively easy to detect.

Fig. 6 compares four different representations of the RM effect drawn from the literature. The upper left

panel shows a time series of the anomalous radial velocity. The upper right panel shows a “Doppler shadow” as a time series of residual line profiles, derived from cross-correlation. Each row represents an observed line profile after subtracting the best-fitting model of an undisturbed line profile. As time progresses (upward, on the plot), the negative residual caused by the planet moves from the blue end to the red end of the line profile. The lower left panel shows a time series of the sub-planet velocity inferred with the RM Reloaded technique. In the lower right panel, the color scale indicates the strength of the line-profile residuals after shifting and averaging them as a function of the sub-planet velocity at mid-transit (v_{cen}) and the difference in sub-planet velocities at ingress and egress (v_{14}) corresponding to Eqn. 9 and Eqn. 8. Such a data-stacking analysis can be useful in the presence of correlated noise (Johnson et al. 2014) or a low signal-to-noise ratio (Hjorth et al. 2021; Bourrier et al. 2021). Another approach to detecting small RM signals, employing Gaussian Processes, was presented by Kunovac Hodžić et al. (2021).

3.1.4. The photometric RM effect

The intensities of the receding and approaching halves of the stellar disk differ, at least slightly, due to Doppler beaming as well as the ordinary Doppler shift combined with the finite bandpass of the observations. Groot (2012) and Shporer et al. (2012) evaluated the potential of using these effects to measure stellar obliquities with precise light curves. Shporer et al. (2012) presented the following equation to estimate the maximum amplitude of the associated photometric anomaly,

$$A_{\text{PRM}} \approx 10^{-5} \frac{v \sin I}{10 \text{ km s}^{-1}} \frac{\left(\frac{r}{R}\right)^2}{0.1}. \quad (15)$$

They concluded that due to the small amplitude of the effect, obliquity measurements will be challenging. The most promising targets are rapidly rotating early-type stars, and possibly white dwarfs.

3.1.5. Hot stars with hot Jupiters have high obliquities

The top panel of Figure 8 shows the available measurements of the projected obliquity as a function of the star’s effective temperature. Focusing attention on stars with hot Jupiters reveals that cool stars (blue points) tend to have low obliquities, while hot and very-hot stars (red and orange points) have a broad range of obliquities. The transition takes place between approximately 6000 and 6300 K. This trend, noted by Winn et al. (2010a) and based on 19 data points, has persisted even while the sample size has quintupled. None of the HJ hosts cooler than 6000 K is known to be misaligned,

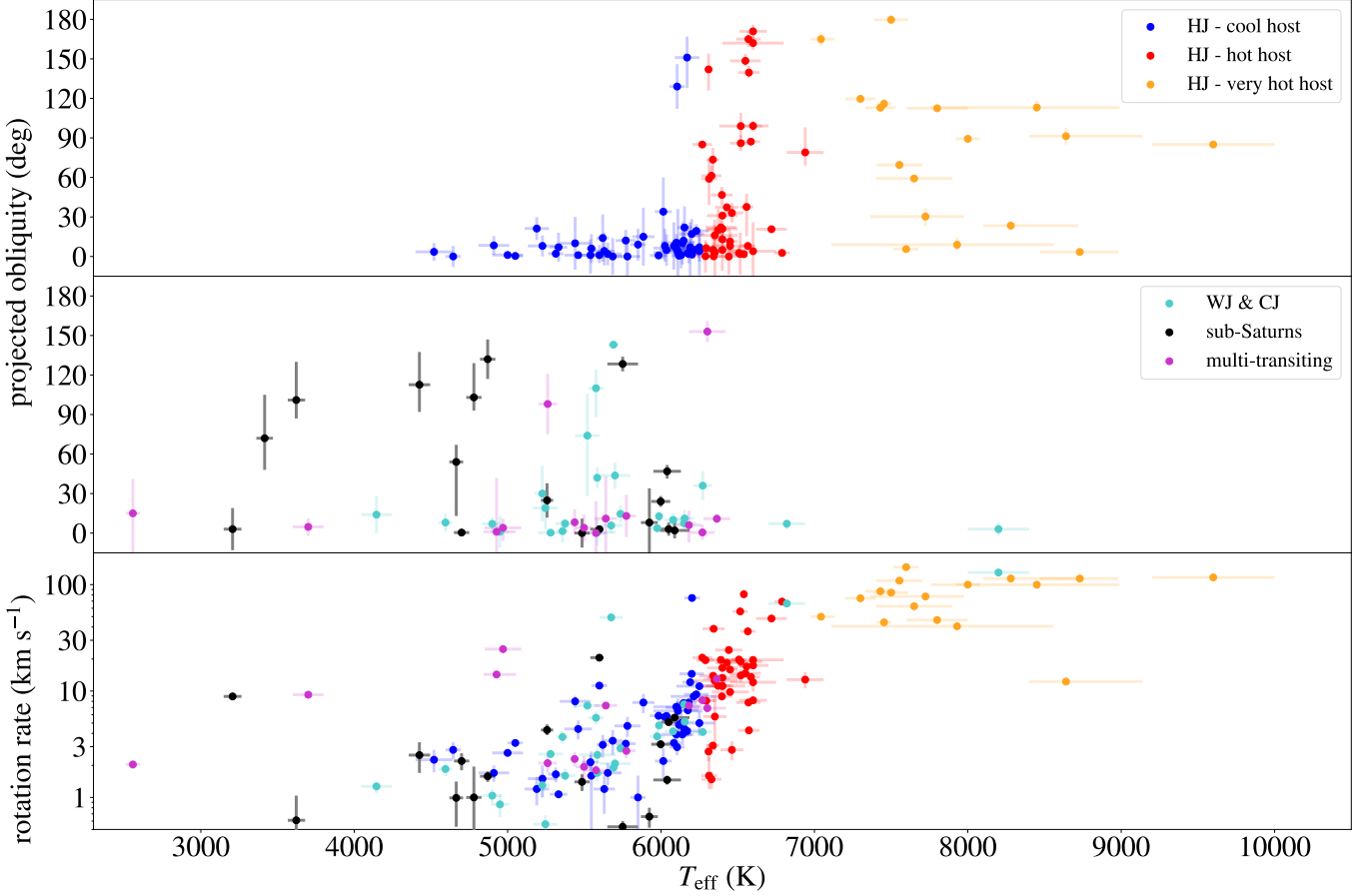


Figure 8. Projected obliquity and rotation velocity vs. effective temperature. Data points are color-coded according to the system's characteristics using the same scheme as in Figure 3. Stars are designated as cool, hot, or very hot, using effective temperature boundaries of 6250 K and 7000 K. Planets with masses exceeding $0.3 M_{\text{Jup}}$ are designated hot Jupiters (HJ) if $a/R < 10$, and warm/cold Jupiters (WJ/CJ) if $a/R > 10$. Planets with masses $\lesssim 0.3 M_{\text{Jup}}$ are designated sub-Saturns. Systems with at least two transiting planets are designated multi-transiting and are represented by only one data point. *Top:* For HJs, the obliquity distribution broadens with effective temperature, with a relatively sharp transition near 6250 K. Cool stars with HJs tend to be well aligned, while hotter stars display misalignments more frequently. *Middle:* Cooler stars with sub-Saturns or WJ/CJs occasionally have high obliquities. Also apparent is that almost all the λ measurements undertaken for hot stars have involved HJs, as opposed to smaller or wider-orbiting planets. *Bottom:* Stellar rotation velocities rise rapidly with effective temperature between about 6000 and 7000 K, a well-known trend attributed to the magnetic braking of cool stars.

where “misaligned” is defined (here and elsewhere in this article) as a reported value of λ that exceeds 10° and excludes 0° with $>3\sigma$ confidence. Between 6250 and 7000 K, the ratio of misaligned to aligned systems is 1.7 (22 vs. 13). Above 7000 K, the ratio rises to 4 (12 vs. 3), and a Kolmogorov-Smirnov test cannot reject the hypothesis that the stars are randomly oriented.

The range of effective temperatures between 6000 and 6300 K, where the obliquity distribution is observed to change, has long been known to be significant in stellar astrophysics. Observationally, this is the division between the lower and upper main sequences, where the stellar mass-radius relationship changes slope and stellar rotation velocities rise sharply with temperature, as shown in the lower panel of Figure 8. Theoretically,

these changes are explained as consequences of differing internal structures. Loosely speaking, a lower main-sequence star has a convective envelope surrounding a radiative interior, while an upper main-sequence star has a radiative exterior and may have a convective core (see page 259 of Kippenhahn et al. 2012). Lower main-sequence stars rotate more slowly because of “magnetic braking,” the steady loss of angular momentum through a magnetized wind, which only develops in stars with outer convective zones. The correct explanation for the obliquity trend seen in the top panel of Figure 8 is likely to involve these differences in the interior structure of the host stars, as discussed further in Section 4.1.

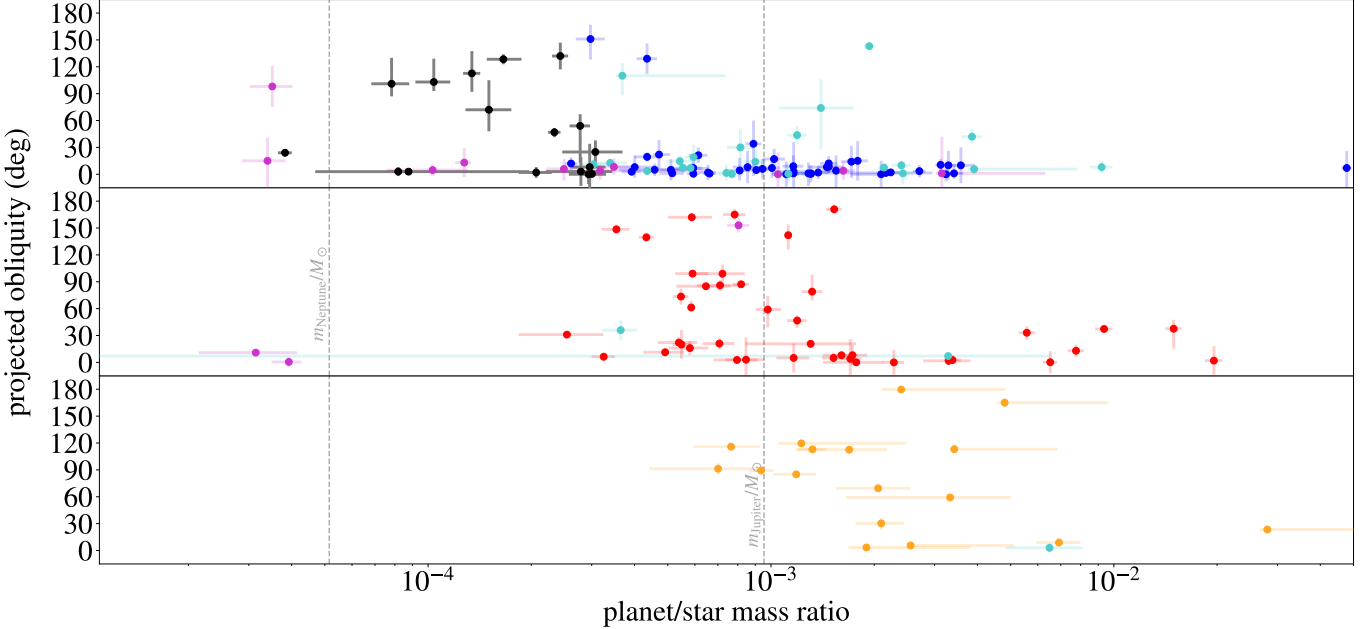


Figure 9. Projected obliquity vs. the planet-to-star mass ratio. Same color scheme as in Figure 8. The three panels are for the three different ranges of effective temperature. For mass ratios exceeding 0.5×10^{-3} , cool host stars have low obliquities, with the exception of three WJ hosts. Hot and very-hot stars have a broad range of obliquities regardless of mass ratio, although hot stars appear to lack retrograde systems for mass ratios exceeding 2×10^{-3} .

3.1.6. Stars with especially massive planets have lower obliquities

Figure 9 displays the projected obliquity as a function of m/M , the planet-to-star mass ratio. For both cool and hot stars, the obliquities tend to be lower when m/M is larger, a trend noted by Hébrard et al. (2011a) using a smaller sample. All the cool HJ hosts with $m/M < 0.5 \times 10^{-3}$ are well aligned. The three misaligned cool stars with $m/M > 10^{-3}$ are WASP-8, Kepler-420, and HD 80606, which all have $a/R > 10$ and are thereby classified as warm Jupiter hosts. For hot stars, the transition to lower obliquities appears to occur for a higher value of m/M , approximately 2×10^{-3} , above which no retrograde systems are seen. Very hot stars do not show evidence for any dependence on mass ratio.

3.1.7. Cool stars with warm Jupiters have high obliquities

Figure 10 displays the projected obliquity as a function of a/R , the orbital semimajor axis divided by the stellar radius. As noted by Albrecht et al. (2012b), cool stars orbited by giant planets with $a/R \lesssim 10$ tend to be well aligned, while those with more distant giant planets have a high obliquity dispersion. Out of the 47 HJs orbiting cool stars with $a/R < 10$, 36 are well aligned, 3 are misaligned, and 8 have an ambiguous status according to our definitions. The misaligned cases are WASP-60 ($\lambda = 19.4^{+4.9}_{-5.1}$ deg; Brown et al. 2017), WASP-94 A

(151^{+23}_{-16} deg; Neveu-VanMalle et al. 2014), and WASP-60 (129 ± 17 deg; Mancini et al. 2018). All three systems have stars hotter than 6100 K and orbits with $a/R > 7$. For hot and very-hot stars (the middle and lower panels of Figure 10), there are no obvious trends with a/R . However, as shown in § 3.7, the misaligned hot stars with $a/R \lesssim 7$ tend to have $\psi \approx 100$ deg.

3.1.8. Some cool stars with HJs are very well aligned

For the stars that are compatible with good alignment, it would be interesting to measure the obliquity dispersion and compare it to the Sun's obliquity as well as the mutual inclination distribution of the planetary orbits in the Solar System. A very low dispersion would suggest that dissipative processes have damped obliquities, although demonstrating that the dispersion is very low would require very precise measurements.

The inset panel within Figure 10 displays all the projected obliquity measurements for cool stars with prograde orbits and measurement uncertainties of 2° or better. Positive and negative values of λ are plotted to allow a better look at the region near 0° . These stars all have projected obliquities lower than the (unprojected) solar obliquity of 6.2° with respect to the plane defined by the total orbital angular momentum of the planets. The standard deviation of the measured values of λ for the prograde cool HJ hosts is 0.91° , and the average formal measurement uncertainty is 0.82° .

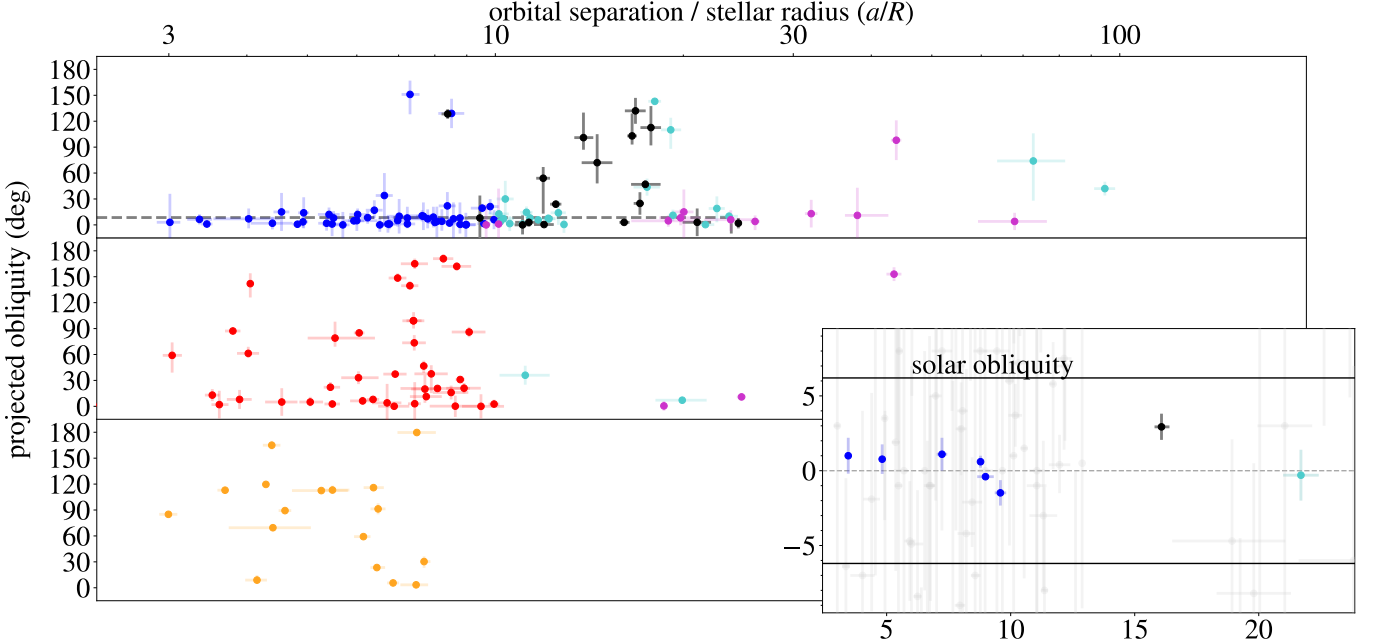


Figure 10. Projected obliquity vs. a/R . Same color scheme as in Figure 8. The obliquity distribution of hot and very-hot stars does not appear to depend on a/R . In contrast, cool stars tend to be aligned whenever $a/R < 10$. The inset panel highlights cool stars for which the measurement uncertainty is below 2° , which appear to have lower obliquities than the Sun. Not shown in this plot is the special case of β Pic, which has $a/R \approx 10^3$ and $\lambda = 3 \pm 5^\circ$ as determined by spectro-interferometry (Kraus et al. 2020).

Thus, the upper limits on the obliquities of the pro-grade cool stars with the best measurements are on the order of a degree, which is several times lower than the solar value. This might be a hint that at some point during the formation or evolution of HJs around cool stars, the obliquities were damped by a dissipative process. The upper limit on the obliquity dispersion is also comparable to the inferred mutual inclination dispersion of compact systems of more than four planets (Zhu et al. 2018). It seems worthwhile to expand on the sample of systems with measurement uncertainties better than 2° and perform a more thorough statistical inference of the underlying obliquity dispersion.

3.1.9. Obliquities and stellar age

Figure 11 displays the projected obliquity as function of isochrone age, i.e., the age determined by fitting stellar-evolutionary models to the observed stellar properties such as effective temperature, surface gravity, metallicity, spectral energy distribution, and luminosity. The HJ hosts older than about 3 Gyr tend to be well-aligned, as noted by Triaud (2011). As discussed by Albrecht et al. (2012b), this correlation is closely related to the previously noted trend involving effective temperature. Cool stars have a broader range of ages than hot stars, because cool stars have longer main-sequence lifetimes. Thus, if misalignments tend to involve hot stars,

the misaligned systems will tend to appear at the young end of the age distribution. Safsten et al. (2020) used statistical tests to conclude that the obliquity distribution is more strongly correlated with effective temperature than age.

3.1.10. Are very young giant-planet hosts well-aligned?

Obliquity measurements for stars younger than 100 Myr are scarce, because not many planets have been detected around such young stars, and because the intrinsic photometric and spectroscopic variations of young stars interfere with detailed characterization. Figure 12 shows the available data for stars younger than 1 Gyr that have age uncertainties below 0.25 Gyr. The data are based on the RM method as well as stellar inclination measurements (from the $v \sin i$ and spectro-interferometric methods). So far, all of the stars younger than 100 Myr are consistent with good alignment.

AU Mic b is one of two known transiting planets that orbit a bright 22-Myr star with an edge-on debris disk (Plavchan et al. 2020). Measurements of the inclination angles of the planetary orbit and the debris disk are consistent with alignment, and RM observations have shown the star to have a low projected obliquity (Hirano et al. 2020a; Palle et al. 2020; Martioli et al. 2020; Addison et al. 2021).

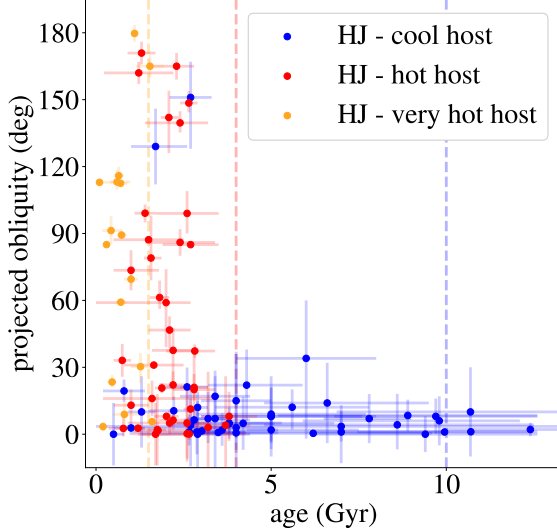


Figure 11. Projected obliquity vs. age. Same color scheme as in Figure 8. Cool stars have a broader age distribution than hot stars because cool stars have longer main-sequence lifetimes.

Another bright and young star with an edge-on debris disk is β Pic, which has two directly-imaged giant planets on orbits that are closely aligned with the disk. Using the spectro-interferometric method (§ 3.3), Kraus et al. (2020) found the star to have a projected obliquity of $3 \pm 5^\circ$. This system is quite different from all the others described in this article because of the large orbital distances, 4.2 and 10.0 au (Lacour et al. 2021).

DS Tuc A is a solar-mass star with an estimated age of 45 Myr, which is separated by 180 au from a K3V binary companion, and has a transiting sub-Saturn planet (Newton et al. 2019). RM observations revealed a projected obliquity of $2.5 \pm 1.0^\circ$, and the $v \sin i$ method also gave results consistent with a low obliquity. The $v \sin i$ method (§ 3.4) is well suited to stars such as DS Tuc A, which rotate rapidly and undergo large-amplitude light variations that reveal the stellar rotation period.

The youngest star known to be misaligned is TOI-811, which has an isochrone age of 117^{+37}_{-43} Myr (Carmichael et al. 2020). The transiting body in that case has a mass of $59.9^{+8.6}_{-13} M_{\text{Jup}}$ and should probably be considered a brown dwarf rather than a planet. The youngest planetary-mass object known to have a misaligned star is Kepler-63 b (210 ± 45 Myr, Sanchis-Ojeda et al. 2013). Another young and misaligned system is KELT-9, a very hot star with $\lambda = 85.01 \pm 0.23^\circ$ and an estimated age of 300 Myr (Gaudi et al. 2017). KELT-9 does not appear in Figure 12 because the reported age did not include an uncertainty estimate. Age determinations for rapidly rotating A stars based on photometry and spectroscopy

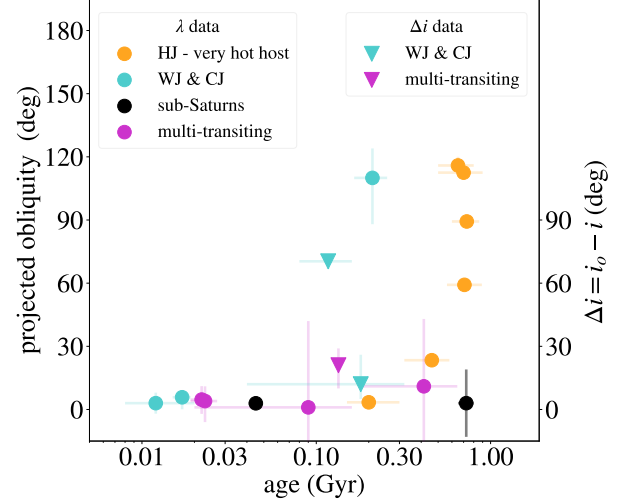


Figure 12. Spin-orbit alignment for the youngest stars? Shown are the projected obliquity measurements (circles) and stellar inclination measurements (triangles) of transit hosts younger than 1 Gyr for which the age uncertainty is smaller than 0.3 Gyr.

are subject to systematic errors due to gravity darkening and rotational oblateness (see, e.g., Jones et al. 2015). The youngest star known to have a well-aligned planet is HIP 67522, with an age of 17 ± 2 Myr (Heitzmann et al. 2021). The planet’s mass has not been measured; it could be a hot Jupiter or an inflated planet of lower mass.

While we cannot draw any firm conclusions from the small sample of young stars, it is noteworthy that the available data for stars with ages $\lesssim 100$ Myr are consistent with low obliquities. If this trend persists for close-orbiting giant planets, it would be an important clue about obliquity excitation. For example, it might be the case that very young hot Jupiters formed *in situ* or underwent disk migration, either of which would preserve the initial alignment, while late-arriving hot Jupiters formed through orbit-tilting interactions. We refer the reader to Dawson & Johnson (2018) for more discussion of the possible origins of hot Jupiters, and to § 4 for more discussion of the relevance of obliquity measurements.

3.1.11. Obliquity & eccentricity

Dynamical interactions such as planet-planet scattering and Kozai-Lidov cycles, which are often invoked to explain high obliquities, are also expected to excite orbital eccentricities (§ 4.3). One might therefore expect an association between obliquity and eccentricity. It is difficult to check for such a statistical association, because there are relatively few systems for which both obliquity and eccentricity are well determined; often, one or the other has a large observational uncertainty.

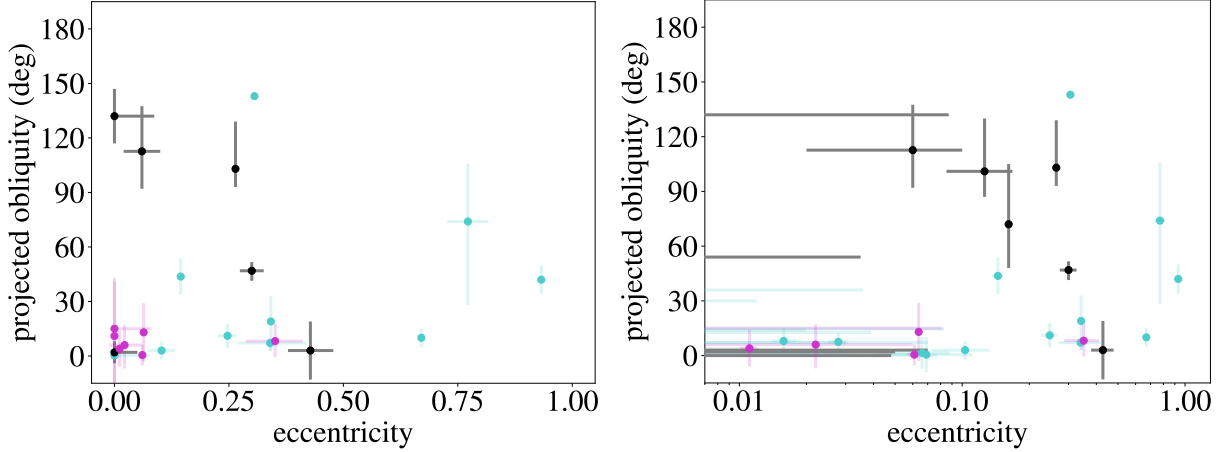


Figure 13. **Obliquity and eccentricity**, for all systems with $a/R > 10$ for which the uncertainty in eccentricity is below 0.1. The lower limit on a/R is intended to exclude systems subject to rapid tidal circularization. The right panel shows the same data with a logarithmic scale for the eccentricity axis. Many systems display nearly circular and aligned architectures, while systems with spin-orbit misalignments tend to travel on eccentric orbits. We note that our restrictions on distance and eccentricity might bias this sample. In particular, hot host stars are nearly all excluded because eccentricity measurements for such stars are more difficult.

The possible effects of tidal interactions also complicate the interpretation of the data. Wang et al. (2021) noted that cool stars with $a/R \lesssim 10$ tend to have both low obliquity and low eccentricity. This could be due to damping of both obliquity and eccentricity by tides (§ 4.1), although according to standard theoretical assumptions, eccentricity damping is mainly caused by dissipation within planets and obliquity damping is mainly caused by dissipation within the star (see, e.g., Schlaufman & Winn 2013).

Rice et al. (2022) found that cool stars with planets on eccentric orbits tend to have higher obliquities than similar stars with planets on low-eccentricity orbits. This is an intriguing finding, although high obliquity is associated not only with high eccentricity, but also lower planet masses and wider orbits (Figures 9 and 10; see also Appendix B of Rice et al. 2022), which complicates the interpretation of the results.

Figure 13 displays the sample of systems for which $a/R > 10$ and the eccentricity is known with a precision of 0.1 or better. This plot is similar to the one presented by Rice et al. (2021), although they omitted planets on circular orbits. The restriction on orbital separation was imposed to select systems that are probably unaffected by tides. (See Tables 4 and 5 for the relevant parameters and references.)

Two of the systems for which the orbit is consistent with circular are misaligned at the 2σ level: HAT-P-12 ($\lambda = 54_{-41}^{+13}$ deg) and TrES-1 (31 ± 21 deg). KELT-6 is misaligned with a formal significance of 3σ (36 ± 11 deg), but the results are more vulnerable than usual to systematic effects because no pre-ingress data are available. The only clearly misaligned system with $e < 0.1$ and $\sigma_e < 0.1$ is HAT-P-18, which has a retrograde orbit and an upper limit of 0.087 on the eccentricity. HAT-P-18 also appears to be one of the oldest systems in the sample, although with large uncertainties ($12.4_{-6.4}^{+4.4}$ Gyr). Only HAT-P-22 appears to be comparably old. It might be relevant that the systems with large obliquities and small eccentricities have sub-Saturn planets. Under standard assumptions in tidal theory, lower-mass planets are more likely to undergo orbital circularization prior to realignment of the host star. There are also four systems with high eccentricities and low obliquities: HAT-P-17, HD 17156, Kepler-448, and K2-25.

In summary, we do not think the current data provide a clear answer to the question of whether misalignment is associated with orbital eccentricity. The relevant sample is small and heterogeneous, and tidal damping of both eccentricities and obliquities – possibly at very different rates – complicates the picture.

Table 2. Key parameters of systems with multiple transiting planets for which λ , i , or both were determined. For the λ measurements, we provide the parameters of the planet for which the measurement was made. In the reference column, the boldface number refers to the work from which we drew the λ measurement. The other numbers refer to works reporting additional measurements of λ or other system parameters not taken from [TEPCat](#) (Southworth 2011).

Planet	T_{eff}	a/R	r	λ	i	ψ	References
	(K)		(R _{Jup})	($^{\circ}$)	($^{\circ}$)	($^{\circ}$)	
(1)	(2)	(3)	(4)	(5)	(6)	(7)	(8)
AU Micb	3700 ± 100	$18.92^{+2.15}_{-2.42}$	0.38 ± 0.02	$4.7^{+6.4}_{-6.8}$	$90.0^{+0.0}_{-19.5}$	$12.1^{+11.3}_{-7.5}$	1,2,3,4,5
HD 3167b	5261 ± 60	$4.08^{+0.99}_{-0.46}$	$0.14^{+0.00}_{-0.00}$	$6.6^{+7.9}_{-6.6}$	—	—	6,7
HD 3167c	5261 ± 60	$43.86^{+0.82}_{-0.86}$	$0.27^{+0.04}_{-0.03}$	98.0 ± 23.0	—	—	8
HD 63433b	5640 ± 74	$16.74^{+1.00}_{-1.11}$	0.19 ± 0.01	$8.0^{+33.0}_{-45.0}$	$90.0^{+0.0}_{-18.7}$	$25.6^{+22.5}_{-15.3}$	9,2
HD 63433c	5640 ± 74	$38.00^{+4.60}_{-1.70}$	2.71 ± 0.14	$11.0^{+32.0}_{-35.0}$	$90.0^{+0.0}_{-18.7}$	$25.6^{+22.5}_{-15.3}$	10,2
HD 106315c	6364 ± 87	$24.79^{+0.39}_{-0.43}$	0.39 ± 0.01	$10.9^{+3.8}_{-3.6}$	—	—	11
K2-290b	6302 ± 120	13.15 ± 0.69	0.27 ± 0.01	$173.0^{+45.0}_{-53.0}$	39.0 ± 7.0	124.0 ± 6.0	12,13
K2-290c	6302 ± 120	43.50 ± 1.20	0.77 ± 0.05	153.0 ± 8.0	39.0 ± 7.0	124.0 ± 6.0	12,13
Kepler-9b	5774 ± 60	32.05 ± 0.74	0.74 ± 0.01	13.0 ± 16.0	$71.9^{+18.1}_{-8.8}$	$28.1^{+13.0}_{-13.6}$	14,2
Kepler-25c	6270 ± 79	18.62 ± 0.24	$0.47^{+0.01}_{-0.01}$	0.5 ± 5.7	$90.0^{+0.0}_{-21.3}$	$5.7^{+4.2}_{-3.2}$	15,16,2,17
Kepler-30c	5498 ± 54	67.86 ± 8.57	1.07 ± 0.03	4.0 ± 10.0	—	—	18
Kepler-50b	6225 ± 66	$10.48^{+1.64}_{-2.73}$	$0.15^{+0.00}_{-0.01}$	—	$82.0^{+8.0}_{-7.0}$	—	19
Kepler-56b	4840 ± 97	5.23 ± 0.26	0.58 ± 0.03	—	47.0 ± 6.0	—	20
Kepler-65b	6211 ± 66	$5.24^{+0.32}_{-0.18}$	$0.13^{+0.00}_{-0.00}$	—	$81.0^{+9.0}_{-16.0}$	—	19
Kepler-89d	6182 ± 82	23.82 ± 2.22	1.00 ± 0.10	$6.0^{+11.0}_{-13.0}$	—	—	21,15
TOI-451b	5550 ± 56	$6.93^{+0.11}_{-0.16}$	0.17 ± 0.01	—	$69.0^{+11.0}_{-8.0}$	—	22
TOI-942b	4928^{+125}_{-85}	$10.12^{+0.13}_{-0.18}$	$0.43^{+0.02}_{-0.00}$	$1.0^{+41.0}_{-33.0}$	$76.0^{+9.0}_{-11.0}$	$2.0^{+27.0}_{-33.0}$	23,24
TRAPPIST-1b	2557 ± 47	$20.04^{+0.72}_{-0.69}$	$0.10^{+0.00}_{-0.00}$	$15.0^{+26.0}_{-30.0}$	$90.0^{+0.0}_{-17.4}$	$23.3^{+17.0}_{-13.6}$	25,2
TRAPPIST-1e	2557 ± 47	$50.82^{+1.83}_{-1.75}$	$0.08^{+0.00}_{-0.00}$	$9.0^{+45.0}_{-51.0}$	$90.0^{+0.0}_{-17.4}$	$23.3^{+17.0}_{-13.6}$	25,2
TRAPPIST-1f	2557 ± 47	$66.85^{+2.40}_{-2.31}$	$0.09^{+0.00}_{-0.00}$	21.0 ± 32.0	$90.0^{+0.0}_{-17.4}$	$23.3^{+17.0}_{-13.6}$	25,2
V1298 Taub	4970 ± 120	26.06 ± 0.46	$0.92^{+0.05}_{-0.05}$	$4.0^{+7.0}_{-10.0}$	$51.0^{+25.0}_{-21.0}$	$8.0^{+4.0}_{-7.0}$	26,27,28,29
V1298 Tauc	4970 ± 120	$13.19^{+0.15}_{-0.13}$	$0.92^{+0.05}_{-0.05}$	5.0 ± 15.0	—	—	26,30,28
WASP-47b	5576 ± 67	9.67 ± 0.15	1.12 ± 0.01	0.0 ± 24.0	—	—	31
WASP-148b	5437 ± 21	19.80 ± 1.50	$0.80^{+0.02}_{-0.02}$	$8.2^{+9.7}_{-8.7}$	—	—	32,33

NOTE—All data were taken from [TEPCat](#) (Southworth 2011) or the following references: 1 (Hirano et al. 2020a), 2 (Albrecht et al. 2021), 3 (Martioli et al. 2020), 4 (Palle et al. 2020), 5 (Addison et al. 2021), 6 (Christiansen et al. 2017), 7 (Bourrier et al. 2021), 8 (Dalal et al. 2019), 9 (Mann et al. 2020), 10 (Dai et al. 2020), 11 (Zhou et al. 2018), 12 (Hjorth et al. 2019a), 13 (Hjorth et al. 2021), 14 (Wang et al. 2018), 15 (Albrecht et al. 2013), 16 (Campante et al. 2016), 17 (Benomar et al. 2014), 18 (Sanchis-Ojeda et al. 2012), 19 (Chaplin et al. 2013), 20 (Huber et al. 2013), 21 (Hirano et al. 2012), 22 (Newton et al. 2021), 23 (Zhou et al. 2021), 24 (Wirth et al. 2021), 25 (Hirano et al. 2020b), 26 (David et al. 2019b), 27 (Johnson et al. 2022), 28 (Biddle et al. 2014), 29 (Gaidos et al. 2022), 30 (Feinstein et al. 2021), 31 (Sanchis-

Ojeda et al. 2015), 32 (Wang et al. 2022), 33 (Hébrard et al. 2020)

3.1.12. Interlude: Mutual orbital inclinations

Most of the available RM data are for stars with close-orbiting giant planets. Many of the theories for obliquity excitation involve the same processes that are hypothesized to allow giant planets to form far from the star and move inward. On the other hand, there might be reasons for high obliquities that are unrelated to close-orbiting giant planets, such as ‘primordial’ misalignments between stars and their protoplanetary disks, i.e., occurring before planet formation. This makes it interest-

ing to expand the domain of obliquity measurements to smaller and wider-orbiting planets.

The *Kepler* mission led to the discovery of hundreds of systems of multiple transiting planets in compact configurations. The known planets are typically between the Earth and Uranus in size and have orbital periods shorter than a year. Through various means, the mutual inclinations between the orbits have been estimated to be $\lesssim 5^\circ$ (Fabrycky et al. 2014; Xie et al. 2016; Zhu et al. 2018; Herman et al. 2019). Thus, the compact multi-planet systems appear to be at least as flat as the Solar System, and some are definitely much flatter (see, e.g., Agol et al. 2021). The very innermost planets with periods $\lesssim 1$ day tend to have somewhat larger mutual inclinations than more distant planets (Dai et al. 2018a), but even in those cases the angles are $\lesssim 15^\circ$. If we assume the nearly coplanar orbits trace out the plane of the long-gone protoplanetary disk, then we can test for primordial misalignments by measuring the stellar obliquity. More generally, we can test for differences in obliquity excitation and evolution between stars with compact multi-planet systems and those with close-orbiting giant planets.

3.1.13. Compact multi-transiting systems: aligned with notable exceptions

The first five obliquity measurements of stars with compact multi-transiting systems were all consistent with good alignment (Albrecht et al. 2013). Since then, the sample size has increased to 18 stars. Of these, 15 have low obliquities. There are also three stars with high obliquities: Kepler-56 (Huber et al. 2013), HD 3167 (Dalal et al. 2019; Bourrier et al. 2021), and K2-290 A (Hjorth et al. 2021). Thus, high obliquities are not confined to stars with close-orbiting giant planets. In a fourth system, Kepler-129, there is tentative evidence of a high obliquity from asteroseismology (Zhang et al. 2021). As discussed in Section 4, the high obliquities in these systems might have been caused by gravitational perturbations from wide-orbiting companions — a stellar companion in the case of K2-290 A, and a planetary-mass companion in the case of Kepler-56. The properties of the multi-transiting systems are included in Tables 4 and 5, along with those of the single-transiting systems. Table 2 highlights the data for multi-transiting systems, in particular, including whether spin-orbit information is available for more than one planet.

3.2. Asteroseismology

Just as observing vibrations of the Earth’s crust can be used to study wave propagation in the Earth’s mantle and core, observing the vibrations of stellar surfaces can

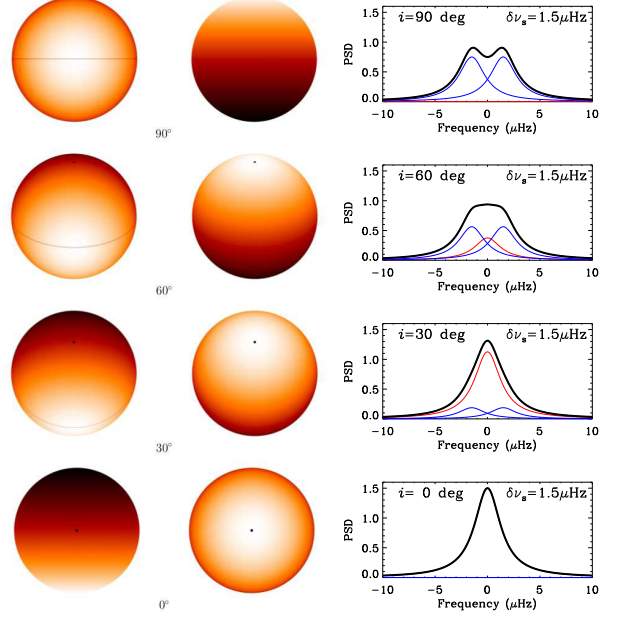


Figure 14. Mode visibility for different stellar inclinations. Left and middle columns: Theoretical intensity perturbations for an $l = 1$ mode with $m = 1$ (left) and $m = 0$ (middle). The top row is for a line of sight along the equatorial plane ($i = 90^\circ$) while the lowest row is for a line of sight along the spin axis ($i = 0^\circ$). Right column: Theoretical frequency profiles of the $l = 1$, $m = \pm 1$ (blue lines) and $m = 0$ (red) modes, as well as the combined signal (black line). The observed amplitude of the $m = \pm 1$ modes is reduced as the inclination is lowered. The reverse is true for the $m = 0$ mode. Adapted from Figures 6 and 7 of Chaplin et al. (2013).

be used to study the deep interiors of stars. This technique, asteroseismology, has seen astonishing advances over the last 15 years due to the availability of photometric time-series data of long duration, fine time sampling, and high signal-to-noise ratio (Kurtz 2022). Among the information that can be retrieved from the frequency spectrum of a star’s oscillation modes is the inclination of the star’s rotation axis with respect to the line of sight (Gough & Kosovichev 1993; Gizon & Solanki 2003; Chaplin & Miglio 2013).

Similar to the eigenstates of the hydrogen atom, the oscillation modes of a star are classified by three integers: the radial order n , the latitudinal degree $l \leq n$, and the azimuthal order m which ranges from $-l$ to l . Mode patterns with different m but the same n and l are related by rotation, and therefore, they would have the same frequency for a stationary spherical star. Stellar rotation breaks this symmetry. Each degenerate group of $2l + 1$ modes is split into a multiplet with

$$\nu_{nlm} \approx \nu_{nl} + \frac{m\Omega}{2\pi} , \quad (16)$$

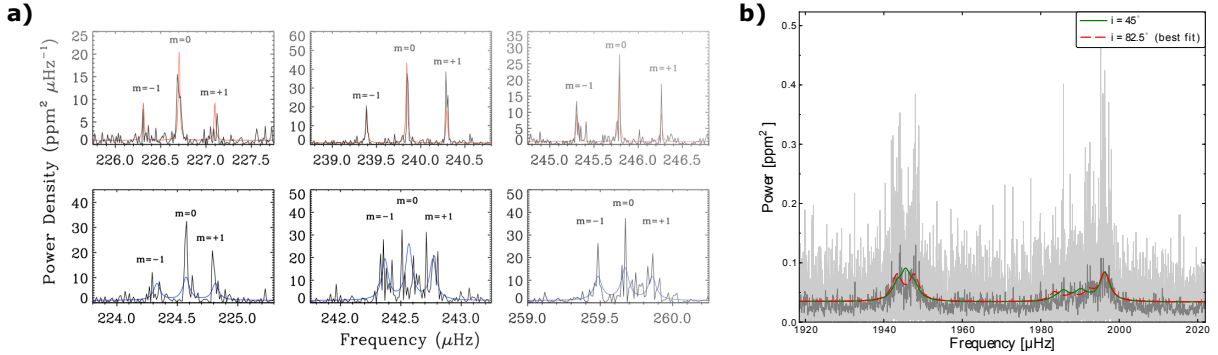


Figure 15. Stellar inclinations from asteroseismology. Shown are the power spectra of two transiting-planet hosts, based on *Kepler* light curves. *Left:* Kepler-56, a subgiant star (Huber et al. 2013). The top row shows gravity-dominated modes and the bottom row shows pressure-dominated dipole modes. Each mode is split into a triplet by rotation. All three modes are visible, indicating a moderate inclination. Quantitatively, the inclination was found to be $47 \pm 6^\circ$. *Right:* Kepler-410, a hotter and less evolved star (Van Eylen et al. 2014). The data are shown as gray and dark gray curves (after smoothing). The red and green curves are models with $i = 90^\circ$ and 45° . Although the triplets are not as well resolved as in Kepler-56, the $m = \pm 1$ modes are more prominent than the $m = 0$ mode, indicating a high inclination.

where Ω is the star’s average angular rotation rate. For the Sun, $\Omega/2\pi$ is approximately $0.43\,\mu\text{Hz}$.

For Sun-like stars, the modes are stochastically excited by convection, making it reasonable to assume that the modes in a given multiplet are excited to the same intrinsic amplitude. However, the observed mode amplitudes in a power spectrum depend on the viewing angle, because they are based on the integrated flux over the visible stellar hemisphere. Consider dipole modes ($l = 1$). When $i = 90^\circ$, the $m = 0$ mode is invisible because the intensity pattern of the mode is antisymmetric about the stellar equator, and integrates to zero over the entire disk. The $m = \pm 1$ modes are seen at maximum amplitude (Figure 14). In contrast, when $i = 0^\circ$, the $m = 0$ mode is seen with maximum amplitude and the $m = \pm 1$ modes are invisible. In general, as shown by Gizon & Solanki (2003), the relative amplitudes are proportional to

$$\begin{aligned} \mathcal{E}_{l=1,m=0} &= \cos^2 i, \\ \mathcal{E}_{l=1,m=\pm 1} &= \frac{1}{2} \sin^2 i, \\ \mathcal{E}_{l=2,m=0} &= \frac{1}{4} (3 \cos^2 i - 1)^2, \\ \mathcal{E}_{l=2,m=\pm 1} &= \frac{3}{8} \sin^2 2i, \\ \mathcal{E}_{l=2,m=\pm 2} &= \frac{3}{8} \sin^4 i. \end{aligned} \quad (17)$$

Therefore, by measuring the relative amplitudes of the modes in each multiplet, we can determine the inclination. When this technique succeeds for a star with a transiting planet, we can compare the orbital and stellar inclinations and thereby obtain a constraint on the stellar obliquity. More details on the extraction of the inclination from the photometric power spectrum are

given by Gizon & Solanki (2003); Ballot et al. (2006, 2008) and Kuszlewicz et al. (2019). See also Grundahl et al. (2017), who discuss the extraction of the inclination from radial-velocity data, instead of photometric data.

The observational requirements are demanding. To measure the relative amplitudes of the members of the multiplets, and thereby constrain the inclination, it is necessary to resolve the multiplets by obtaining a long-duration time series. For uniformly-sampled data, the frequency resolution is $\sim 1/T$ where T is the total duration of a time series. By this criterion, resolving a Sun-like splitting of $0.43\,\mu\text{Hz}$ requires a total duration of a month. In most applications, a much longer time series has been needed to achieve a sufficiently high signal-to-noise ratio. In addition, the intrinsic frequency widths of the modes need to be small in comparison to the splittings, and the mode amplitudes need to be large enough to detect, factors that favor evolved and rapidly-rotating stars. Figure 15 illustrates the method with two cases: one in which the multiplets are well resolved (left panel), and another in which they are barely resolved (right panel).

The left panel features the most striking result so far from the asteroseismic technique for inclination determination: the high obliquity of the subgiant star Kepler-56 (Huber et al. 2013). This star has two transiting planets of radii 6.5 and $9.8 R_\oplus$, which are engaged in a $2:1$ mean-motion resonance. The stellar and orbital inclinations differ by 45° . This system is discussed further in § 4. Using the same method, Zhang et al. (2021) found tentative evidence for a misalignment in the Kepler-129 system, which has two transiting sub-Neptunes. Kamiaka et al. (2019) found a misalignment of at least 42°

in the Kepler-408 system, which has a super-Earth on a 2.5-day orbit.

So far, those are the only misalignments that have been reported using the asteroseismic method. [Chaplin et al. \(2013\)](#) found that the data for the Kepler-50 and Kepler-65 systems, which have multiple transiting super-Earths, are consistent with low obliquities. [Van Eylen et al. \(2014\)](#) found agreement between i and i_o for Kepler-410, a multi-planet system featuring a transiting mini-Neptune on an eccentric orbit (see the right panel of Figure 15). [Campante et al. \(2016\)](#) performed a comprehensive study of the 25 Kepler systems that appeared to have the most favorable properties for the asteroseismic technique. They confirmed that HAT-P-7 has a nearly polar orbit, as had been found by [Lund et al. \(2014\)](#). Since RM data were also available for this retrograde-rotating star ([Winn et al. 2009a; Narita et al. 2009a; Albrecht et al. 2012b](#)), HAT-P-7 was one of the first stars for which the 3-d obliquity (ψ) could be determined. The data for the rest of the systems analyzed by [Campante et al. \(2016\)](#) were consistent with good alignment, although in many cases only weak constraints could be obtained (e.g., $i \gtrsim 20^\circ$).

The RM effect would have been difficult to detect for most of the systems described in this section, because of the small signal sizes. As noted in § 3, the asteroseismic signal depends only on the properties of the star, rather than the planet. Once a transiting planet has been detected, the applicability of the asteroseismic method is independent of the properties of the planet. At this point, though, the only successful applications of this method have been based on data from the Kepler mission. More detections might come from the ongoing Transiting Exoplanet Survey Satellite (TESS) mission ([Ricker et al. 2015](#)), and especially the future PLATO mission ([Rauer et al. 2014](#)).

3.3. Spectro-interferometry

Optical and near-infrared interferometers can resolve the disks of main-sequence stars in the solar neighborhood. If equipped with a spectrograph capable of resolving stellar absorption lines, an interferometer can measure the orientation of the stellar rotation axis as projected on the sky plane ([Albrecht et al. 2010](#)). The approaching and receding halves of the stellar disk have slightly different locations on the sky. Therefore, the photocenters of the red and blue wings of a rotationally-broadened absorption line are slightly displaced. This displacement is manifested as a phase shift in the fringe pattern recorded by a pair of telescopes in an interferometer. For marginally resolved stars, the differential phase between the interferometric fringes of the two pho-

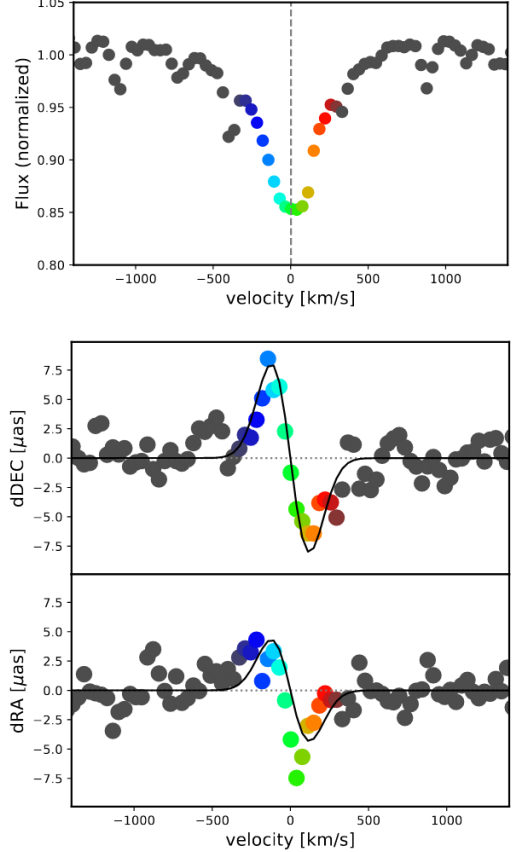


Figure 16. Spatially resolved Br γ absorption line of β Pic. From [Kraus et al. \(2020\)](#). The top panel displays the spatially integrated Br γ absorption line. The two lower panels display the spatial offsets of the photocenter relative to the continuum. The approaching (blue) side of the star is displaced north and east of the receding (red) side of the star.

tocenters is (see [Le Bouquin et al. 2009](#), and Eqn. B.5 of [Lachaume 2003](#))

$$\rho = -2\pi p \frac{B}{\lambda_w} [\text{rad}], \quad (18)$$

where B is the baseline length between the telescopes, p is the angular sky separation of the two photocenters projected onto B , and λ_w is the observing wavelength. More details are given by [Petrov \(1989\)](#) and [Chelli & Petrov \(1995\)](#).

So far, this technique has worked in two cases: (1) [Le Bouquin et al. \(2009\)](#) showed that Fomalhaut is aligned on the sky with its debris disk to within a few degrees, and (2) [Kraus et al. \(2020\)](#) showed that β Pic is aligned with its debris disk and with the orbital planes of two directly imaged planets (see Figure 16). Good alignment for β Pic had already been suspected, based on asteroseismology ([Zwintz et al. 2019](#)). Both

of these stars are bright and rapidly rotating, and in both cases the inclination was derived from the pressure-broadened Br γ line. It would be advantageous to observe metal absorption lines, because they are not subject to strong pressure broadening, but no current interferometer can resolve metal lines in late-type main-sequence stars. Preparations are underway for interferometers with higher spectral resolving power at the CHARA array (Mourard et al. 2018) and the VLT Interferometer (Kraus 2019). These newer instruments will be able to perform improved fringe tracking, which will increase the allowable integration time of the spectrograph and thereby extend the applicability of the technique to fainter stars.

For this method to provide obliquity information, we must also know the position angle on the sky of the plane of the surrounding disk, or a planetary orbit. The position angle of a planetary orbit cannot be obtained from RV or transit observations, but it can be obtained from direct-imaging or astrometric observations. Time-series astrometry from the Gaia mission is expected to lead to the detection of thousands of exoplanets for which the orbital orientation will be known (Perryman et al. 2014). The brightest and nearest stars with Gaia planets might provide a new pool of targets for interferometric observations of stellar obliquities.

Some other relevant and potentially observable interferometric effects are worth noting. In the presence of differential rotation, it may be possible for interferometry to constrain the stellar inclination (Domiciano de Souza et al. 2004). For the most rapidly-rotating and centrifugally flattened stars, interferometry can determine the star’s sky-projected shape without the need for spectroscopy (see, e.g., Domiciano de Souza et al. 2003).

In addition to studying planetary systems, interferometers can be used to study the alignment of stars in binary systems, star-forming regions, and stellar clusters. Such measurements would shed light on the initial conditions of star and planet formation (as discussed further in section 4).

3.4. The projected rotation velocity technique

By combining estimates of a star’s radius, R , rotation period, P_{rot} , and projected rotation velocity, $v \sin i$, and neglecting any differential rotation, the inclination can be calculated as

$$i = \sin^{-1} \left(\frac{v \sin i}{v} \right) = \sin^{-1} \left(\frac{v \sin i}{2\pi R / P_{\text{rot}}} \right). \quad (19)$$

This method is not as straightforward as it might seem. Measurements of $v \sin i$ are obtained by analyzing a

star’s spectral absorption lines or cross-correlation function. The contribution to line broadening from rotation must be separated from those of other sources, such as turbulence and the finite instrumental resolution. To put this into perspective, consider that the Sun’s rotation velocity is 1.9 km s^{-1} and the best available spectrographs have a spectral resolution of $\sim 10^5$, corresponding to a velocity resolution of 3 km s^{-1} . Thus, data with a very high signal-to-noise ratio are required to disentangle the sources of broadening for solar-type stars – and even then, the results are subject to systematic uncertainties.

The rotation period can be measured by observing the quasiperiodic brightness variations due to rotating spots and plages. The advent of the Kepler and TESS missions has made it possible to measure the rotation periods of thousands of planet-hosting stars (McQuillan et al. 2013; Mazeh et al. 2015a; see also the review by Maxted 2018). When the rotation period of a solar-type star cannot be directly measured (because there are no suitable data, or because photometric modulation is not detected), one can guess the rotation period based on the star’s mass and age. This is because the rotation of main-sequence solar-type stars tends to slow down according to the Skumanich (1972) law, $P_{\text{rot}} \propto t^{1/2}$, with a coefficient depending on mass (e.g. Barnes 2010; Epstein & Pinsonneault 2014; Meibom et al. 2015; van Saders et al. 2016). However, this is not a safe procedure to follow for stars with hot Jupiters. Such stars need not obey the usual pattern because of tidal spin-up (see, e.g., Tejada Arevalo et al. 2021).

A subtlety in the statistical inference of i from Equation 19 is that v and $v \sin i$ are not independent variables. Masuda & Winn (2020) discussed the diagnosis and treatment of this problem. A relatively simple method to account for the interdependent variables is to employ a Monte Carlo Markov Chain method in which the parameters are R , P_{rot} , and $\cos i$, with a uniform prior on $\cos i$ and measurement-informed priors on R , P_{rot} , and $(2\pi R / P_{\text{rot}})\sqrt{1 - \cos^2 i}$.

In an important early application of the $v \sin i$ technique, Schlaufman (2010) studied a sample of 75 transiting planets for which the stellar rotation periods had been estimated from an age-mass-rotation relationship. He found 10 stars with unusually low values of $v \sin i$, suggesting that they have high obliquities. This was true even though most of the planets were hot Jupiters and might have been expected to spin up their stars. All 10 misaligned stars were in the mass range from 1.2 to $1.5 M_{\odot}$, despite such stars constituting only $\approx 40\%$ of the sample. This suggested that misalignments are preferentially found in massive stars, although this was not

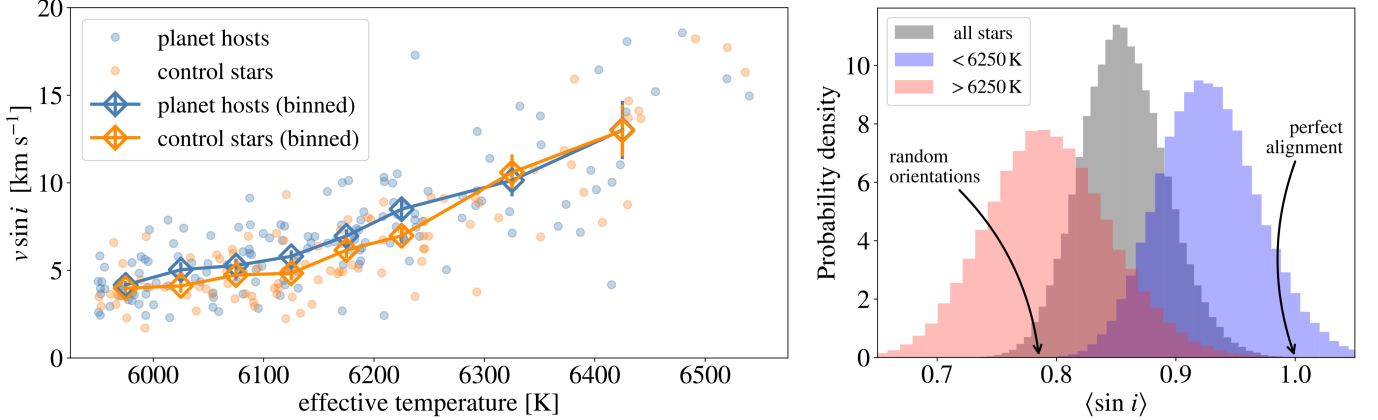


Figure 17. The projected rotation velocity method applied to Kepler stars, from Louden et al. (2021). *Left:* Projected rotation velocities of stars with and without detected transiting planets. For stars cooler than 6250 K (the Kraft break), the average value of $v \sin i$ is higher for transit hosts than for the non-transit hosts, by approximately the factor one would expect if the transit hosts have low obliquities and the other stars are randomly oriented. For hotter stars, no difference is detected. *Right:* Posterior probability distributions for the mean value of $\sin i$ of the cool stars (blue), the hot stars (red), and the entire sample (gray).

necessarily a valid conclusion because the $v \sin i$ method is less sensitive to misalignments of lower-mass stars, due to their slower rotation. Nevertheless, results from the RM effect and other methods have indeed shown that misalignments in hot-Jupiter systems are more common for massive stars hotter than ≈ 6250 K (see § 3.1.5).

This method was further developed to take advantage of the large sample of transiting planets and planet candidates supplied by the Kepler mission. The Kepler data not only led to the detection of thousands of planets, but also the measurement of the rotation period for about one-third of the host stars. Therefore, to apply the $v \sin i$ method, the only new observations that were required were a single good spectrum of each host star. This made it possible to study the obliquity distribution of large samples of stars with non-giant planets, for the first time. The first such studies, by Hirano et al. (2012), Walkowicz & Basri (2013), and Hirano et al. (2014), identified some candidate misaligned systems. Morton & Winn (2014) took a different approach: Instead of searching for individual cases of misalignment, they performed a hierarchical Bayesian analysis of the obliquity distribution of 70 Kepler stars. In terms of the vMF model (see § 2), they found tentative evidence ($p \approx 0.03$) that stars with multiple detected transiting planets have a higher κ (lower obliquities) than stars with only a single detected transiting planet.

Winn et al. (2017) performed a larger and more homogeneous study as part of the California Kepler Survey (CKS; Johnson et al. 2017; Petigura et al. 2017), which obtained high-resolution optical spectra of $\approx 10^3$ Kepler stars. The analysis of this expanded sample did not confirm the previously reported candidate misalign-

ments, nor did it confirm the difference between single and multiple-transiting planets. Muñoz & Perets (2018) performed a similar study. In general, both groups found the Kepler stars with non-giant planets to have obliquities lower than about 30° .

A problem with these population-level analyses is that the stars with measurable rotation periods might be biased with respect to age and inclination, complicating the interpretation of the results. To overcome this problem, Louden et al. (2021) returned to the method of Schlaufman (2010), wherein the $v \sin i$ distribution of a sample of transiting-planet hosts is compared with the $v \sin i$ distribution of a sample of control stars. The control stars were selected to have a distribution of masses, ages, and metallicities indistinguishable from those of the planet hosts. To the extent that the planet hosts have low obliquities, their $v \sin i$ distribution should be shifted to higher values. Using this method, Louden et al. (2021) found evidence for a difference between the hot and cool Kepler stars with transiting planets, see Figure 17. The stars cooler than 6250 K had $\langle \sin i \rangle = 0.928 \pm 0.042$ (1.7σ away from zero obliquity), while the hotter stars had $\langle \sin i \rangle = 0.794 \pm 0.052$ (consistent with random orientations). Thus, they suggested that hot stars with Kepler-like planets ($R \lesssim 4/R_\oplus$, $P \lesssim 1$ year) have a broad obliquity distribution, as was already known to be the case for hot Jupiters. A similar finding was reported earlier by Mazeh et al. (2015b) using a technique described below. These results pertain mainly to stars with compact multi-planetary systems, which dominate the Kepler sample. Even the Kepler stars with only a single detected transiting planet probably are thought to have additional, non-transiting

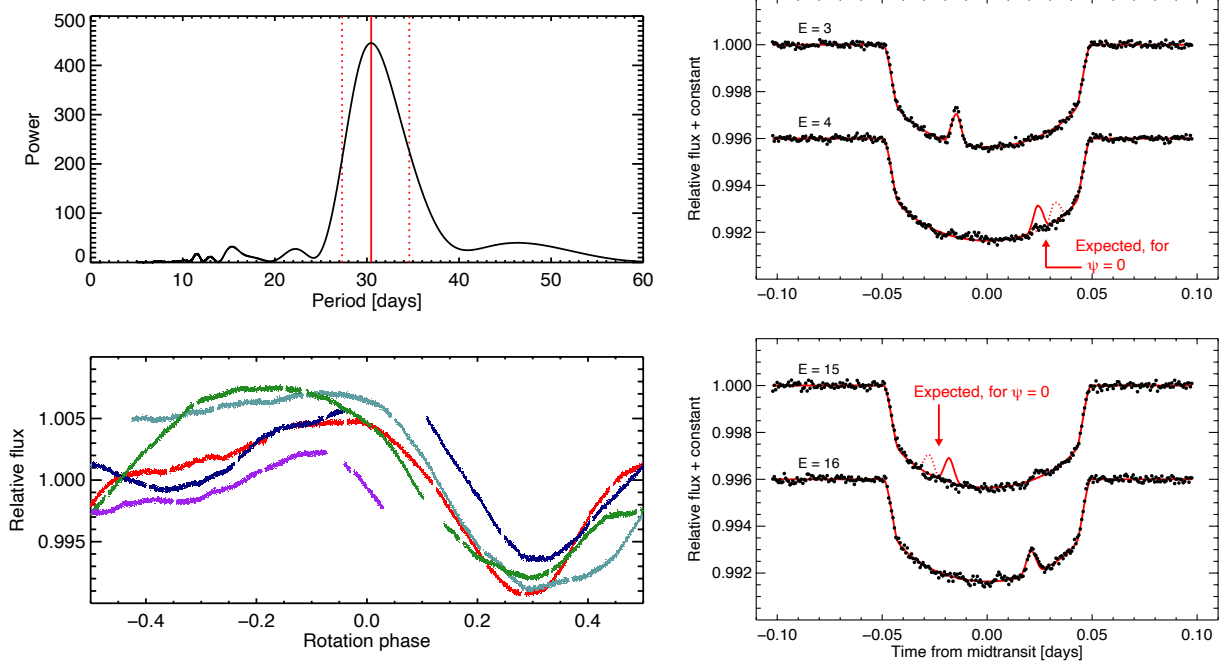


Figure 18. QPVs and spots crossing transits. From Sanchis-Ojeda & Winn (2011). *Upper left:* Lomb-Scargle periodogram of *Kepler* photometry of HAT-P-11, indicating a rotation period of $30.5^{+3.1}_{-3.2}$ days. *Lower left:* Phase-folded light curve, illustrating the quasi-periodic variability. *Upper right:* Light curves of two consecutive transits. Given the orbital and rotation periods, the starspot-crossing anomaly seen in the first transit should have appeared in the second transit (red line), if the star had a low obliquity. *Lower right:* A different pair of transits illustrating the same effect.

planets most of the time (see, e.g., Zhu et al. 2018; Mill-holland et al. 2021).

3.5. Starspots

3.5.1. Quasi-Periodic Variation

Any inhomogeneities on a star’s photosphere (which we will call spots, for simplicity) will lead to variations in the star’s observed brightness with a period equal to the star’s rotation period and its harmonics. These variations are quasi-periodic, rather than strictly periodic, because of the evolution of spot properties with time as well as differential rotation. As described in the preceding section, observing the quasi-periodic variation (QPV) can be used to measure the rotation period, which can be combined with R and $v \sin i$ to measure or constrain the stellar inclination.

The QPV amplitude, by itself, also bears some information about inclination. Sun-like stars tend to have spots appear near the equator. For such stars, all other things being equal, the observed QPV amplitude is maximized at high inclination. This is because in the high-inclination configuration, the spots appear and disappear completely from view. At low inclination, the spots are limb-darkened and circulate around the stellar disk, leading to weaker photometric variability. (The QPVs of

stars with polar or nearly-polar spots, such as young and rapidly rotating stars, might show the opposite trend.)

The amplitude of the QPVs also depends on the spot pattern, which varies with time and from star to star. Mazeh et al. (2015b) dealt with this complication by averaging the QPV amplitudes of large numbers of stars drawn from the *Kepler* survey. When considering stars cooler than the Sun, they found the average QPV amplitude of stars without transiting planets (“control stars”) to be about 0.8 times that of stars with transiting planets. This is consistent with a picture in which the QPV amplitude is proportional to $\sin i$, the transit hosts have low obliquities ($\sin i = 1$), and the control stars are randomly oriented ($\langle \sin i \rangle \approx 0.8$). Thus, this study supported the idea that the cool Kepler stars tend to have low obliquities.

For stars between 5800 and 6100 K, Mazeh et al. (2015b) found the transit hosts and the control stars to have similar QPV amplitudes. This suggests that the pattern found earlier for stars with close-orbiting giant planets — hotter stars have a broader obliquity distribution — is also shared by stars with smaller Kepler-type planets. The transition temperature of 6000 K in the QPV study appears to be a few hundred degrees lower than that of the RM studies (§ 3.1.5), although it is difficult to compare them directly.

For stars hotter than 6100K, Mazeh et al. (2015b) found the control stars to have *higher* QPV amplitudes than the planet hosts, with an amplitude ratio of about 1.6. This inverted ratio was surprising. Interpreted purely in terms of geometry, and assuming that the latitudinal distribution of starspots of hot stars is similar to that of cool stars (which might be incorrect), the results imply that stars tend to rotate perpendicular to the planetary orbits. At least part of the reason for the inverted ratio is a selection effect: Transiting planets are easier to detect when the QPV amplitude is low. However, Mazeh et al. (2015b) argued that this bias is not likely to be responsible for the entire observed effect. There is also relatively new evidence for a tendency toward perpendicularity based on individual obliquity measurements (§ 3.7). It will be interesting to probe further with these two techniques and understand the relationship (if any) between the results.

3.5.2. Starspot-tracking method

If a transiting planet moves in front of a starspot, the light curve shows a glitch. During such a spot-crossing event, the portion of the star blocked by the planet is not as bright as the surrounding photosphere, thereby reducing the usual loss of light. When the spots are dark and localized, the glitches take the form of brief and partial rebrightenings, as observed for HAT-P-11 (Sanchis-Ojeda et al. 2011, see Figure 18). When the photosphere is mottled with a more complex pattern, the light curve becomes jagged, as observed for Kepler-17 (Désert et al. 2011).

A sequence of transit observations of a star with long-lived spots can sometimes reveal the obliquity, or at least reveal whether the obliquity is lower than about 10° . When the obliquity is lower than about 10° , the transiting planet’s trajectory is aligned well enough with the trajectories of spots as they move across the stellar disk to allow for recurrences of spot-crossing events at predictable times. When the obliquity is high, recurrences require a special coincidence and are rarer. This type of logic was used to argue that HAT-P-11, Kepler-63, and WASP-107 have high obliquities (Sanchis-Ojeda et al. 2011, 2013; Dai & Winn 2017), and in all three cases the misalignments were confirmed via the RM effect (Winn et al. 2010b; Sanchis-Ojeda et al. 2013; Rubenzahl et al. 2021). The analysis of starspot crossings was also the technique used in the first obliquity measurement for a star with multiple transiting planets (Kepler-30; Sanchis-Ojeda et al. 2012). Many other stars have been shown to have low obliquities through this technique, including 10 hot-Jupiter systems analyzed by Dai

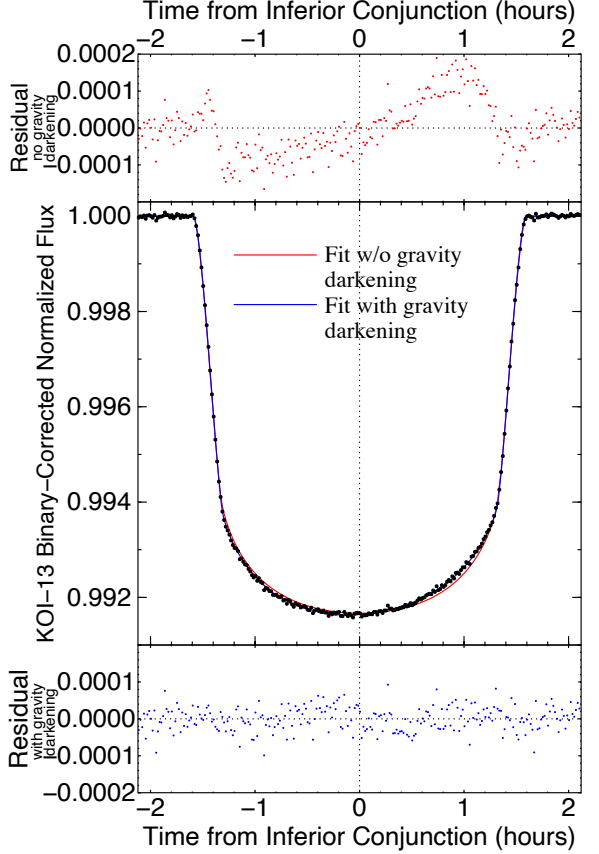


Figure 19. Gravity darkened transit light curve. From Barnes et al. (2011). *Middle:* Phase folded transit light curve of the fast rotating A type star in the Kepler-13 system. *Top:* Residuals relative to a light curve model without the effects of gravity darkening. *Bottom:* Residuals relative to light curve model including the effects of gravity darkening and a non zero misalignment.

et al. (2018b) using a statistical test for correlations between the residuals of a sequence of transit light curves.

Even when spot-crossing events cannot be well resolved, it is sometimes possible to tell whether a star is rotating in a prograde or retrograde direction. Suppose there is a spot on the approaching side of the star, at a latitude that coincides with the trajectory of a transiting planet. The stellar flux will be observed to decrease slowly as the spot rotates toward the meridian. A transiting planet on a prograde orbit would encounter the spot in the first half of the transit. If, instead, the planet’s orbit is retrograde, then the spot-crossing anomaly would occur during the second half of the transit. Therefore, one can distinguish prograde from retrograde orbits by comparing the overall asymmetry of the transit light curve and the trend in the stellar flux outside the transit. Complications arise when the star has multiple spots. Nevertheless, a few systems have been

shown to have prograde orbits in this fashion (Nutzman et al. 2011; Mazeh et al. 2015b; Holczer et al. 2015).

3.6. Gravity darkening, fast rotators

Another reason for intensity variations across the disk of a star is gravity darkening. The equatorial zone of a rapidly rotating star is centrifugally lifted to higher elevation, causing it to become cooler and darker than the polar regions. This pattern is superimposed onto the usual center-to-limb intensity variation due to limb darkening. Under standard assumptions, the local effective temperature of the photosphere obeys the von Ziepel theorem (see, e.g., Barnes 2009, and references therein)

$$T_{\text{eff}} \propto g^{\beta}, \quad (20)$$

where g is the local acceleration due to gravity, and $\beta = 0.25$ for bolometric observations of radiative stars. The exponent varies with the stellar spectral type and the observing bandpass.

The rotationally-induced intensity variations are manifested as slight perturbations of the transit light curve. For the aligned and anti-aligned cases ($\lambda \approx 0^\circ$ or 180°), the transit light curve retains its usual symmetry about the midpoint, making it difficult to use gravity darkening to constrain the obliquity. Intermediate values of λ give rise to transit asymmetries that are easier to isolate and interpret (Barnes 2009).

The first observation of this effect for an exoplanet system was for an A type star, Kepler-13 (Barnes et al. 2011; Szabó et al. 2011). See Figure 19. The light-curve anomalies in that case were on the order of 0.01% and indicated an obliquity of $\approx 60^\circ$. Other observations with this technique include HAT-P-7 (Masuda 2015), KOI 368 (Ahlers et al. 2014) as well as a less secure detection in KOI 2138 (Barnes et al. 2015).⁸ Gravity darkening has also been used to determine obliquities in a few TESS systems (Ahlers et al. 2020a,b).

Gravity darkening is of particular interest because the transit light curve depends on both λ and i , offering the possibility of determining the 3-d obliquity from the light curve (Masuda 2015; Zhou et al. 2019a; Ahlers et al. 2020b). Even when the data are not precise enough for an unambiguous determination of both λ and i , the combination of information from gravity darkening and the RM effect can provide good constraints on the 3-d obliquity, which can lead to additional insights, as discussed below.

3.7. A Preponderance of Perpendicular Planets?

⁸ Misalignment had been reported for KOI-89 (Ahlers et al. 2015), but this result was contested by Masuda & Tamayo (2020).

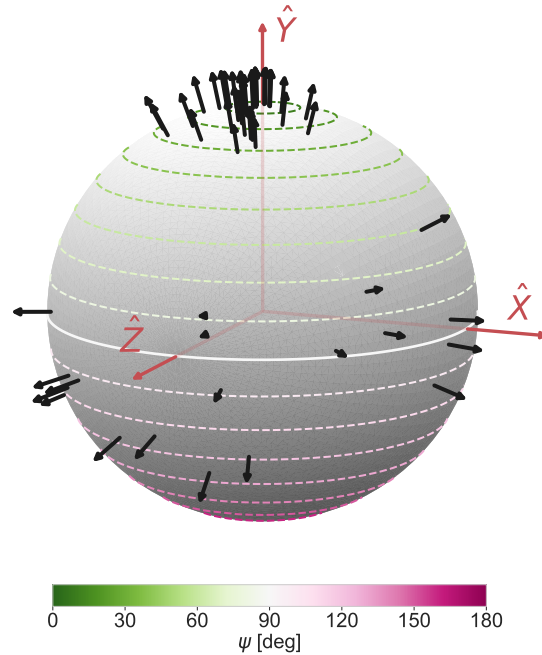


Figure 20. Obliquity distribution in 3-d. From Albrecht et al. (2021). Stellar spin axes in the 57 systems analyzed by Albrecht et al. (2021) are represented by arrows. Here the z -axis points along the line of sight, and the y -axis points along the orbital axis. For plotting purposes i and i_o were chosen to be $\leq 90^\circ$ and the signed value of λ from the literature was adopted.

There is a growing number of stars for which both λ and i have been determined, most often through the combination of RM and $v \sin i$ methods. Albrecht et al. (2021) analyzed 57 such cases and found a surprising feature in the resulting distribution of ψ , the 3-d obliquity. Even though the results for λ span the full range from 0° to 180° , the range of ψ appears to be limited to a maximum of about 120° , with apparent preferences for values near 0° and 100° (Figure 20). There were 38 well-aligned stars, most of which are consistent with zero obliquity, and 19 misaligned stars, of which 18 have values of ψ between 80° and 125° . The sole exception was Kepler-13, with $\psi \approx 60^\circ$. Notably, the planets with nearly polar orbits have a wide range of masses (0.1 to 3 Jupiter masses; see also Fig. 9), orbital separations (a/R from 3 to 30), and stellar effective temperatures (3000 to 8000 K).

It will be interesting to see if this pattern becomes more statistically significant after collecting additional data. If so, the pattern would seem to be an important clue about the processes sculpting the obliquity distribution. Since the study by Albrecht et al. (2021), at least two additional ψ measurements of mis-

aligned systems have been published: MASCARA-1 b ($\psi = 72.1 \pm 2.5$ deg) by Hooton et al. (2022), and GJ 3470 b ($\psi = 97^{+16}_{-11}$ deg) by Stefansson et al. (2022).

Looking further ahead, highly precise light curves from TESS, CHEOPS (Benz et al. 2021), and eventually PLATO may provide additional opportunities to measure 3-d obliquities using the gravity darkening method. PLATO may also enable additional asteroseismic inclination measurements to complement λ measurements (§ 3.2).

3.8. Interlude: Planetary obliquities

Although this article is about stellar obliquities, there have been some interesting developments regarding *planetary* obliquities. Some of the proposed techniques for exoplanet obliquity measurements are related to the techniques developed for stars.

The planets of the Solar System show a wide range of obliquities. Earth's obliquity is famously 23.5 deg, Venus rotates very slowly in the retrograde direction, and Uranus is tipped over on its side. The root-mean-squared obliquity of the other five planets is 20.7 deg. The planetary obliquities are not considered to be primordial Laskar & Robutel (1993); instead, planetary obliquities are thought to have been influenced by a variety of processes. Collisions can lead to large obliquities (Dones & Tremaine 1993; Li & Lai 2020), as can earlier interactions with the protoplanetary or external perturbers (Tremaine 1991; Jennings & Chiang 2021). Nonzero planetary obliquities in exoplanet systems might also lead to important tidal effects (Heller et al. 2011; Millholland & Laughlin 2018, 2019; Su & Lai 2022; see also Winn & Holman 2005 and Fabrycky et al. 2007). A planet's obliquity evolution can be coupled to the properties of its moons, if it has any (Atobe & Ida 2007). Moons can stabilize the planet's spin-axis orientation, as appears to be the case for the Earth (Laskar et al. 1993). Moons can also drive large obliquity variations (Saillenfest et al. 2021). Finally, planetary obliquities have been discussed as possible factors in the habitability of planets (Deitrick et al. 2018).

An early idea for measuring planetary obliquities was based on the slight difference between the transit light curve of a spherical planet and an oblate planet with the same cross-sectional area (Seager & Hui 2002; Barnes & Fortney 2003), which was used by Carter & Winn (2010a) to set joint upper limits on the oblateness and obliquity of HD 189733 b. Soon after, Carter & Winn (2010b) proposed a related detection method based on the transit depth variations induced by the spin precession of an oblique planet, which was put into practice

by (Biersteker & Schlichting 2017, although without any secure detections).

More recently, with the advent of high-resolution spectroscopy of directly imaged planets, it became possible to use the $v \sin i$ method (§ 3.4) to constrain planetary obliquities. The broadening of the planet's spectral lines is used to measure $v \sin i$, the planet's photometric variations reveal the rotation period, and the planet's radius is estimated from its spectrum and thermal evolution models. Using this technique, Bryan et al. (2020, 2021) found evidence for large obliquities of two different planets, a major step forward. With current and forthcoming high-resolution infrared spectrographs, it may be possible to apply this method to a larger sample (Snellen et al. 2014).

Further in the future, it may become possible to detect moons around directly imaged planets. Spectroscopic observations of the transit of a moon would allow the planet's obliquity to be constrained via the RM effect (Heller & Albrecht 2014).

4. PROCESSES THAT INFLUENCE OBLIQUITIES

In this section, we review the physical mechanisms that might be responsible for establishing and altering a star's obliquity. We compare the predictions of some specific models with the available data. We also suggest future measurements that would help to clarify which mechanisms are operative, both for individual systems and in general.

We treat separately the subjects of obliquity *excitation* and *damping*. There are observational clues for obliquity damping due to tidal dissipation in systems with low-mass stars and hot Jupiters (§ 4.1). In contrast, the observations do not appear to single out any particular mechanism for obliquity excitation. A similar situation occurs in the interpretation of orbital eccentricities: It is widely accepted that tidal circularization occurs for at least some hot Jupiters, while the mechanisms for eccentricity excitation of giant planets are still debated. The proposed mechanisms for obliquity excitation fall into three groups: primordial misalignment, i.e., occurring before the formation of the planet (§ 4.2), post-formation misalignment (§ 4.3), and changes in the stellar spin vector that are not associated with planet formation (§ 4.4). The predicted obliquity trends for the different categories of processes are summarized in Table 3 and Figure 21 is a graphical summary of this categorization.

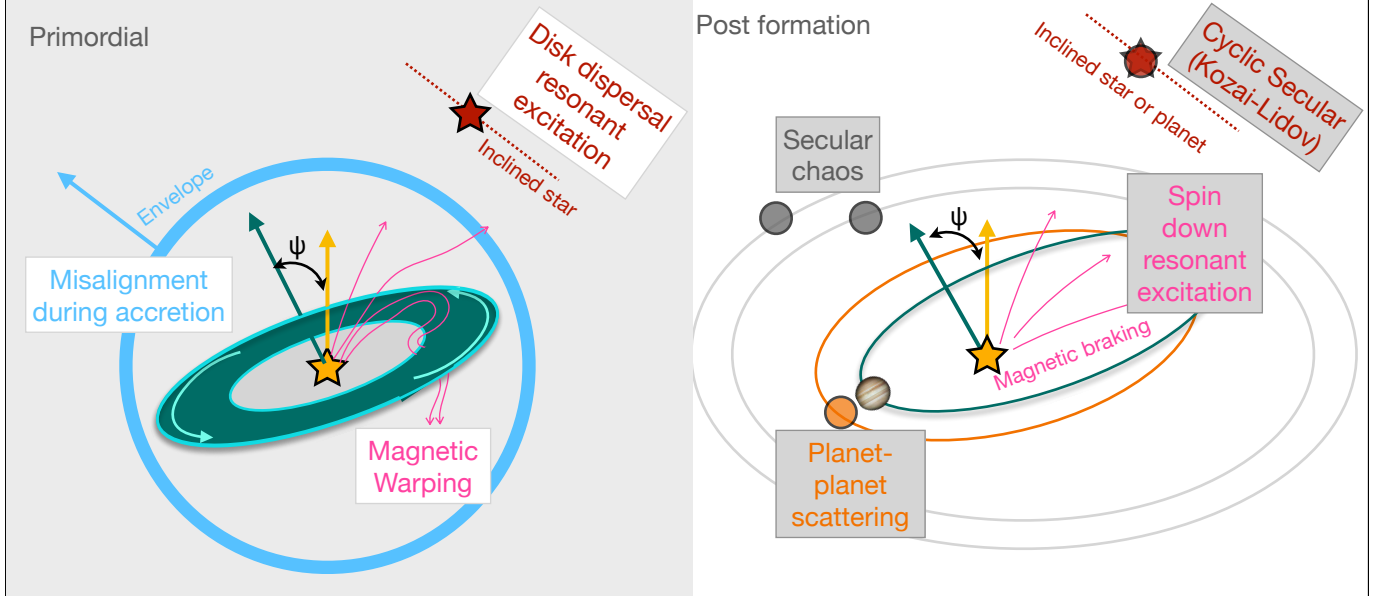


Figure 21. Processes that create spin-orbit misalignments before (left) or after (right) planet formation.

4.1. Tidal realignment

Tidal dissipation in any binary system typically tends to circularize the orbit, align the rotational and orbital axes, and synchronize the rotational and orbital periods.⁹ It is straightforward to demonstrate these facts based on simple considerations of energy and angular momentum (see, e.g., Hut 1980), but it is much more difficult to model the specific processes by which angular momentum is exchanged and energy is dissipated. For reviews of tidal phenomena in binary-star and exoplanet systems, we refer the reader to Zahn (2008), Mazeh (2008), and Ogilvie (2014).

Obliquity damping — if it occurs — must happen after obliquity excitation. Nevertheless, we discuss obliquity damping first, because the interpretation of the data seems clearer and because obliquity damping must be kept in mind when evaluating the evidence for obliquity excitation mechanisms. We summarize here the evidence for tidal obliquity damping:

1. The narrowing of the obliquity distribution of hot Jupiter hosts as the effective temperature becomes lower than about 6250 K (§ 3.1.5). The transi-

⁹ For binary systems in general, tidal interactions can temporarily excite instead of damp eccentricities and inclinations, depending on the starting ratio between rotational & orbital angular momenta, the rotational and orbit frequencies, and the orbital eccentricity. However, the eccentricity and obliquity are damped for typical parameters of exoplanet host stars with close-in planets. Many observed short period planets have insufficient angular momentum to synchronize their stars (Section 4.1.1). See Hut (1981); Barker & Ogilvie (2009); Ogilvie (2014).

tion temperature appears to be coincident with the “Kraft break,” below which cool stars have deep convective envelopes and undergo magnetic braking. The different internal structure and slower rotation of cooler stars may hasten the effects of tidal dissipation.

2. The exceptions to the preceding statement — cool stars with misaligned planets — are generally the systems with lower planet masses and wider orbital separations than the others (§ 3.1.6 and § 3.1.7). Tidal dissipation is expected to be weaker in such cases; thus, the exceptions seem to prove the rule.
3. The most precise measurements of λ involving low-mass stars with hot Jupiters are consistent with zero within about a degree (§ 3.1.8), which is smaller than the Sun’s obliquity and smaller than the typical mutual inclinations of the known multi-planet systems.
4. Low-mass stars with hot Jupiters tend to rotate more rapidly than similar stars without hot Jupiters (Brown 2014; Poppenhaeger & Wolk 2014; Maxted et al. 2015; Tejada Arevalo et al. 2021). This is evidence that hot Jupiters tidally affect the spin rates of their host stars, which in turn suggests that hot Jupiters can also tidally affect the stars’ obliquities.

Although this evidence points toward tidal dissipation in general, the issue of tidal dissipation has raised interesting theoretical questions related to which types of

Predicted Obliquity Trends								
Category	Scenario	Low mass planets	Multis	Low mass stars (M dwarfs)	Young stars (10-100 Myr)	Long period planets	Obliquity distribution	Non-exoplanet systems
Tidal interactions (Section 4.1)	Realignment with orbital angular momentum to spare	Low mass planets are more likely to be misaligned than high mass planets	Wide separation companions may be misaligned with inner planet Uncertain Uncertain. Depends on presence of decoupled outer layer.	Low mass stars are likely to be aligned	Young stars are more likely to be misaligned	Long period planets are more likely to be misaligned Realignment is faster than ~100 Myr, for short orbital periods Massive planets are more likely to be prograde	Realignment is possible even for polar/retrograde planets Produces pile-ups of stars with 90° and 180° obliquities	Binary stars realign at wider separations than planet hosts; otherwise, similar trends as planets
	Realignment through inertial wave tidal dissipation	Low mass planets are more likely to be misaligned than high mass planets, but the mass boundary is uncertain		Uncertain	Realignment is faster than ~100 Myr, for short orbital periods			
	Skin deep realignment							
Primordial misalignment (Section 4.2)	Chaotic accretion	No predicted dependence on planet mass	Star is misaligned with respect to multiple coplanar planets. Star is misaligned with respect to multiple coplanar planets, unless the innermost planet is strongly coupled to the star	No strong dependence on stellar mass Unknown: parameters probably depend on stellar mass Unclear: depends on ratio of stellar radius to disk size	Young and old stars have similar obliquity distributions	No predicted dependence on orbital period Long period planets are more likely to be misaligned	Misalignments are smaller than 20° Prograde misalignments; retrograde only if suitable companion exists Depends on details	Debris and protoplanetary disks are often misaligned
	Magnetic warping							
	Protoplanetary disk is tilted during resonance crossing by wide-orbiting, highly-inclined planet or star							
Post formation misalignment (Section 4.3)	Planet-planet scattering	Low-mass planets are rarely misaligned by more than 45°	Stars with compact coplanar multis have low obliquities Suitable companion must exist. Compact multis may be misaligned if decoupled from star. Suitable companion must exist	No strong dependence on stellar mass Late-arriving hot Jupiters are misaligned Young stars are typically aligned, depending on timing of resonance and magnetic braking	Late-arriving hot Jupiters are misaligned Properties of suitable companion depend on orbital period	No predicted dependence on orbital period Depends on details N/A	Mostly prograde planets	N/A
	Secular cycles	Low mass planets are slightly easier to misalign than high mass planets					Triple stars have a similar obliquity distribution to planet hosts	
	Secular chaos						N/A	
	Secular resonance	Properties of suitable companion depend on planet mass	Low mass stars are more likely to be misaligned	Young and old stars have similar obliquity distributions	Long period planets are less likely to be misaligned	Can be arranged to produce polar planets	Tight binaries in triples have a broad obliquity distribution	
	Dispersing gas disk	Low mass planets are easier to misalign						
Internal gravity waves (Section 4.4)		Obliquity distribution is independent of planet properties	Low mass stars are aligned	Young and old stars have similar obliquity distributions	Obliquity distribution is independent of planet properties	Uncertain	Binary stars with hot components are often misaligned	

Table 3. This table summarizes what might be observed in different populations of systems if any or some of the various proposed processes are shaping spin-orbit angles of exoplanet host stars.

tidal oscillations are relevant, and how long it takes for obliquity damping to occur. Before getting to these details, though, we present below a simplified tidal model that is consistent with the patterns seen in the data.

4.1.1. Simplified tidal friction model

In the theory of the *equilibrium tide*, fluid elements of the star closer to the planet feel a stronger gravitational force than those farther away, stretching the star into a slightly ellipsoidal shape. The near and far ends of the ellipsoid are the “tidal bulges.” Unless the planet’s orbit is aligned and synchronized with the star’s spin, the tidal bulges are not stationary in the rotating frame of the star. If the response of the stellar fluid is delayed by viscosity, the tidal bulges point toward a previous position of the planet instead of the instantaneous position. This offset leads to a torque on the star that transfers angular momentum and also a steady loss of energy from the system. When the orbital period P_{orb} is shorter than the star’s rotation period P_{rot} , the planet drags the bulges in the prograde direction, spinning up the star. Conversely, when $P_{\text{orb}} > P_{\text{rot}}$, the planet drags the bulges in the retrograde direction, slowing down the star’s rotation. When there is a spin-orbit misalignment, the tidal bulges oscillate in latitude in addition to being dragged around the star’s circumference.

Stars also experience *dynamical tides*. The star can be modeled as a fluid oscillator that is being driven by the planet’s periodic tidal perturbations. The oscillations take different forms, depending on the characteristics of the perturbations and the structure of the star. For example, in the radiative zone of a star, tidal perturbations can generate gravity waves (in which the restoring force is gravity), and in the convective zone, tidal perturbations that can generate inertial waves (in which the restoring force is the Coriolis force) that reflect off the radiative core. Any dissipation of the energy associated with the star’s oscillations ultimately comes at the expense of the kinetic and potential energy associated with orbital motion and rotation.

Figure 22 shows the measurements of λ as a function of an approximate tidal scaling factor $(m/M)^{-2}(a/R_*)^6$ taken from the equilibrium-tide theory of (Zahn 1977). For cool host stars, the systems with the lowest values of the tidal scaling factor tend to have low obliquities. The systems with larger values of the tidal scaling factor show a much broader range of obliquities, while also including a concentration of well-aligned systems. Less of a trend is seen for the hotter host stars, and no trend is seen for stars with $T_{\text{eff}} > 7000$ K. Overall, the data appear consistent with the hypothesis of tidal damping. This type of argument was first made by Albrecht et al.

(2012b), and the trend still holds true after the sample has more than tripled in size.

Despite the agreement between the data and the simple scaling relation drawn from equilibrium-tide theory, we must acknowledge that dissipation of the equilibrium tide is not a realistic model for obliquity damping in star-planet systems. In that theory, the timescales for realignment and orbital decay should be comparable, and therefore, there is only a fleeting time interval when the star has been realigned and the planet still exists. The orbit decays because a short-period planet (even a giant planet) generally does not have enough orbital angular momentum to synchronize the star and thereby halt the dissipation. Tidal dissipation ultimately causes the planet to transfer all its angular momentum to the star and become engulfed or tidally disrupted. Observing hot Jupiters around cool stars that have been tidally realigned is most likely when the realignment timescale is much shorter than the orbital decay timescale. In the context of the equilibrium-tide theory, this condition, in turn, implies that the angular momentum ratio $\frac{L_{\text{orb}}}{L_*}$ should be much smaller than one. However, the actual ratios are on the order of unity:

$$\begin{aligned} \frac{L_{\text{orb}}}{L_*} &= \frac{ma^2(2\pi/P_{\text{orb}})}{k_*MR^2(2\pi/P_{\text{rot}})} \\ &\sim 2.5 \left(\frac{0.1}{k_*}\right) \left(\frac{m/M}{0.001}\right) \left(\frac{a/R}{5}\right)^2 \left(\frac{P_{\text{rot}}/P_{\text{orb}}}{10}\right). \end{aligned} \quad (21)$$

4.1.2. More realistic tidal models

Many possible answers have been offered to the question of how to tidally damp a star’s obliquity without destroying the planet, and how to account for the difference in the obliquity distributions of hot and cool stars.

- **Planets with orbital angular momentum to spare:** For systems with unusually massive planets, wide orbits, or slowly rotating stars, the ratio $\frac{L_{\text{orb}}}{L_*}$ can exceed 10, and the realignment timescale becomes shorter than the orbital decay timescale (see, e.g., Hansen 2012; Valsecchi & Rasio 2014). These planets may be able to realign their stars without undergoing much orbital decay over the star’s lifetime.

- **Inertial wave dissipation:** Tidal perturbations can launch inertial waves within the convective zone of a cool star. As noted above, the restoring force is the Coriolis force. Their dispersion relation is: $\omega = 2\vec{k} \cdot \vec{\Omega}_*$, where ω is the angular frequency, \vec{k} is the direction of the wavevector and phase velocity, and $\vec{\Omega}_* \equiv 2\pi/P_{\text{rot}}$. Thus, inertial waves always

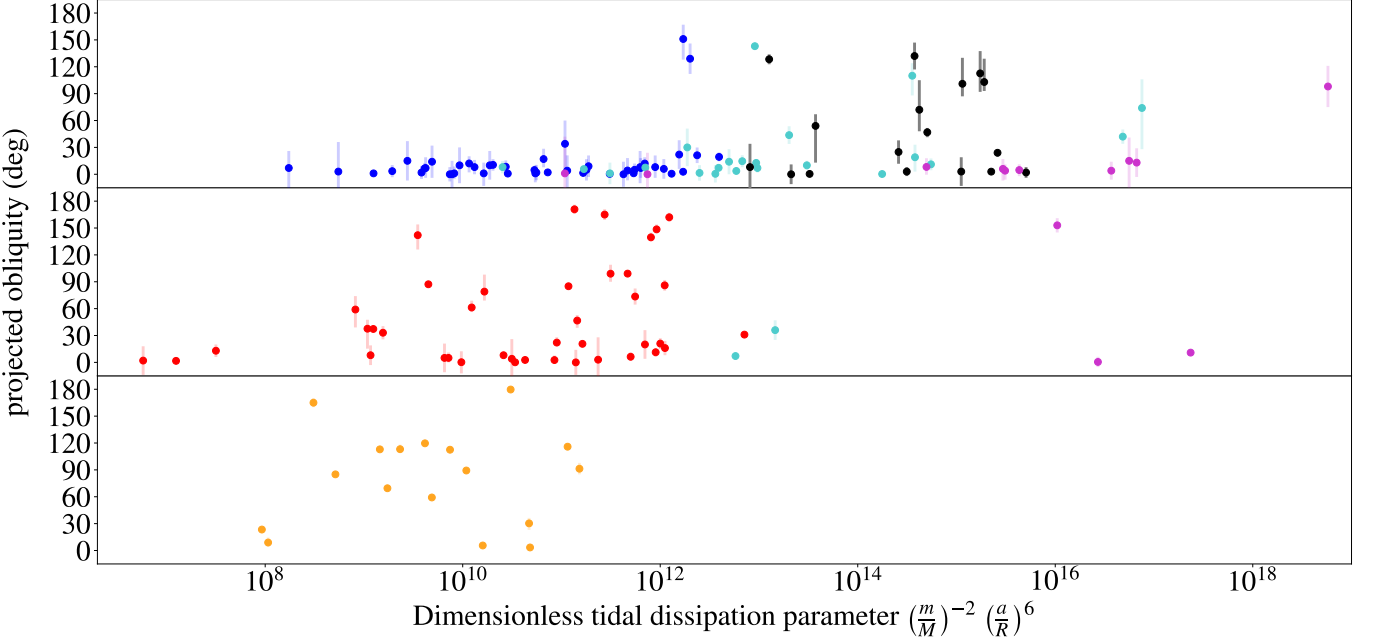


Figure 22. Projected obliquities of exoplanet systems as a function of expected tidal dissipation timescale. Plotted on the x -axis is a dimensionless parameter $(m/M)^{-2}(a/R)^6$ that appears in a simple theory for tidal dissipation. For cool host stars, the systems with the shortest expected tidal dissipation timescales tend to have low projected obliquities. For hotter hosts, any such a trend is less obvious or absent.

have frequencies lower than $2\Omega_*$, and cannot be excited by perturbations with higher frequencies. For a short-period planet, most of the components of the tidal perturbation are too fast to excite inertial waves — but when the star is misaligned, there is a component that oscillates at the frequency Ω_* . This component affects the spin direction, but not the orbital distance (see, e.g., Lai 2012; Lin & Ogilvie 2017; Damiani & Mathis 2018). By itself, inertial wave tidal dissipation would drive the star toward one of three equilibrium orientations: $\psi = 0, 90$, or 180° . The destination depends on the initial condition, the ratio of orbital to spin angular momentum (smaller ratios lead to more $\psi = 90^\circ$ planets), and the ratio between the rates of inertial-wave tidal dissipation and equilibrium tidal dissipation (larger ratios lead to more $\psi = 90^\circ$ planets). For more details, see Xue et al. (2014) and Li & Winn (2016). For an attempt to use this theory to constrain the timing of hot Jupiter formation, see Spalding & Winn (2022).

- **Steeply frequency-dependent tidal dissipation:** The tidal dissipation rate is likely to depend strongly on the forcing period. If the rate of tidal dissipation drops sharply with decreasing period, then a hot Jupiter can realign the star while its orbit decays by a moderate amount, before tidal

evolution slows to a crawl as its orbital period decreases. There is some empirical evidence for such a sharp frequency dependence, based on the observed degree of tidal spin-up as a function of the system parameters (Penev et al. 2018; Anderson et al. 2021). Although resonance locking to a tidally excited stellar gravity mode can generate such a frequency dependence, but the waves break at the core, preventing effective dissipation (Barker & Ogilvie 2010). Thus, it is thought to only operate for very massive stars with convective cores or for Neptune-mass and lower-mass planets around Sun-like stars (Ma & Fuller 2021). In this scenario, the differences in the obliquity distributions of hot and cool stars might arise because hot stars have a lower tidal dissipation efficiency, a different frequency dependence, or both.

- **Realignment is only skin deep:** The planet might realign only the outer convective zone of the star, if this outer zone could somehow remain decoupled from the interior (e.g., Dobbs-Dixon et al. 2004; Winn et al. 2010a). This would lower the amount of orbital angular momentum required for realignment. Stars lacking an outer convective zone would, naturally, remain misaligned. Moderately hot stars could also remain misaligned because they rotate quickly (due to a lack of mag-

netic braking; Dawson 2014), because their convective outer layers couple strongly to the interior, or because they have less efficient tidal dissipation.

Cébron et al. (2013) proposed that, rather than damping the obliquity of cool stars, tides could excite the obliquities of hot stars. However, later global simulations found that the mechanism would tend to damp obliquities (Barker 2016) and that obliquity excitation would require tides to generate rather than dissipate energy (Ogilvie 2014).

Figure 23 shows the results of a toy population-synthesis model, which is described in detail in Appendix A. The first column shows the observed distributions of λ , T_{eff} , and $v \sin i$ for stars having planets with $a/R < 10$ and $m > 0.5M_{\text{Jup}}$.¹⁰ The second column shows a hypothetical initial distribution of stellar properties, before any tidal effects. The next four columns show the final distributions according to four of the proposed solutions to the realignment problem described above.

In the equilibrium-tide theory (third column), the most massive planets manage to realign their stars, but lower-mass hot Jupiters remain misaligned even around cool stars, contradicting the data.

With inertial waves excited by dynamical tides (fourth column), cool stars are realigned. However, some simulated systems end up stalled at $\psi = 180^\circ$, even though the effects of equilibrium tides are also being taken into account (Xue et al. 2014; Li & Winn 2016). We have not observed a population of anti-aligned stars, neither in exoplanet systems nor binary stars. We think it would be difficult to resolve the disagreement by altering the initial obliquity distribution; even stars that start with obliquities near 90° can evolve to 180° by the end of the simulation.

Theories in which tidal dissipation declines sharply with frequency (fifth column) and in which tidal realignment is only skin deep (sixth column) successfully reproduce the observed broadening of the obliquity distribution at the Kraft break. However, these models are *ad hoc*. Further work needs to be done to try connecting them to more physically grounded theories of stellar oscillations. In particular, skin-deep realignment would require the outer and inner zones of the star to rotate with different rates and in different directions for billions of years, which seems at odds with the observation that the Sun’s convective zone rotates at the same rate as its

radiative interior. On the other hand, the Sun does have a thin near-surface shear outer layer (starting at around $0.95 R_\odot$) which rotates at a different rate from the rest of the convective zone (see, e.g., Thompson et al. 1996).

In summary, tidal alignment appears to play an important role in shaping the obliquity distribution of stars with close-orbiting giant planets. However, there is no completely satisfactory theory that specifies the nature of the tidal perturbations and how they are damped.

4.2. Primordial misalignment

One might expect a star to be well-aligned with its protoplanetary disk, because the star and the disk both inherit their angular momentum from the same part of a collapsing molecular cloud. Furthermore, gas funnels onto the young star through the disk, a process that would help maintain good alignment. Nevertheless, three processes have been proposed to generate a “primordial misalignment”: chaotic accretion, magnetic warping, and tilting by a companion star. Figure 21 illustrates these possibilities.

Chaotic accretion refers to the fact that stars form in the dense and chaotic environment of a gravitationally collapsing and fragmenting molecular cloud. Interactions between a protostar and neighboring protostars or clumps of gas might cause the early-accreting gas to arrive from a different direction than the gas that accretes later. The late oblique infall of material might warp or tilt the disk away from the star (Bate et al. 2010; Thies et al. 2011; Fielding et al. 2015; Bate 2018; Kuffmeier et al. 2021). This possibility was studied further by Takaishi et al. (2020), who found that subsequent accretion from the disk onto the star tends to eliminate any temporary misalignments. According to this work, by the time planets form, the disk and star are probably aligned to within 20° .

Magnetic warping occurs when differential rotation between a young star and the ionized inner disk twists the magnetic field lines that link them, generating a toroidal magnetic field. The toroidal magnetic field, in turn, generates an electrical current in the inner disk. The Lorentz force on this current generates a misaligning torque that would amplify any initially small misalignment and warp the inner disk (Foucart & Lai 2011; Lai et al. 2011; see also Romanova et al. 2013, 2021, for three-dimensional magnetohydrodynamical simulations). Modest misalignments can be generated by this torque if the toroidal field is sufficiently strong and the realigning torques are sufficiently weak. Realigning torques are caused by accretion, magnetic braking, disk winds (which transport angular momentum from the star to the disk), and viscosity (which cou-

¹⁰ We decided not to show predictions for low-mass planets because the mass cut-off for alignment is very sensitive to uncertain tidal dissipation parameters.

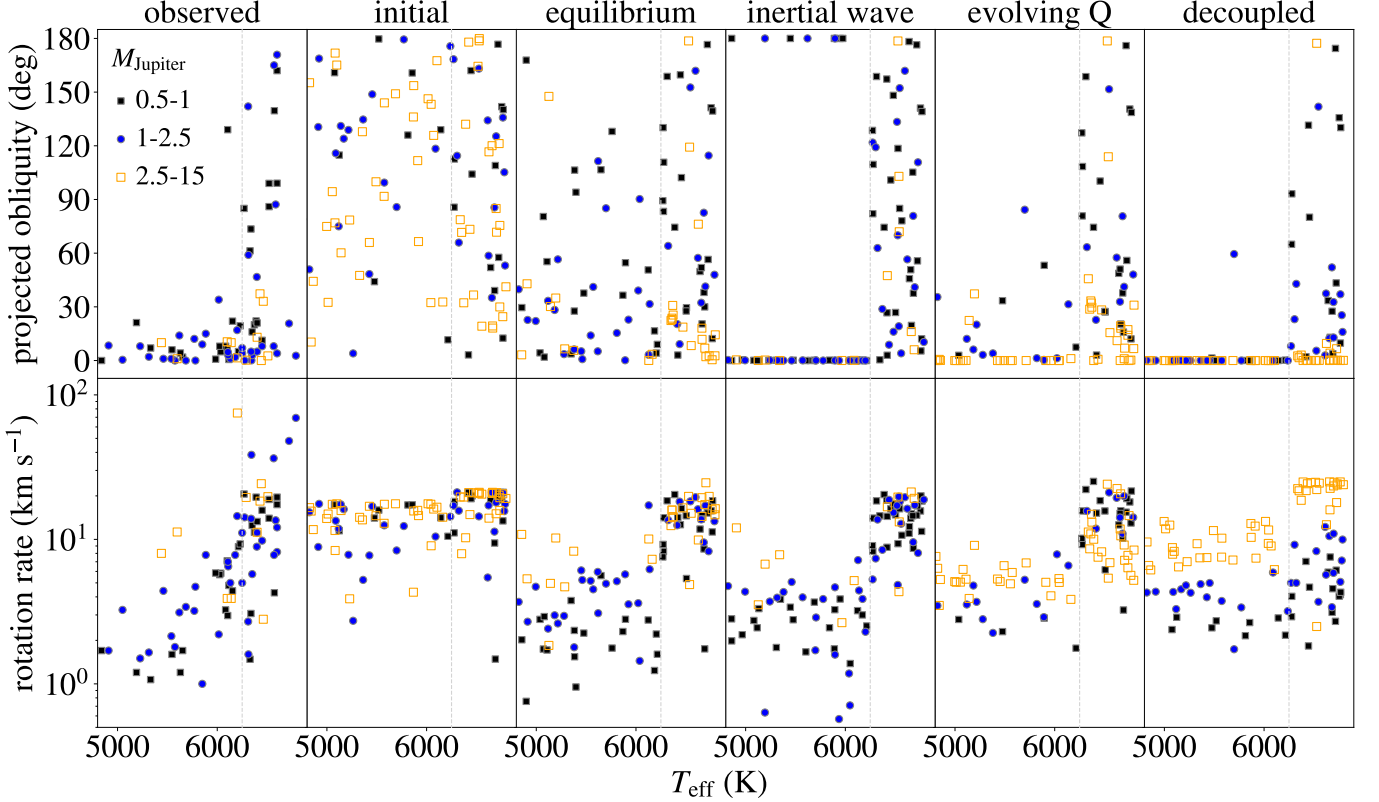


Figure 23. Results of illustrative population-synthesis models for tidal realignment. Column 1 shows real data. Column 2 shows the initial properties of the simulated distribution. Columns 3–6 show the final distributions. See the text, and Appendix, for more details.

ples the misaligned inner disk to the aligned outer disk). A realigning torque can also be created if the magnetic field becomes wrapped around the stellar rotational axis instead of around the disk axis (Romanova et al. 2021). A broad distribution of obliquities (including retrograde stars) can be achieved if the warping torques are accompanied by an external disturbance to the outer disk, perhaps generated by a stellar companion (Foucart & Lai 2011).

Inclined stellar or planetary companions can tilt disks (see, e.g., Borderies et al. 1984; Lubow & Ogilvie 2000; Batygin 2012; Matsakos & Königl 2017). Although the disk is coupled to the star through accretion, a misalignment can be generated if the system encounters a resonance between the spin precession period of the star around the disk axis, and the nodal precession period of the disk around the binary axis (Batygin & Adams 2013; Lai 2014). Such a “secular resonance crossing” might be encountered as a disk’s precession period gradually changes in response to mass loss (see, e.g. Spalding et al. 2014). However, hot Jupiters are tightly coupled by gravitational forces to the spins of their host stars. Zanazzi & Lai (2018) found that this coupling generally prevents misalignments from occurring due to

secular resonance crossings, even if the planet formed at a large orbital distance and underwent disk-driven migration after the resonance crossing. Therefore, this mechanism is unlikely to be responsible for the observed high obliquities of stars with hot Jupiters.

Among the three primordial misalignment mechanisms, magnetic warping (under certain disk conditions) remains viable as an explanation for the observed obliquity distribution. The incidence of primordial misalignments might increase with stellar mass. For example, Spalding & Batygin (2015, 2016) proposed that young stars with masses lower than about $1.2 M_{\odot}$ are able to realign their disks due to their stronger magnetic fields. However, in that case, misalignment would more strongly correlate with the initial main sequence effective temperature than with the present-day effective temperature. Because primordial misalignment occurs prior to planet formation, the observed correlations between misalignment and planet mass and orbital separation (§ 3.1.6) and 3.1.7 would need to have a different explanation, such as tidal realignment.

What about stars with other kinds of planets, besides hot Jupiters? A star that was primordially misaligned might be expected to have multiple coplanar planets

that are all misaligned with the star by the same angle. As noted in § 3.4 and § 3.5, there is indeed evidence for a broad obliquity distribution among hot stars hosting Kepler-type planets, many of which are in flat multi-planet systems. However, this is not true of cool stars, and it is hard to understand why primordial misaligning mechanisms would leave the cool stars alone. Planet-star tides are weak and probably irrelevant for almost all the Kepler systems.

Regarding individual systems, the sample of 17 compact multi-transiting systems with obliquity measurements presented in § 3.1.13 contains 14 well-aligned systems of super-Earths and mini-Neptunes. There are three misaligned systems:

- HD 3167 is a K dwarf with mass $0.88 M_{\odot}$, two transiting planets, and a third non-transiting planet orbiting in between the transiting planets (Christiansen et al. 2017). The currently available data do not show clear evidence for any wider-orbiting companion, whether planet or star. The orbit of the innermost planet is misaligned on the sky by $-97 \pm 23^{\circ}$ relative to the star (Dalal et al. 2019). The orbit of the outer transiting planet was found to be aligned with the star (Bourrier et al. 2021), implying the two planetary orbits are nearly perpendicular, an extraordinary architecture, although the evidence for this claim relies on a signal that was only barely detected. Reobservation of this remarkable system is warranted.
- Kepler-56 is a $1.3 M_{\odot}$ star with two transiting planets, and is misaligned by at least 45° with respect to both of their orbits (Huber et al. 2013). Kepler-129 is a $1.2 M_{\odot}$ star that also has two transiting planets, for which a $\approx 40^{\circ}$ misalignment was tentatively detected (Zhang et al. 2021). Both stars have wide-orbiting massive planets with properties that make them good candidates for tilting the orbital plane of the inner planets, either before or after these planets have formed (Gratia & Fabrycky 2017; Zhang et al. 2021).
- K2-290 is a $1.2 M_{\odot}$ star with two transiting planets — a warm Jupiter and an inner Neptune-sized planet — and has an obliquity of $124 \pm 6^{\circ}$ (Hjorth et al. 2019a, 2021). A stellar companion, K2-290 B (projected separation ≈ 110 au), was also detected and appears capable of tilting the protoplanetary disk but not capable of tilting the system today. This system is probably the best known candidate for a primordial misalignment, although a recent study by Best & Petrovich (2022) suggested an alternative possibility: The third known star in that

system, K2-290 C (projected separation ≈ 2500 au) might have been responsible for the misalignment.

To make further progress, it would be helpful to measure the obliquities of stars that still have protoplanetary disks. The problem is that the disks and the surrounding material often blocks the stellar photosphere. It may be relevant that misalignments have been found between the planes of the inner and outer parts of a protoplanetary disk (see, e.g., Marino et al. 2015; Sakai et al. 2019; Ginski et al. 2021; or Casassus 2016 for a review). However, the occurrence rate of such misalignments is not known. These internally misaligned or “broken” disks might form planets with large mutual inclinations, setting the starting conditions for some of the obliquity-excitation processes discussed in the next section. The obliquities of stars with resolved debris disks have been investigated, usually using the projected rotation velocity method, and have generally been found to be lower than $\approx 30^{\circ}$ (Watson et al. 2011; Greaves et al. 2014; Davies 2019).

To complete the discussion of stars and disks, we note that there are a few wide binary systems in which the two protoplanetary disks are misaligned with respect to each other and with respect to the orbital plane. These findings are based on polarization observations of disk jets (Monin et al. 2007, and references therein) and interferometric imaging of protoplanetary disks (e.g., HK Tauri, Jensen & Akeson 2014, IRS 43 Brinch et al. 2016). Misaligned circumbinary debris disks have also been found, such as the disk surrounding and eclipsing the two stars of KH 15D (Winn et al. 2004; Chiang & Murray-Clay 2004; Poon et al. 2021).

The $v \sin i$ method has been used to test for alignment in binaries with separations of several au (e.g. Weis 1974; Hale 1994; Glebocki & Stawikowski 1997; Howe & Clarke 2009). However, Justesen & Albrecht (2020) argued that the available data do not allow for strong conclusions, contradicting previous results.

4.3. Post-formation misalignment

After formation, gravitational interactions between a planet and other bodies could alter the planet’s orbital plane, leading to misalignment with the host star’s spin. These gravitational interactions might also initiate high-eccentricity tidal migration, in which a giant planet forms on a distant orbit and acquires a high orbital eccentricity, bringing it close enough to the star for tidal dissipation to shrink and circularize the orbit.¹¹

¹¹ In this case, tidal evolution can be driven by dissipation within both the star and the planet. The planetary contribution is thought to be dominant (see, e.g., Mazeh 2008).

An appealing aspect of this scenario is that it has the potential to explain three things at once: hot Jupiters, eccentric orbits, and misaligned stars (see Dawson & Johnson 2018, for a review of theories for the origins of hot Jupiters).

Since the discovery of misaligned hot Jupiters, it was hoped that stellar obliquities would provide clues about the dynamical histories of hot Jupiters. Specifically, many authors have interpreted a low obliquity as a sign that a hot Jupiter formed through disk-driven migration or *in situ* formation, and a high obliquity as an indicator of high-eccentricity migration (see, e.g., Fabrycky & Winn 2009). The picture has become more complicated, partly because of the evidence for tidal sculpting of the obliquity distribution (Section 4.1). If tides can damp obliquities, then a low obliquity cannot necessarily be counted as evidence for disk-driven migration or *in situ* formation. The initial obliquity distribution could have been very broad (Figure 21). Some of the proposed primordial theories for obliquity excitation, discussed in Section 4.2, can generate a broad initial obliquity distribution and also account for the statistical evidence for misalignments of hot stars hosting compact coplanar systems (Sections 3.4 and 3.5).

Planet-planet scattering can tilt orbits with respect to each other and the host star, on timescales as short as thousands of years. Close encounters between planets disturb their orbits, causing eccentricities and mutual inclinations to undergo random walks. Planet-planet scattering can take place shortly after the dissipation of the gas disk, when it becomes possible for large eccentricities to develop. Scattering might also occur when planets are brought together by longer-timescale chaotic evolution (see below) or the influence of a passing star (Malmberg et al. 2011).

When the planets have low masses or small orbits (i.e., when the escape velocity from the surface of the planet is less than the planet’s orbital velocity), encounters tend to lead to collisions rather than scattering. In such cases, planet-planet scattering can only produce small mutual inclinations (see, e.g., Goldreich et al. 2004). For giant planets on wide orbits — the types of planets that might become hot Jupiters — the expected distribution of mutual inclinations ranges up to about 60° and does not include retrograde systems (Chatterjee et al. 2008). This is a problem when trying to match the data. Possibly, planet-planet scattering establishes the initial conditions for subsequent secular interactions that further broaden the obliquity distribution (see, e.g., Nagasawa et al. 2008; Nagasawa & Ida 2011; Beaugé & Nesvorný 2012). In Figure 24, which compares the obliquity distributions predicted by various excitation theories, the top

purple histogram is for planet-planet scattering (taken from Beaugé & Nesvorný 2012).

A related mechanism that can produce a more isotropic distribution is the direct disturbance of a giant planet’s orbit through a hyperbolic encounter with another star. This is very improbable in general, but it might occur in a very dense cluster environment, such as the center of a globular cluster where stars are moving in random directions (Hamers & Tremaine 2017). Unfortunately, we do not yet know of any hot Jupiters in globular clusters (Gilliland et al. 2000; Masuda & Winn 2017).

Secular cyclic interactions refers to processes that allow planets and stars to gradually and periodically exchange angular momentum, over timescales of thousands of orbits or more. Eccentricities and mutual inclinations oscillate as the bodies torque each other. When the oscillations of a close binary are driven by a distant tertiary object on a highly inclined or highly eccentric orbit, these interactions are known as **Kozai-Lidov cycles** (Kozai 1962; Lidov 1962). They can be driven by either a stellar or planetary companion. Many authors have investigated Kozai-Lidov cycles as a possible route to the formation of hot Jupiters; see, e.g., Wu & Murray 2003; Fabrycky & Tremaine 2007; Naoz et al. 2011, or Naoz 2016 for a review. The period of the secular oscillations depends on the separation and mass of the perturbing companion, with typical timescales on the order of millions of years. Most calculations of secular interactions have assumed that the protoplanetary disk has already disappeared. However, mutual inclinations can also be excited through secular interactions between a planet, a protoplanetary disk, and a companion (Picogna & Marzari 2015; Lubow & Martin 2016; Franchini et al. 2020).

Secular resonant excitation of the stellar obliquity can occur if a resonance is encountered between a secular frequency and some other frequency in the system. In a triple system, as the primary star spins down due to magnetic braking, the star’s rotational precession around the planet’s orbital axis slows down, possibly leading to a resonance between the stellar spin precession frequency and the nodal precession of the inner planet’s orbital axis about the outer companion’s orbital axis. The result would be a large misalignment (Anderson & Lai 2018).

Because of the reliance on magnetic braking, we would expect this mechanism to work only for cool stars. Thus, this mechanism might struggle to explain the high obliquities of hot and rapidly rotating stars. It also has trouble producing retrograde obliquities, as illustrated in the second histogram (blue) in the top panel of Figure 24

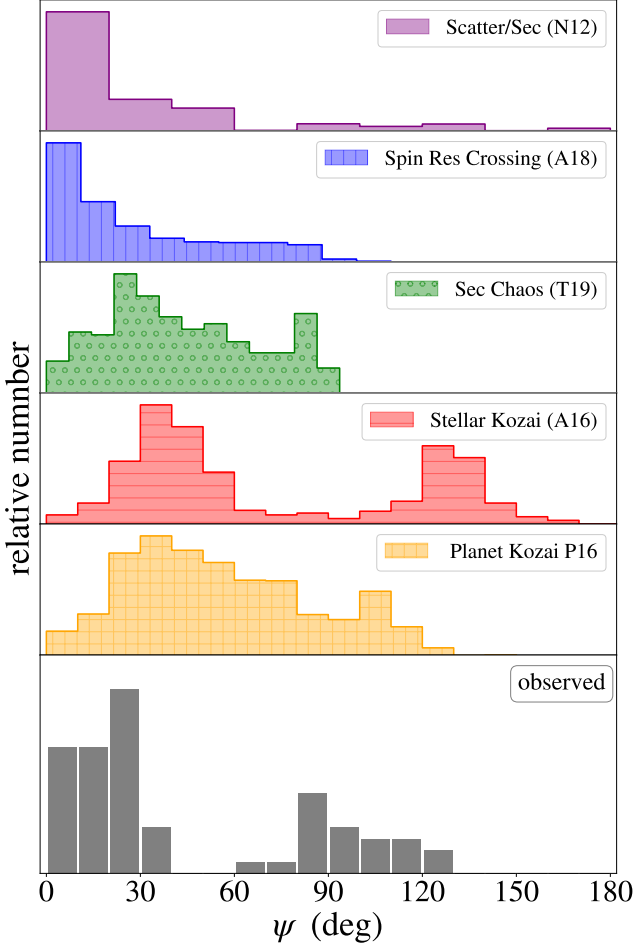


Figure 24. Population-synthesis predictions for the 3-d obliquity distributions based on different misalignment mechanisms: planet-planet scattering with secular cycles (Beaugé & Nesvorný 2012; see their Fig. 16 for hot Jupiters from systems with four planets at 3 Gyr), resonance crossing for hot Jupiters (Fig. 9 of Anderson & Lai 2018; secular chaos (Fig. 11 of Teyssandier et al. 2019), star-planet Kozai-Lidov cycles for a $1 M_{\text{Jup}}$ HJ orbiting an F star (Fig. 14 of Anderson et al. 2016), and planet-planet Kozai-Lidov cycles (Fig. 10 of Petrovich & Tremaine 2016). Bottom: Observed distribution of ψ .

when initial mutual inclinations are small. Larger initial mutual inclinations – for example, if the third body is a binary, or if other interactions tilts its plane – would produce more retrograde orbits.

In a system with an outer planetary companion and a dispersing gas disk, the outer planet's precession frequency (due to the inner planet and to the disk) might come to coincide with the inner planet's precession frequency (due to the outer planet and to the star's rotation). Such a resonance crossing is capable of generating a large mutual inclination between the inner and outer

planetary orbits. With the aid of general relativistic precession, the stellar obliquity can be driven to 90° (Petrovich et al. 2020). This mechanism is most effective for close-in Neptune-mass planets with outer Jupiter-mass companions, such as HAT-P-11.

Secular chaos refers to the stochastic growth of eccentricities and mutual inclinations due to the overlap of secular frequencies in multi-planet systems (Laskar 2008; Wu & Lithwick 2011; Hamers et al. 2017; Teyssandier et al. 2019) or multiple-star systems (Hamers 2017; Grishin et al. 2018). The growth takes place over many secular timescales, typically hundreds of millions of years or longer. The resulting obliquity distribution depends on the initial architecture. Producing planets on retrograde orbits requires initially large eccentricities and inclinations (see, e.g., Lithwick & Wu 2014), which could have been established by planet-planet scattering (Beaugé & Nesvorný 2012) or stellar flybys (see, e.g., Hao et al. 2013). Teyssandier et al. (2019) argued that secular chaos has an insurmountable problem in producing retrograde planets, as illustrated with the green histogram in Figure 24. This is because the planet's orbit tends to circularize and decouple from the companion before the obliquity grows very large.

Kozai-Lidov cycles with tidal friction tend to produce a bimodal obliquity distribution (Fabrycky & Tremaine 2007), as illustrated with the red histogram in Figure 24. The location of the peaks and the degree of bimodality depend on the properties of the star and the perturber, including the star's oblateness and spin evolution (Damiani & Lanza 2015; Petrovich 2015; Anderson et al. 2016). The spin evolution of the star can also lead to chaotic obliquity variations (Storch et al. 2014). The expected obliquity distribution can be broadened (and the fraction of retrograde obliquities can be increased) by placing the companion on an eccentric or nearby orbit (Naoz et al. 2011; Teyssandier et al. 2013; Li et al. 2014b,a; Petrovich & Tremaine 2016). Such companions might result from planet-planet scattering. The case of an eccentric or nearby planet perturber is illustrated with the yellow histogram in Figure 24. Intriguingly, there is evidence for a peak in the observed obliquity distribution near 100° (§ 3.7) which might be related to Kozai-Lidov cycles. More work needs to be done to see if theory and observations can be brought into better agreement.

For Kozai-Lidov cycles to significantly raise the mutual inclination, the orbital precession induced by the companion must be faster than precession from other sources, such as stellar oblateness, tides, and general relativity. In compact systems where planets are more tightly coupled to each other than to an exterior com-

panion, the exterior companion can misalign the entire interior system relative to the host star's equatorial plane, as observed for Kepler-56 (see, e.g., Innanen et al. 1997; Takeda et al. 2008; Kaib et al. 2011; Boué & Fabrycky 2014; Li et al. 2014c; Gratia & Fabrycky 2017). This explanation does not work for K2-290 (a system highlighted in § 4.2) because oblateness-induced precession is too fast (Hjorth et al. 2021).

In summary, none of the proposed mechanisms, by itself, seem capable of producing a broad obliquity distribution with plenty of retrograde planets. However, more complex and multistep dynamical histories, such as planet-planet scattering followed by secular cycles, are at least qualitatively consistent with the hot Jupiter data (Fig. 24). The low probability of retrograde outcomes in these models might not be a fatal problem. Although a fair fraction of hot stars have retrograde hot Jupiters, the measured 3-d obliquities are almost all below 130° (§ 3.7). In addition, a low initial fraction of retrograde systems might remove one of the objections to the idea that obliquities are damped due to inertial-wave dissipation, by reducing the probability of systems evolving into the anti-aligned state (see § 4.1).

The possible influence of tidal damping — which might play a role even for hot stars — complicates the effort to compare the theoretical and observed obliquity distributions and tease out the relative contributions of different mechanisms (see, e.g., Morton & Johnson 2011; Naoz et al. 2012). Achieving an isotropic distribution for small, compact, coplanar planets orbiting hot stars (see § 3.4) may be even more challenging; it has not yet been attempted, to our knowledge.

As noted above, the basic premise of all the theories described in this section is that a hot Jupiter forms far away from the star, undergoes interactions that raise its orbital eccentricity and inclination, undergoes high eccentricity tidal migration, and arrives in its final orbit in a misaligned state. None of the obliquity excitation mechanisms would work well after the giant planet is already in a tiny orbit. Planet-planet scattering generally fails to generate large misalignments very close to the star. Secular mechanisms would require very nearby planets to overcome the coupling between the hot Jupiter and the star, and hot Jupiters only rarely have such companions (see below).

Can post-formation misalignment scenarios be tested with stellar ages? Like the primordial misalignment mechanisms (Section 4.2), the disk-companion secular mechanism and disk dispersal mechanism predict that misaligned planets are in place as soon as the gas disk disperses. In contrast, the magnetic braking resonance crossing mechanism generally needs billions of years to

generate misaligned planets. For the mechanisms that act in concert with high-eccentricity tidal migration, the migration time (rather than the eccentricity excitation timescale) typically dominates the time to deliver a misaligned hot Jupiter. Depending on the planet's periastron distance after eccentricity excitation, the planet can achieve a short orbital period on timescales ranging from less than a Myr to several Gyr.

The current sample of obliquity measurements for young stars ($\lesssim 100$ Myr) contains only well-aligned systems (§ 3.1.10), but it is not yet possible to use this sample to rule out any of the proposed post-formation misalignment mechanisms. This is partly because the sample is small. In addition, the planets in the sample are not of the types that are commonly found to be misaligned around older stars. To derive constraints on the timing of misalignments, it would be more useful to obtain measurements for young stars with close-orbiting giant planets, which are often seen to be misaligned around older stars.

If a larger sample of young systems, including hot Jupiters, still shows very few misalignments, then the primordial misalignment scenario would be cast into doubt. Such a result would be consistent with the magnetic braking resonance crossing mechanism. It would also be consistent with the hypothesis of dual origins for hot Jupiters: a population of initially aligned orbits from disk-driven migration, along with late-arriving hot Jupiters from high-eccentricity migration. If the sample could be enlarged to include stars with accurately determined ages spanning a wide range, we may be able to test other predictions as well. For example, Beaugé & Nesvorný (2012) predicted that retrograde orbits generated by planet-planet scattering and secular interactions should go hand in hand with small periastron distances, and are thus more likely to experience tidal decay, leading to a dearth of retrograde orbits around older stars.

One way to test the secular cycle hypothesis, in particular, is to search for companions capable of driving Kozai-Lidov cycles. A prime example is the HD 80606 double star system with its highly eccentric warm Jupiter (Naef et al. 2001) on an oblique orbit (Winn et al. 2009c; Hébrard et al. 2010). This planet may be in the midst of high-eccentricity tidal migration Wu & Murray (2003). The Friends of Hot Jupiters survey (Knutson et al. 2014; Ngo et al. 2015; Piskorz et al. 2015; Bryan et al. 2016; Ngo et al. 2016) found that most hot Jupiters lack a stellar companion capable of driving Kozai-Lidov oscillations — but also that many hot Jupiters do have potentially suitable planetary companions. Time-series astrometry from the Gaia mission will probe whether these companions have sufficiently

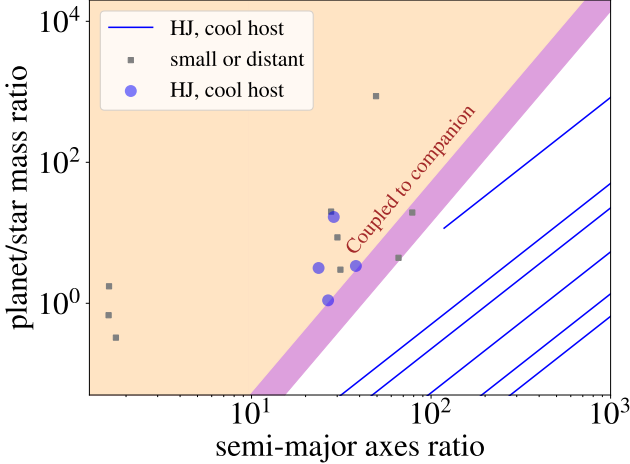


Figure 25. Planet-planet coupling. A handful of cool stars with HJs and low obliquities (blue symbols in the orange region) are strongly coupled to a nearby companion, preventing tidal realignment. Lines represent companions that are detected as radial velocity trends (for which the companion mass and semi-major axis cannot be independently determined).

high mutual inclinations. Using the currently available Gaia data, several groups have found correlations between the orbital orientation of a planet and the orbital orientation of a stellar companion (Dupuy et al. 2022; Behmard et al. 2022; Christian et al. 2022). Future Gaia data releases are expected to significantly improve our understanding of companionship and mutual orbital inclinations.

Searching for wide-orbiting companions to hot Jupiters can also shed light on the tidal realignment hypothesis. A mutually inclined companion can continue to drive secular cycles (Becker et al. 2017) or, with sufficient tidal dissipation, drive the hot Jupiter to a mutually inclined equilibrium known as a Cassini state (Correia 2015). However, the mutually inclined companion must be nearby and massive enough to compete with the spin-orbit coupling arising from stellar oblateness (Lai et al. 2018), i.e., a giant planet companion interior to ~ 1 au. The majority of known companions are too far away or too low in mass to compete with the stellar oblateness coupling (Figure 25). Qatar-2, HAT-P-13, WASP-41, and WASP-47 are currently known systems with an aligned hot Jupiter and a nearby, massive companion; the mutual inclinations of the companions for these systems must be small.

4.4. Altering the stellar spin vector

The processes discussed so far involve tilting a planet’s orbital plane or reorienting a star with an external torque. Some theorists have proposed that a star is ca-

pable of reorienting itself. Based on 2-d hydrodynamical simulations, Rogers et al. (2012, 2013) argued that stars with convective cores and radiative envelopes have photospheres that undergo random tumbling. This is because internal gravity waves (IGW), generated at the radiative/convective boundary, propagate upward within the radiative zone and crash near the stellar surface, depositing angular momentum stochastically. The imperfect cancellation of prograde and retrograde waves leads to a self-reinforcing effect that causes the net orientation of the photosphere to wander randomly, potentially by large angles. The timescale of the changes would be on the order of 10^4 rotation periods or shorter.

Because upward-propagating IGWs are only expected in hot stars, this hypothesis can explain why hot stars have a broader obliquity distribution than cool stars (§ 3.1.5). The IGW hypothesis is also compatible with the evidence that hot stars are misaligned in general, even when they host Kepler-type planets instead of hot Jupiters (§ 3.4 and § 3.5). However, this mechanism does not provide an explanation for the high obliquities that are observed for some cool stars with low-mass or wide-orbiting giant planets (§ 3.1.6, 3.1.7).

The IGW theory might be tested by seeking evidence for time variations of λ and $v \sin i$ for hot stars. The interpretation of any observed changes would be complicated by the possibility of precession caused by other effects (see, e.g., Szabó et al. 2012; Johnson et al. 2015; Masuda 2015). Another signature of IGWs would be the asteroseismic detection of radial differential rotation within the host stars (Christensen-Dalsgaard & Thompson 2011).

We might also test the IGW theory using binaries with separations beyond the reach of tides that contain both a cool star and a hot star. Assuming initial spin-orbit alignment, IGWs would tend to cause the hot star to become misaligned with the binary orbit, while leaving the cool star alone. Obliquities have been measured in a few double-star systems (see Marcussen & Albrecht 2021, for a listing) but none of them fulfill all these requirements. There are two systems, DI Her and CV Vel, in which both components have radiative envelopes and measured obliquities — but in those systems, the time variations in λ and $v \sin i$ are caused by the precession of the misaligned stars around the total angular momentum vector (Reisenberger & Guinan 1989; Albrecht et al. 2009; Philippov & Rafikov 2013; Albrecht et al. 2014; Liang et al. 2022).

5. SUMMARY AND DISCUSSION

The textbook picture of a planetary system features a star rotating around the axis defined by the plane of its

protoplanetary disk or the orbits of its planets. Experience has shown that this picture is missing some aspects of planet formation or the long-term evolution of planetary systems. Here, we summarize the general trends in the data that were discussed in more detail in Section 3. Table 1 provides an even more concise summary.

- The orbital planes of hot Jupiters orbiting G and K dwarfs are almost always found to be aligned with the stellar equatorial plane. However, misalignments are at least occasionally found in all the other classes of systems that have been investigated (Figure 2).
- The risk factors for a star with a close-orbiting giant planet to develop a high obliquity are: a stellar mass exceeding about $1.2 M_{\odot}$ or an effective temperature exceeding 6250 K (§ 3.1.5), a relatively low planet mass (Neptunian instead of Jovian; § 3.1.6), and a relatively wide orbit ($a/R \gtrsim 10$; § 3.1.7).
- The most precise measurements so far show that giant planets traveling on short-period orbits around stars with deep convective envelopes tend to be aligned to within about 1 degree (§ 3.1.8), i.e., more closely aligned than the Sun is with respect to the orbits of the planets of the Solar System.
- The two preceding observations can be interpreted as evidence for tidally-driven spin-orbit alignment, although we lack a good theoretical understanding of the process (§ 4.1).
- The occurrence of misalignments for the youngest systems that have been investigated ($\lesssim 100$ Myr) appears to be lower than for their older siblings, although this is not a firm conclusion because of the small sample size (§ 3.1.10).
- One might expect high obliquities and high eccentricities to be correlated. Such a correlation might already be present in the current data, though the interpretation is complicated by the possibility of tidal alignment and tidal circularization, by the difficulty of measuring both eccentricity and obliquity in the same system, and by the inhomogeneity of the sample (§ 3.1.11).
- Coplanarity of orbits does not guarantee alignment between the planetary orbital plane and the stellar equator. Most multi-transiting systems for which a component of the obliquity vector has

been measured tend to be consistent with alignment, but exceptions do exist (§ 3.1.13). Statistical studies also suggest that alignment is not universal among multi-transiting systems, at least for hot stars (§ 3.5.1 and 3.4).

- Planets comparable in size to Neptune, or smaller, have been found both on well-aligned orbits and on misaligned orbits (§ 3.1 and § 3.2). Statistical studies point toward widespread misalignments up to about 30° (§ 3.4 and § 3.5.1).
- Studies of planets with orbital distance larger than ~ 1 au are only just becoming possible (§ 3.3).
- Almost all the 3-d obliquities that have been determined fall into two groups: Most are lower than 40° , and the rest are between about 80 and 125° (§ 3.7). The misaligned systems do not seem to have much in common: they include planets ranging from mini-Neptunes to Jupiter-sized, and stars ranging from spectral type M to A.

The observational evidence does not single out a unique explanation for spin-orbit misalignments. Many plausible theoretical mechanisms have been proposed. The multiplicity of mechanisms is not too surprising. Undoubtedly, there is more than one way to perturb stars and planetary orbits. To paraphrase Tolstoy: circular and coplanar systems are all alike; each eccentric and misaligned system is eccentric and misaligned in its own way. We do not yet know which of the proposed misalignment mechanisms actually occurs, and if so, how often. Nevertheless, there is evidence for at least two pathways to spin-orbit misalignment: primordial misalignment between a star and its protoplanetary disk, and gravitational dynamical processes taking place after planet formation.

Evidence for **primordial misalignment** comes from the small collection of misaligned stars with multiple coplanar planets (Kepler-56, K2-290 A, and possibly Kepler-129 and HD 3167). In particular, K2-290 A is known to have a companion star with properties suitable for misaligning the protoplanetary disk. In addition, the $v \sin i$ and photometric-variability statistical techniques have provided evidence that hot Kepler stars have a broad distribution of obliquities. This suggests that misalignment operates independently of the size or orbital period of the planets. Primordial misalignment is such a mechanism.

Furthermore, observations of jets and disks in young stellar systems show indirect evidence for occasional misalignments between a star and the surrounding protoplanetary disk. Some young binary systems observed

with ALMA have circumstellar disks tilted with respect to the orbital plane and each other, such as HK Tauri. However, based on theoretical work, observations of resolved debris disks, obliquity measurements in a few young exoplanet systems, and obliquity measurements in compact transiting multi planet systems with cool host stars suggest primordial misalignments do not seem to be widespread — or perhaps they do not persist throughout the entire planet formation epoch. The evidence for **post-formation gravitational dynamical interactions** comes from systems with close-orbiting giant planets. Observational support comes from the higher incidence of misalignments for close-orbiting giant planets compared to compact systems of multiple coplanar planets. The observations of alignment in the (admittedly small) number of systems younger than 100 Myr systems with close-orbiting giant planets suggests that misalignments occur later, as expected from long-term dynamical interactions that stimulate high-eccentricity migration.

There are a few “poster child” systems for Kozai-Lidov cycles caused by stellar companion, such as HD 80606. Of all the post-formation misalignment scenarios, Kozai-Lidov cycles can most easily generate retrograde orbits. However, surveys have generally not found evidence for stellar companions with suitable properties. This still leaves open the possibility of Kozai-Lidov cycles induced by wide-orbiting massive planets, if these companions somehow acquire large mutual inclinations. Different post-formation mechanism scenarios lead to different predictions for the obliquity distribution, which can in principle be used as an observational test. The possibility of tidal realignment, and our lack of a quantitative understanding of tidal timescales, complicates such tests.

Tidal interactions between the star and planet appear to be important in the subset of systems with short-period hot Jupiters and stars with thick convective envelopes. While tides are not fully understood, there are several indications that the problem of tidal realignment without catastrophic orbital decay might not be as severe as originally feared. Tides are successful in explaining observational trends with stellar structure, orbital separation, and planetary mass. Tides also explain why the hot Jupiters with cool host stars and the most precisely measured obliquities are very well aligned, with an inclination dispersion on the order of 1° .

The **current sample of systems with obliquity measurements is biased**, and especially favors close-in giant planets orbiting main sequence FGK stars.

New projects and space missions have the potential to end this preoccupation with a small subset of

planetary systems. Bright and well-characterized TESS systems allow for more precise RM and $v \sin i$ measurements over a more diverse range of system properties. For example, it will be interesting to see if the obliquity distribution of M-dwarf planet hosts differs from that of G and K dwarfs. PLATO will follow TESS in this regard, while also providing longer time baselines for seismic and starspot-based measurements. Gaia will dramatically improve our understanding of companionship and measure orbital inclinations in some systems. This in turn will motivate and enable obliquity measurements for such systems via some of the methods discussed above. Together with the availability of future spectrographs and interferometers, there will be many ways to improve our knowledge, including:

- Bright and well-studied TESS systems harboring close-in giant planets will allow for precise RM measurements ($\lesssim 2^\circ$) employing new ground-based spectrographs. Such observations would be useful in testing whether tidal obliquity damping occurs.
- Theories of primordial misalignment can be tested by observing young systems, planets with large orbital separations, systems with multiple transiting planets with and without wide-orbiting companions, and resolved disks with stars amenable to the $v \sin i$ technique. Also relevant are observations of misalignments and warps between the inner and outer portions of disks, and the angles between disks around the members of wide double stars.
- The increasing number of transiting planets found around bright stars will allow for more precise obliquity and eccentricity measurements in systems with lower stellar masses, wider orbits, and smaller planets. It also allows for a more complete characterization of companionship. Combined with a better understanding of tidal alignment (first point above), it may be possible to make meaningful comparisons between the measured obliquity distribution and predictions of post-formation misalignment mechanisms.
- Obliquity measurements in multiple-star systems over a wide range of separations may help to determine whether primordial disk misalignment mechanisms and stellar KL-cycles are important. These samples could also serve to better test the role of internal gravity waves.

Measurements of the stellar obliquity have opened a new window through which we can observe the 3-d structure of exoplanetary systems. However, the currently

available measurements are mainly confined to stars with close-orbiting giant planets or Kepler-type compact multi-planet systems. Other classes of exoplanets have been left out, so far. Two related types of information, mutual orbital inclinations and planetary obliquity, have proven more difficult to obtain. Not before long, all of these quantities will be more accessible for a more diverse exoplanet population. This will be thanks to time-series astrometric data from Gaia, advances in spectroscopic and interferometric instrumentation, and newly discovered exoplanet systems with nearby and bright host stars. The combined information on the orientation of the various components of angular momentum in a planetary system will have an impact on our understanding of star and planet formation, exoplanet orbital dynamics, and theories of tidal interactions between stars and planets. The drama of planet formation and evolution — initially portrayed on a two-dimensional, planar stage — is gradually becoming a three-dimensional spectacle.

S.A. acknowledges the support from the Danish Council for Independent Research through the DFF Sapere Aude Starting Grant No. 4181-00487B, as well as a DFF Research Project 1 grant No.2032-00230B, and the Stellar Astrophysics Centre whose funding is provided by The Danish National Research Foundation (Grant agreement no.: DNRF106). R.I.D. acknowledges the support from grant NNX16AB50G awarded by the NASA Exoplanets Research Program and the Alfred P. Sloan Foundation's Sloan Research Fellowship. The Center for Exoplanets and Habitable Worlds is supported by Pennsylvania State University, the Eberly College of Science, and the Pennsylvania Space Grant Consortium. J.N.W. gratefully acknowledges the hospitality and support of the Institute for Advanced Study.

We thank J.J. Zanazzi and Hans Kjeldsen for insightful comments on a manuscript draft. We are grateful for feedback and helpful suggestions from Adrian Baker, Subo Dong, Dan Fabrycky, René Heller, Emil Knudstrup, David Latham, Marcus Marcussen, Gordon Ogilvie, Malena Rice and Scott Tremaine. We thank the anonymous reviewer for helpful comments that improved the review. We thank John Southworth for curating the [TEPCat](#) catalog.

APPENDIX

A. POPULATION SYNTHESIS SIMULATIONS

The simulations are based on work by [Dawson \(2014\)](#), with updates to incorporate options for inertial wave tidal dissipation and a frequency dependent tidal dissipation efficiency. We numerically integrate the planet's specific orbital angular momentum vector \vec{h} and the host star's spin angular frequency vector, assuming a circular orbit. The equations here correspond to [Barker & Ogilvie \(2009\)](#), Eqns. A7 and A12 with the eccentricity vector $\vec{e} = 0$.

$$\begin{aligned} \left(\dot{\vec{h}} \right)_{eq} &= -\frac{1}{\tau_{eq}} \vec{h} + \frac{1}{\tau_{eq}} \frac{\Omega_*}{2n} \left(\frac{\vec{\Omega}_* \cdot \vec{h}}{\Omega_* h} \cdot \vec{h} + \frac{h}{\Omega_*} \vec{\Omega}_* \right) \\ \left(\dot{\vec{\Omega}}_* \right)_{eq,\alpha} &= -\frac{m}{k_{*,\text{eff}} MR^2} \dot{\vec{h}}_{eq} - \alpha_{\text{brake}} \Omega_*^2 \vec{\Omega}_*, \end{aligned} \quad (\text{A1})$$

for which

$$\begin{aligned} \tau_{eq} &= \frac{Q}{6k_L} \frac{M}{R^5(M+m)^8 G^7} \frac{M}{m} h^{13} \\ &= \tau_{eq,0} \left(\frac{h}{h_0} \right)^{13} \frac{0.5 M_{\text{Jup}}}{m} \end{aligned} \quad (\text{A2})$$

is an orbital decay timescale, k_L is the Love number, Q is the tidal quality factor, $k_{*,\text{eff}}$ is the effective constant of the stellar moment of inertia participating in the tidal realignment, α_{brake} is a braking constant, and $h_0 = \sqrt{a_0 G(M+m)}$ is the initial specific angular momentum. By default, we use $k_{*,\text{eff}} MR^2 = 0.08 M_{\odot} R_{\odot}^2$ for cool stars, $k_{*,\text{eff}} MR^2 = 0.08(1.2M_{\odot})(1.4R_{\odot})^2$ for hot stars, and $\Omega_{s,0} = 800 \text{ AU}^2 \text{yr}^{-1}$. We use $\alpha = 3 \times 10^{-16}$ for hot stars, $\alpha = 1.4 \times 10^{-14}$ for cool stars, $\tau_{eq,0} = 500 \text{ Gyr}$, and $h_0 = 1.33 \text{ au}^2 \text{yr}^{-1}$. For the pure equilibrium tides simulation, we use $h_0 = 1.68 \text{ au}^2 \text{yr}^{-1}$. For the frequency-dependent Q simulations, we use $\tau_{eq,0} = 20 \text{ Gyr}$, and $h_0 = 2 \text{ au}^2 \text{yr}^{-1}$. For inertial wave

tidal dissipation, we use $\tau_{eq,0} = 50$ Gyr for cold stars, $\tau_{eq,0} = 5 \times 10^6$ Gyr for hot stars, and $h_0 = 1.25 \text{ au}^2 \text{ yr}^{-1}$. For the decoupled outer envelope simulations, we use $\tau_{eq,0} = 100$ Gyr, $\alpha = \times 10^{-13}$ for cool stars, $k_{\star,\text{eff}} MR^2 = 0.0008 M_{\odot} R_{\odot}^2$ for cool stars, and $k_{\star,\text{eff}} MR^2 = 0.0004(1.2M_{\odot})(1.4R_{\odot})^2$ for hot stars.

For inertial wave tidal dissipation, the tidal forcing component that excites inertial waves exerts a torque. Here, we follow Lai (2012) to compute the resulting effects on \vec{h} and $\vec{\Omega}_{\star}$. One component is parallel to the stellar spin, i.e., in the $\vec{\Omega}_{\star}$ direction. A second component is perpendicular to both \vec{h} and $\vec{\Omega}_{\star}$, i.e., in the $\vec{\Omega}_s \times \vec{h}$ direction, and is ignored in our calculations because it does not affect the alignment. The third component is perpendicular to the other two, and thus we compute its unit vector as:

$$\hat{x} = (\vec{h} \times \vec{\Omega}_s) \times \frac{\vec{\Omega}_s}{\Omega_{\star}^2 h \sin \psi} \quad (\text{A3})$$

where

$$\begin{aligned} \cos \psi &= \frac{\vec{\Omega}_{\star} \cdot \vec{h}}{\Omega_{\star} h} \\ \sin \psi &= \frac{|\vec{\Omega}_{\star} \times \vec{h}|}{\Omega_{\star} h} \end{aligned} \quad (\text{A4})$$

We add the following terms to Eqn. A1.

$$\begin{aligned} \left(\dot{\vec{\Omega}}_{\star} \right)_{dy} &= -\frac{1}{\tau_{dy}} \left(1 - \frac{\tau_{0,dy}}{\tau_{0,eq}} \right) \\ &\quad \left[(\sin \psi \cos \psi)^2 \vec{\Omega}_{\star} - \sin \psi \cos \psi^3 \vec{\Omega}_{\star} \hat{x} \right] \\ \left(\dot{\vec{h}} \right)_{dy} &= -\frac{k_{\star,\text{eff}} MR^2}{m} \left(\dot{\vec{\Omega}}_{\star} \right)_{dy} \end{aligned} \quad (\text{A5})$$

where

$$\tau_{dy} = \frac{\tau_{0,dy}}{\tau_{0,eq}} \frac{\Omega_{\star}}{\Omega_{\star,0}} \frac{h_0}{h} \tau_{eq}. \quad (\text{A6})$$

We set $\frac{\tau_{0,dy}}{\tau_{0,eq}} = 10^{-5}$ for Fig. 23.

For the frequency-dependent tidal dissipation efficiency model (Penev et al. 2018), we use Eqn. A1 with a modified value of t_{eq} :

$$t_{eq,f} = t_{eq} \frac{\max\{10^6/P_{\text{tide}}^{3.1}, 10^5\}}{\max\{10^6/P_{\text{tide},0}^{3.1}, 10^5\}} \quad (\text{A7})$$

where $P_{\text{tide}} = \pi/(n - \Omega_s)$ is in units of days.

To generate the populations for Fig. 23, we select an effective temperature drawn randomly from a uniform distribution between 4800 and 6800 K, a planet mass drawn from a log-uniform probability distribution between 0.5 and 15 Jupiter masses, an initial obliquity ψ drawn from an isotropic distribution, an evolution time drawn from a uniform distribution between 0 and 10 Gyr for cool stars ($T_{\text{eff}} < 6250$ K) and between 0 and 4 Gyr for hot stars, and a longitude of ascending node drawn from a uniform distribution between 0 and 360° . We integrate the momentum equations given above, between $t = 0$ and $t = t_{\star}$. We compute $\sin i = \sqrt{1 - (\sin \psi \cos \Omega)^2}$, $v \sin(i)/R = \Omega_{\star} \sin i$, and $\lambda = \tan^{-1}(\tan \psi \sin \Omega)$ (Fabrycky & Winn 2009, Eqn. 11; Column 2 of our Fig. 23 shows the initial distribution of λ).

B. HISTOGRAM PLOT

C. SYSTEMS

Here we describe the sources of the system parameters and our vetting process that led to the sample of obliquity data that forms the basis of many of the figures in this article. On 5 January 2021, we downloaded the data from the TEPCat catalog, which is curated by John Southworth and is available here: [TEPCat Southworth \(2011\)](#).

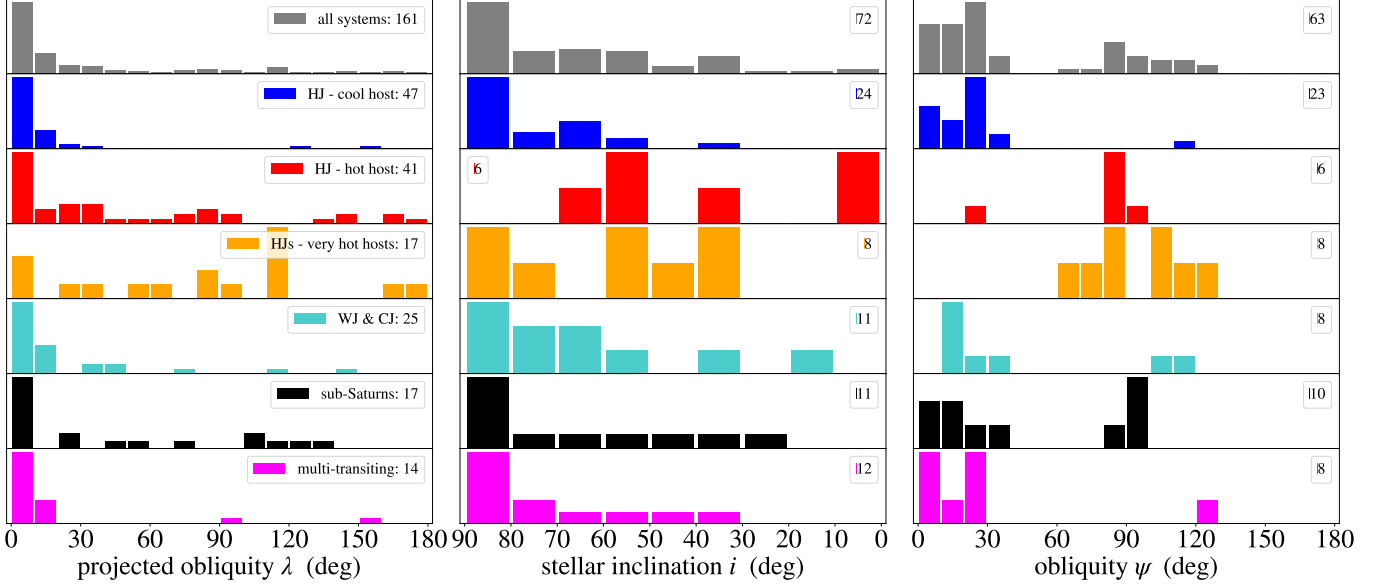


Figure 26. Overview: Histograms of host star obliquities. *Left:* Projected obliquities λ folded onto the range $[0, 180^\circ]$. *Middle:* Stellar inclination measurements folded onto $[0, 90^\circ]$. *Right:* Three-dimensional obliquities (ψ), for the cases in which λ and i have both been measured. Histograms are color-coded according to the system’s characteristics. Stars are designated as cool, hot, or very hot, using effective temperature boundaries of 6250 K and 7000 K. Planets with masses exceeding $0.3 M_{\text{Jup}}$ are designated hot Jupiters (HJ) if $a/R < 10$, and warm/cold Jupiters (WJ/CJ) if $a/R > 10$. Planets with masses $\lesssim 0.3 M_{\text{Jup}}$ are designated sub-Saturns.

We added the following obliquity measurements which were not in TEPCat at the time of download: β Pic (Kraus et al. 2020), HD 332231 (Knudstrup & Albrecht 2022), K2-290 (Hjorth et al. 2021), a measurement of the second planet in HD 63433 (Dai et al. 2020), TOI-942 (Wirth et al. 2021), HIP 67522 (Heitzmann et al. 2021), GJ 3470 (Stefansson et al. 2022), V1298 Tau c (Feinstein et al. 2021) & V1298 Tau b (Johnson et al. 2022), K2-140 (Rice et al. 2021), K2-232 (Wang et al. 2021), TOI-1518 (Cabot et al. 2021), WASP-148 (Wang et al. 2022), HD 3167 b (Bourrier et al. 2021), TOI-2109 Wong et al. (2021), KELT-25 and KELT-26 Rodríguez Martínez et al. (2020), and TOI-1268 Dong et al. (2022).

We also included some stellar inclination measurements obtained with the method described by Masuda & Winn (2020). These were: TOI-251 & TOI-942 (Zhou et al. 2021), TOI-451 (Newton et al. 2021), TOI-811 & TOI-852 (Carmichael et al. 2020), and TOI-1333 (Rodríguez et al. 2021).

For some systems, more than one measurement of the stellar inclination or projected obliquity have been reported. TEPCat indicates a “preferred” measurement, which we adopted except for the following cases: for HAT-P-7, we chose “Solution 1” of Masuda (2015); for HAT-P-16, we chose Moutou et al. (2011); for Kepler-25, we chose (Albrecht et al. 2013); for MASCARA-4, we chose Dorval et al. (2020); for WASP-18 & WASP-31, we chose Albrecht et al. (2012b); and for WASP-33, we chose the 2014 data of Johnson et al. (2015). We do not think that different choices would have led to significantly different conclusions.

We folded all the measurements of projected obliquity onto a half circle ranging from 0° to 180° . (The only exception is one panel in Fig. 10.)

We obtained orbital eccentricity data either from the papers reporting on radial-velocity data of individual objects, or, whenever possible, from the comprehensive work by Bonomo et al. (2017). For Kepler-448, we used the eccentricity determined by Masuda (2017). We obtained information on companionship from the “Friends of hot Jupiters” series of papers (Knutson et al. 2014; Piskorz et al. 2015; Ngo et al. 2016).

We excluded systems with uncertainties in the projected obliquity larger than 50 deg, specifically HAT-P-27 (Brown et al. 2012a) and WASP-49 (Wyttenbach et al. 2017). We also excluded the following specific systems, for which we think the true uncertainties are larger than the formal uncertainties would suggest. For the hot Jupiter system CoRoT-1, two RM datasets have been reported, one indicating good alignment (Bouchy et al. 2009), and one indicating strong misalignment (Pont et al. 2010). For CoRoT-19, Guenther et al. (2012) found a projected obliquity of $\lambda = -52^{+27}_{-22}$ deg.

However, no post-egress data were obtained, and the RM effect was only detected with 2.3σ confidence. For HATS-14, Zhou et al. (2015) reported a misaligned orbit ($|\lambda| = 76_{-5}^{+4}$ deg). However, there are no post-egress data and, as highlighted by the authors, making different assumptions about the orbital semi-amplitude leads to different conclusions about the obliquity. For similar reasons, the WASP-134 results by (Anderson et al. 2018a) were excluded. WASP-23 has a low transit impact parameter and a low $v \sin i$, which prevented Triaud et al. (2011) from drawing any conclusions other than that the orbit is probably prograde. We excluded the WASP-1 and WASP-2 systems (Triaud et al. 2010; Simpson et al. 2011) for reasons that were discussed in detail by Albrecht et al. (2011) and Triaud (2018). Bourrier & Hébrard (2014) presented evidence for a significant misalignment in the 55 Cnc system, but López-Morales et al. (2014) presented other data suggesting that the detection of misalignment had been spurious. There was also a tentative detection of misalignment in KOI-89 (Ahlers et al. 2015), but a recent reanalysis of the Kepler data showed that the obliquity is unconstrained by the data (Masuda & Tamayo 2020).

Most of the $v \sin i$ measurements adopted for our sample were obtained by modeling the RM effect. However, for some cases in which the RM data have a low signal-to-noise ratio (e.g., Qatar-2 Esposito et al. 2017), we opted to report the value of $v \sin i$ based on the observed line broadening. It is also worth noting that in general, the $v \sin i$ value derived from line broadening is based on the disk-integrated stellar spectrum, whereas the value obtained by modeling the RM effect is more closely connected to the spectrum of the portion of the star hidden by the planet.

Table 4. Key properties of the systems considered in this review. Additional planetary parameters are given in Table 5.

System	T _{eff}	M	R	age	$v \sin i$	References
	(K)	(M _⊕)	(R _⊕)	(Gyr)	(km s ⁻¹)	
(1)	(2)	(3)	(4)	(5)	(6)	(7)
AU Mic	3700 ± 100	0.50 ± 0.03	0.75 ± 0.03	0.02 ± 0.00	$9.23_{-0.31}^{+0.79}$	1,2
Beta PIC	8200 ± 200	$1.75_{-0.02}^{+0.03}$	1.87 ± 0.03	$0.01_{-0.00}^{+0.01}$	130.00 ± 10.00	3,4,5,6
CoRoT-2	5598 ± 50	1.00 ± 0.05	0.90 ± 0.02	2.66 ± 1.62	11.25 ± 0.45	7,8
CoRoT-3	6558 ± 44	1.40 ± 0.06	1.58 ± 0.09	2.20 ± 0.60	17.00 ± 1.00	9,10
CoRoT-11	6343 ± 72	1.26 ± 0.14	1.37 ± 0.06	2.66 ± 1.62	38.47 ± 0.07	11,12
CoRoT-18	5440 ± 100	0.88 ± 0.07	$0.88_{-0.03}^{+0.03}$	10.69 ± 3.82	8.00 ± 1.00	7,13
DS Tuc	5598_{-59}^{+28}	0.96 ± 0.03	0.87 ± 0.03	0.04 ± 0.00	$20.58_{-0.24}^{+0.31}$	14,15
EPIC 246851721	6202_{-50}^{+52}	1.32 ± 0.04	$1.62_{-0.04}^{+0.04}$	$3.02_{-0.46}^{+0.44}$	$74.92_{-0.60}^{+0.62}$	16
GJ 3470	3622_{-55}^{+58}	$0.53_{-0.03}^{+0.02}$	$0.50_{-0.02}^{+0.00}$	1.65 ± 1.35	$0.61_{-0.37}^{+0.43}$	17,18,19
GJ 436	3416 ± 54	$0.51_{-0.06}^{+0.07}$	0.46 ± 0.02	6.00 ± 2.00	$0.33_{-0.07}^{+0.09}$	20
HAT-P-1	5975 ± 50	1.15 ± 0.02	$1.17_{-0.03}^{+0.03}$	1.90 ± 0.60	3.75 ± 0.58	21,22
HAT-P-2	6290 ± 60	1.28 ± 0.05	1.68 ± 0.15	2.60 ± 0.50	19.50 ± 1.40	23,24
HAT-P-3	5190 ± 80	0.93 ± 0.04	0.85 ± 0.02	2.60 ± 0.60	1.20 ± 0.36	25
HAT-P-4	6036 ± 46	$1.27_{-0.07}^{+0.12}$	$1.60_{-0.04}^{+0.12}$	$4.20_{-0.60}^{+2.60}$	5.83 ± 0.30	26,27
HAT-P-6	6570 ± 80	1.29 ± 0.07	1.52 ± 0.07	$2.30_{-0.70}^{+0.50}$	7.80 ± 0.60	28,29
HAT-P-7	6310 ± 15	1.59 ± 0.03	2.02 ± 0.01	$2.08_{-0.23}^{+0.28}$	2.70 ± 0.50	30,29
HAT-P-8	6200 ± 80	1.19 ± 0.07	1.48 ± 0.03	3.40 ± 1.00	14.50 ± 0.80	31,32
HAT-P-9	6350 ± 150	1.28 ± 0.10	1.34 ± 0.08	$1.60_{-1.40}^{+1.80}$	12.50 ± 1.80	33,32
HAT-P-11	4780 ± 50	0.80 ± 0.03	0.68 ± 0.01	$6.50_{-4.10}^{+5.90}$	$1.00_{-0.56}^{+0.95}$	34,35
HAT-P-12	4665 ± 45	0.69 ± 0.02	0.68 ± 0.01	2.50 ± 2.00	$0.99_{-0.46}^{+0.42}$	36,25
HAT-P-13	5653 ± 90	1.32 ± 0.06	1.76 ± 0.05	$5.00_{-0.70}^{+2.50}$	1.70 ± 0.40	37,38
HAT-P-14	6600 ± 90	1.42 ± 0.05	1.59 ± 0.06	1.30 ± 0.40	8.18 ± 0.40	39,27
HAT-P-16	6140 ± 72	1.22 ± 0.06	1.16 ± 0.03	1.30 ± 0.40	3.90 ± 0.80	40,32
HAT-P-17	5246 ± 80	0.86 ± 0.04	0.84 ± 0.02	7.80 ± 0.30	$0.56_{-0.14}^{+0.12}$	41,42
HAT-P-18	4870 ± 50	0.77 ± 0.03	0.72 ± 0.03	$12.40_{-6.40}^{+4.40}$	1.58 ± 0.18	43,44
HAT-P-20	4595 ± 45	0.75 ± 0.04	0.68 ± 0.01	$6.70_{-3.80}^{+5.70}$	1.85 ± 0.27	45,46
HAT-P-22	5314 ± 50	0.94 ± 0.04	1.06 ± 0.05	12.40 ± 2.40	1.65 ± 0.26	45,25

Table 4 continued

Table 4 (*continued*)

System	Teff	M	R	age	$v \sin i$	References
	(K)	(M _⊕)	(R _⊕)	(Gyr)	(km s ⁻¹)	
(1)	(2)	(3)	(4)	(5)	(6)	(7)
HAT-P-23	5885 ± 72	1.10 ± 0.05	1.09 ± 0.03	4.00 ± 1.00	7.80 ± 1.60	45,32
HAT-P-24	6373 ± 80	1.19 ^{+0.04} _{-0.04}	1.29 ^{+0.07} _{-0.06}	2.80 ± 0.60	11.20 ± 0.90	47,29
HAT-P-30	6338 ± 42	1.24 ± 0.04	1.22 ± 0.05	1.00 ^{+0.80} _{-0.50}	3.07 ± 0.24	48
HAT-P-32	6269 ± 64	1.18 ± 0.05	1.23 ± 0.02	2.70 ± 0.80	20.60 ± 1.50	9,29
HAT-P-34	6442 ± 88	1.39 ± 0.05	1.53 ^{+0.14} _{-0.10}	1.70 ^{+0.40} _{-0.50}	24.30 ± 1.20	9,29
HAT-P-36	5620 ± 40	1.03 ± 0.04	1.04 ± 0.02	6.60 ^{+2.90} _{-1.80}	3.12 ± 0.75	9,49
HAT-P-41	6390 ± 100	1.42 ± 0.05	1.68 ^{+0.06} _{-0.04}	2.20 ± 0.40	19.60 ± 0.50	9,50
HAT-P-56	6566 ± 50	1.30 ± 0.04	1.43 ± 0.03	2.01 ± 0.35	36.40 ± 0.70	9,51
HAT-P-69	7724 ⁺²⁵⁰ ₋₃₆₀	1.70 ± 0.03	1.85 ^{+0.04} _{-0.02}	1.27 ^{+0.44} _{-0.28}	77.43 ^{+0.64} _{-0.53}	52
HAT-P-70	8450 ⁺⁵⁴⁰ ₋₆₉₀	1.89 ^{+0.01} _{-0.01}	1.86 ^{+0.12} _{-0.09}	0.60 ^{+0.38} _{-0.20}	99.85 ^{+0.64} _{-0.61}	52
HATS-2	5227 ± 95	0.88 ± 0.04	0.90 ± 0.02	9.70 ± 2.90	1.50 ± 0.50	9,53
HATS-3	6351 ± 76	1.21 ± 0.04	1.40 ± 0.03	3.20 ^{+0.60} _{-0.40}	5.75 ± 2.98	9,54
HATS-70	7930 ⁺⁶³⁰ ₋₈₂₀	1.78 ± 0.12	1.88 ^{+0.06} _{-0.07}	0.81 ^{+0.50} _{-0.33}	40.61 ^{+0.32} _{-0.35}	55
HD 332231	6089 ⁺⁹⁷ ₋₉₆	1.13 ± 0.08	1.28 ^{+0.04} _{-0.04}	4.30 ^{+2.50} _{-1.90}	5.63 ± 0.11	56,57
HD 3167	5261 ± 60	0.84 ^{+0.05} _{-0.04}	0.88 ^{+0.01} _{-0.01}	7.80 ± 4.30	2.10 ± 0.40	58,59
HD 17156	6079 ± 56	1.30 ± 0.07	1.49 ± 0.04	3.37 ^{+0.20} _{-0.47}	4.18 ± 0.31	60,61
HD 63433	5640 ± 74	—	—	0.41 ± 0.23	7.30 ± 0.30	62
HD 80606	5584 ± 13	1.02 ± 0.06	1.04 ± 0.04	4.70 ± 0.60	1.70 ± 0.30	63,64
HD 106315	6364 ± 87	1.15 ± 0.04	1.27 ± 0.02	4.00 ± 1.00	13.00 ± 0.28	65,66
HD 149026	6147 ± 50	1.34 ± 0.02	1.54 ^{+0.05} _{-0.04}	2.90 ± 0.30	7.70 ± 0.80	21,29
HD 189733	5050 ± 50	0.84 ± 0.04	0.75 ± 0.03	6.20 ± 3.40	3.25 ± 0.02	21,67
HD 209458	6117 ± 50	1.15 ± 0.04	1.16 ± 0.01	4.00 ± 1.20	4.80 ± 0.20	21,68
HIP 67522	5675 ± 75	1.22 ± 0.05	1.38 ± 0.06	0.02 ± 0.00	49.21 ^{+0.97} _{-0.95}	69,70
K2-25	3207 ± 58	0.26 ± 0.01	0.29 ± 0.01	0.73 ± 0.08	8.90 ± 0.60	71,72
K2-29	5358 ± 38	0.94 ± 0.02	0.86 ± 0.01	2.60 ^{+1.20} _{-2.35}	3.70 ± 0.50	73
K2-34	6131 ± 47	1.20 ± 0.03	1.38 ± 0.05	2.88 ^{+0.26} _{-0.24}	5.00 ^{+1.30} _{-1.40}	74
K2-140	5585 ± 120	0.96 ^{+0.06} _{-0.04}	1.06 ^{+0.07} _{-0.06}	9.80 ^{+3.40} _{-4.60}	2.51 ± 0.38	75,76
K2-232	6154 ± 60	1.19 ^{+0.03} _{-0.03}	1.16 ± 0.02	1.43 ^{+0.82} _{-0.75}	5.15 ± 0.62	77,78
K2-290	6302 ± 120	1.19 ± 0.07	1.51 ^{+0.08} _{-0.08}	4.00 ^{+1.60} _{-0.80}	6.90 ^{+0.50} _{-0.60}	79
KELT-1	6516 ± 49	1.33 ± 0.06	1.47 ^{+0.04} _{-0.04}	1.75 ± 0.25	56.00 ± 2.00	80
KELT-6	6272 ± 61	1.13 ± 0.06	1.53 ^{+0.14} _{-0.14}	4.90 ^{+0.66} _{-0.46}	4.12 ± 0.26	81
KELT-7	6789 ⁺⁵⁰ ₋₄₉	1.53 ^{+0.07} _{-0.05}	1.73 ^{+0.04} _{-0.04}	1.20 ± 0.20	69.30 ± 0.20	82,51
KELT-9	9600 ± 400	2.32 ± 0.16	2.42 ± 0.06	0.30 ± 0.00	116.90 ± 1.80	83,84
KELT-17	7454 ± 49	1.64 ^{+0.07} _{-0.06}	1.65 ^{+0.06} _{-0.06}	0.65 ± 0.15	44.20 ^{+1.50} _{-1.30}	85
KELT-19	7500 ± 110	1.62 ^{+0.25} _{-0.20}	1.83 ± 0.10	1.10 ± 0.10	84.20 ± 2.00	86
KELT-21	7598 ⁺⁸¹ ₋₈₄	1.46 ^{+0.03} _{-0.03}	1.64 ± 0.03	1.60 ± 0.10	146.03 ± 0.48	87
KELT-25	8280 ⁺⁴⁴⁰ ₋₁₈₀	2.18 ^{+0.12} _{-0.11}	2.26 ^{+0.05} _{-0.05}	0.46 ^{+0.12} _{-0.14}	114.20 ± 1.20	88
KELT-26	8640 ⁺⁵⁰⁰ ₋₂₄₀	1.92 ^{+0.14} _{-0.16}	1.80 ^{+0.05} _{-0.05}	0.43 ^{+0.31} _{-0.25}	12.28 ^{+0.78} _{-0.82}	88
Kepler-8	6213 ± 150	1.23 ± 0.07	1.50 ± 0.04	3.80 ± 1.50	8.90 ± 1.00	9,29
Kepler-9	5774 ± 60	1.02 ^{+0.03} _{-0.04}	0.96 ± 0.02	3.00 ± 1.00	2.74 ± 0.40	89,90
Kepler-13	7650 ± 250	1.72 ± 0.10	1.71 ± 0.04	0.71 ^{+0.18} _{-0.15}	62.70 ± 0.20	91,92
Kepler-17	5781 ± 85	1.07 ^{+0.05} _{-0.16}	0.98 ^{+0.02} _{-0.05}	2.90 ^{+1.50} _{-1.60}	4.70 ± 1.00	93
Kepler-25	6270 ± 79	1.17 ^{+0.03} _{-0.03}	1.32 ^{+0.02} _{-0.01}	2.75 ± 0.30	8.20 ± 0.20	94,95
Kepler-30	5498 ± 54	0.99 ± 0.08	0.95 ± 0.12	2.00 ± 0.80	1.94 ± 0.50	96,97
Kepler-50	6225 ± 66	1.24 ± 0.05	1.58 ± 0.02	3.80 ± 0.80	8.00 ^{+1.20} _{-1.00}	98
Kepler-56	4840 ± 97	1.32 ± 0.13	4.23 ± 0.15	3.50 ± 1.30	1.70 ± 1.00	99
Kepler-63	5576 ± 50	0.98 ^{+0.04} _{-0.04}	0.90 ^{+0.03} _{-0.02}	0.21 ± 0.05	5.60 ± 0.80	100
Kepler-65	6211 ± 66	1.25 ^{+0.02} _{-0.02}	1.44 ^{+0.03} _{-0.03}	2.90 ± 0.70	10.40 ± 0.60	98
Kepler-89	6182 ± 82	1.28 ± 0.05	1.52 ± 0.14	3.90 ^{+0.30} _{-0.20}	7.30 ± 0.60	101

Table 4 continued

Table 4 (continued)

System	T _{eff} (K)	M (M _⊕)	R (R _⊕)	age (Gyr)	v sin i (km s ⁻¹)	References
(1)	(2)	(3)	(4)	(5)	(6)	(7)
Kepler-408	6088 ± 65	1.05 ± 0.04	1.25 ± 0.05	4.70 ± 1.20	2.80 ± 1.00	102
Kepler-410	6375 ± 44	1.21 ^{+0.03} _{-0.03}	1.35 ± 0.01	2.76 ± 0.54	12.90 ± 0.60	103
Kepler-420	5520 ± 80	0.99 ± 0.05	1.13 ± 0.14	9.30 ± 0.30	7.30 ± 0.60	104
Kepler-432	5020 ± 60	1.32 ^{+0.10} _{-0.07}	4.06 ^{+0.12} _{-0.08}	9.30 ^{+0.80} _{-1.00}	2.70 ± 0.50	9
Kepler-448	6820 ± 120	1.45 ± 0.09	1.63 ± 0.15	1.40 ± 0.50	66.43 ^{+1.00} _{-0.95}	105,50
MASCARA-1	7554 ± 150	1.72 ± 0.07	2.10 ± 0.20	1.00 ± 0.20	109.00 ± 3.00	106
MASCARA-2	8730 ⁺²⁵⁰ ₋₂₆₀	1.76 ^{+0.14} _{-0.20}	1.56 ^{+0.06} _{-0.06}	0.20 ^{+0.10} _{-0.05}	114.00 ± 3.00	107
MASCARA-3	6508 ± 49	1.46 ^{+0.06} _{-0.06}	1.51 ± 0.02	0.78 ^{+0.61} _{-0.42}	19.76 ± 0.16	108
MASCARA-4	7800 ± 200	1.75 ± 0.05	1.92 ± 0.11	0.70 ± -0.20	46.50 ± 1.00	109
NGTS-2	6450 ± 50	1.30 ± 0.03	1.62 ± 0.09	2.70 ± 0.20	15.91 ± 0.49	110
Qatar-1	4910 ± 100	0.84 ^{+0.04} _{-0.04}	0.80 ± 0.02	8.90 ± 3.70	1.70 ± 0.30	21,111
Qatar-2	4645 ± 50	0.73 ± 0.02	0.70 ± 0.01	9.40 ± 3.20	2.80 ± 0.50	112,113
TOI-1268	5257 ± 40	0.90 ± 0.13	0.86 ± 0.02	280.00 ± 90.00	4.30 ^{+0.55} _{-0.45}	114
TOI-1333	6274 ± 97	1.46 ^{+0.08} _{-0.08}	1.92 ^{+0.06} _{-0.06}	2.33 ^{+0.71} _{-0.56}	14.20 ± 0.50	115
TOI-1518	7300 ± 100	1.79 ± 0.26	1.95 ± 0.05	—	74.40 ± 2.30	116
TOI-2109	6540 ± 16	1.45 ± 0.07	1.70 ^{+0.06} _{-0.06}	1.77 ^{+0.88} _{-0.68}	81.20 ± 1.60	117
TOI-251	5875 ⁺¹⁰⁰ ₋₁₉₀	1.04 ^{+0.01} _{-0.01}	0.88 ^{+0.04} _{-0.05}	0.18 ± 0.14	11.50 ± 1.00	118
TOI-451	5550 ± 56	0.95 ± 0.02	0.88 ± 0.03	0.13 ± 0.01	7.90 ± 0.50	119
TOI-811	6107 ± 77	1.32 ^{+0.05} _{-0.07}	1.27 ^{+0.06} _{-0.09}	0.12 ^{+0.04} _{-0.04}	7.11 ± 0.50	120
TOI-852	5768 ⁺⁸⁴ ₋₈₁	1.32 ^{+0.05} _{-0.04}	1.71 ± 0.04	4.04 ^{+0.68} _{-0.76}	14.50 ± 0.50	120
TOI-942	4928 ⁺¹²⁵ ₋₈₅	0.79 ^{+0.04} _{-0.03}	1.02 ^{+0.02} _{-0.02}	0.09 ± 0.07	14.30 ± 0.50	118
TRAPPIST-1	2557 ± 47	0.09 ± 0.00	0.12 ± 0.00	7.60 ± 2.20	2.04 ± 0.18	121,122
TrES-1	5226 ± 50	0.89 ± 0.05	0.82 ± 0.02	3.70 ^{+3.40} _{-2.80}	1.30 ± 0.30	9,123
TrES-2	5850 ± 50	0.99 ± 0.06	0.96 ± 0.02	5.00 ^{+2.70} _{-2.10}	1.00 ± 0.60	9,124
TrES-4	6295 ± 65	1.45 ± 0.05	1.81 ± 0.08	2.20 ± 0.40	8.10 ± 1.10	9,125
V1298 Tau	4970 ± 120	1.13 ± 0.05	1.41 ^{+0.00} _{-0.02}	0.02 ± 0.00	24.77 ± 0.19	126,127,128
WASP-3	6340 ± 90	1.11 ^{+0.08} _{-0.06}	1.30 ^{+0.05} _{-0.04}	2.10 ± 1.20	13.90 ± 0.03	9,129
WASP-4	5540 ± 55	0.93 ± 0.06	0.91 ± 0.02	7.00 ± 2.90	2.14 ^{+0.38} _{-0.35}	7,130
WASP-5	5770 ± 65	1.03 ± 0.05	1.09 ± 0.04	5.60 ± 2.20	3.20 ± 0.30	9,131
WASP-6	5375 ± 65	0.84 ± 0.07	0.86 ± 0.03	11.00 ^{+3.00} _{-7.00}	1.60 ^{+0.27} _{-0.17}	9,132
WASP-7	6520 ± 70	1.32 ± 0.07	1.48 ± 0.09	2.40 ± 1.00	14.00 ± 2.00	133,134
WASP-8	5690 ± 36	1.09 ± 0.03	0.98 ± 0.02	4.00 ± 1.00	1.90 ± 0.05	135,136
WASP-11	4900 ± 65	0.81 ± 0.04	0.77 ± 0.01	7.60 ^{+5.80} _{-3.00}	1.04 ± 0.15	9,49
WASP-12	6313 ± 52	1.43 ^{+0.11} _{-0.09}	1.66 ^{+0.05} _{-0.04}	2.00 ^{+0.70} _{-2.00}	1.60 ^{+0.80} _{-0.40}	9,29
WASP-13	6025 ± 21	1.22 ± 0.12	1.66 ± 0.08	5.00 ^{+2.60} _{-1.70}	5.70 ± 0.40	9,137
WASP-14	6462 ± 75	1.30 ± 0.06	1.32 ^{+0.10} _{-0.07}	0.75 ± 0.25	2.80 ± 0.57	9,138
WASP-15	6573 ± 70	1.30 ± 0.05	1.52 ± 0.04	2.40 ^{+0.80} _{-1.00}	4.27 ^{+0.26} _{-0.36}	139,131
WASP-16	5630 ± 70	0.98 ± 0.05	1.09 ± 0.04	8.60 ^{+3.90} _{-3.80}	1.20 ^{+0.40} _{-0.50}	139
WASP-17	6550 ± 100	1.29 ± 0.08	1.58 ± 0.04	2.65 ± 0.25	14.67 ^{+0.81} _{-0.57}	9,131
WASP-18	6400 ± 70	1.29 ± 0.06	1.25 ± 0.03	1.00 ± 0.50	11.20 ± 0.60	9,29
WASP-19	5460 ± 90	0.94 ± 0.04	1.02 ± 0.01	9.95 ± 2.49	4.40 ± 0.90	7,29
WASP-20	5987 ± 20	1.11 ± 0.03	1.24 ± 0.04	7.00 ^{+2.00} _{-1.00}	4.75 ± 0.51	9,140
WASP-21	5924 ± 55	0.89 ± 0.08	1.14 ± 0.05	5.50 ± 2.00	0.66 ± 0.14	21,141
WASP-22	6153 ± 46	1.25 ^{+0.07} _{-0.03}	1.25 ± 0.03	4.30 ^{+1.60} _{-1.10}	4.40 ± 0.30	9,142
WASP-24	6107 ± 77	1.17 ± 0.07	1.32 ± 0.04	3.80 ^{+1.30} _{-1.20}	7.00 ± 0.90	9,143
WASP-25	5736 ± 35	1.05 ± 0.04	0.92 ± 0.02	0.02 ^{+3.96} _{-0.01}	2.90 ± 0.30	144,145
WASP-26	6015 ± 55	1.09 ± 0.05	1.28 ± 0.04	6.00 ± 2.00	2.20 ± 0.70	9,29
WASP-28	6084 ± 45	0.99 ± 0.07	1.08 ± 0.03	5.00 ^{+3.00} _{-2.00}	3.25 ± 0.34	140
WASP-30	6190 ± 50	1.25 ^{+0.03} _{-0.04}	1.39 ^{+0.03} _{-0.03}	3.40 ^{+0.30} _{-0.50}	12.10 ^{+0.40} _{-0.50}	146

Table 4 continued

Table 4 (*continued*)

System	T _{eff} (K)	M (M _⊕)	R (R _⊕)	age (Gyr)	v sin i (km s ⁻¹)	References
(1)	(2)	(3)	(4)	(5)	(6)	(7)
WASP-31	6175 ± 70	1.16 ± 0.03	1.25 ± 0.03	1.00 ^{+3.00} _{-0.50}	6.60 ± 0.60	9,145
WASP-32	6100 ± 100	1.10 ± 0.03	1.11 ± 0.05	2.22 ^{+0.62} _{-0.73}	3.90 ^{+0.40} _{-0.50}	9,147
WASP-33	7430 ± 100	1.56 ^{+0.04} _{-0.08}	1.51 ^{+0.02} _{-0.03}	0.10 ^{+0.40} _{-0.09}	86.63 ^{+0.32} _{-0.37}	148,149
WASP-38	6150 ± 80	1.20 ± 0.04	1.33 ^{+0.03} _{-0.03}	3.29 ^{+0.42} _{-0.53}	7.50 ^{+0.10} _{-0.20}	9,147
WASP-39	5485 ± 50	0.91 ± 0.05	0.94 ± 0.02	9.00 ^{+3.00} _{-4.00}	1.40 ± 0.25	9,25
WASP-41	5546 ± 33	0.99 ± 0.03	0.89 ± 0.01	9.80 ^{+2.30} _{-3.90}	1.60 ± 1.10	9,150
WASP-43	4520 ± 120	0.72 ± 0.03	0.67 ^{+0.01} _{-0.01}	7.00 ± 7.00	2.26 ± 0.54	9,46
WASP-47	5576 ± 67	1.04 ± 0.03	1.14 ± 0.01	6.70 ^{+1.50} _{-1.10}	1.80 ^{+0.24} _{-0.16}	151,152
WASP-52	5000 ± 100	0.80 ± 0.05	0.79 ± 0.02	10.70 ^{+1.90} _{-4.50}	2.62 ± 0.07	9,141
WASP-53	4950 ± 60	0.84 ± 0.05	0.80 ± 0.02	—	0.86 ± 0.21	153
WASP-60	6105 ± 50	1.23 ± 0.03	1.40 ± 0.07	1.70 ^{+0.90} _{-0.70}	2.97 ± 0.47	25
WASP-61	6250 ± 150	1.27 ± 0.06	1.39 ± 0.03	2.70 ^{+0.10} _{-0.60}	11.10 ± 0.70	154
WASP-62	6230 ± 80	1.25 ± 0.05	1.28 ± 0.05	0.80 ± 0.60	9.30 ± 0.20	154
WASP-66	6600 ± 150	1.30 ± 0.07	1.75 ± 0.09	3.70 ^{+0.70} _{-1.20}	12.10 ± 2.20	9,155
WASP-69	4700 ± 50	0.83 ± 0.03	0.81 ± 0.03	7.00 ± 7.00	2.20 ± 0.40	9,156
WASP-71	6180 ± 52	1.56 ± 0.06	2.26 ± 0.17	3.60 ^{+1.60} _{-1.00}	7.80 ^{+0.30} _{-0.40}	154
WASP-72	6250 ± 100	1.39 ± 0.06	1.98 ± 0.24	3.20 ± 0.60	5.00 ^{+1.40} _{-1.20}	157,158
WASP-74	5984 ± 57	1.19 ± 0.04	1.54 ± 0.03	3.49 ± 0.65	5.85 ± 0.50	159
WASP-76	6329 ± 65	1.46 ± 0.02	1.76 ± 0.07	1.82 ± 0.27	1.48 ± 0.28	160
WASP-78	6100 ± 150	1.39 ^{+0.09} _{-0.08}	2.35 ^{+0.10} _{-0.09}	2.80 ^{+1.60} _{-0.30}	7.10 ± 0.50	154
WASP-79	6600 ± 100	1.39 ± 0.08	1.51 ^{+0.04} _{-0.03}	1.40 ± 0.30	17.41 ^{+0.20} _{-0.12}	154,50
WASP-80	4145 ± 100	0.60 ± 0.04	0.59 ± 0.01	7.00 ± 7.00	1.27 ^{+0.14} _{-0.17}	9,161
WASP-84	5280 ± 80	0.85 ± 0.06	0.77 ± 0.02	2.10 ± 1.60	2.56 ± 0.08	162
WASP-85	5685 ± 65	1.09 ± 0.08	0.94 ± 0.02	0.50 ^{+0.30} _{-0.10}	3.41 ± 0.89	163,164
WASP-87	6450 ± 120	1.20 ± 0.09	1.63 ± 0.06	3.80 ± 0.80	9.80 ± 0.60	165,155
WASP-94A	6170 ± 80	1.45 ± 0.09	1.62 ^{+0.05} _{-0.04}	2.70 ± 0.60	4.20 ± 0.50	9,166
WASP-100	6940 ± 120	1.47 ^{+0.06} _{-0.05}	1.67 ^{+0.18} _{-0.11}	1.57 ^{+0.30} _{-0.20}	12.80 ^{+2.30} _{-2.20}	9,158
WASP-103	6110 ± 160	1.21 ^{+0.10} _{-0.12}	1.41 ^{+0.04} _{-0.05}	4.00 ± 1.00	6.50 ± 2.00	9,155
WASP-107	4425 ± 70	0.68 ^{+0.02} _{-0.02}	0.67 ± 0.02	6.90 ^{+3.70} _{-3.40}	2.50 ± 0.80	167,168
WASP-109	6520 ± 140	1.20 ± 0.09	1.35 ± 0.04	2.60 ± 0.90	18.90 ^{+2.40} _{-2.30}	158
WASP-111	6400 ± 150	1.50 ± 0.11	1.85 ± 0.10	2.60 ± 0.60	11.12 ± 0.77	165
WASP-117	6040 ± 90	1.13 ± 0.03	1.17 ^{+0.07} _{-0.06}	4.60 ± 2.00	1.46 ± 0.14	9,169
WASP-121	6586 ± 59	1.38 ± 0.02	1.44 ± 0.03	1.50 ± 1.00	13.56 ^{+0.69} _{-0.68}	170
WASP-127	5750 ± 100	0.95 ± 0.02	1.33 ± 0.03	9.66 ± 1.00	0.53 ^{+0.07} _{-0.05}	171
WASP-134	5700 ± 100	1.13 ± 0.04	1.18 ± 0.05	5.10 ± 1.60	2.08 ± 0.26	172
WASP-148	5437 ± 21	0.97 ^{+0.05} _{-0.06}	0.90 ^{+0.01} _{-0.01}	—	2.30 ^{+0.38} _{-0.34}	173
WASP-166	6050 ± 50	1.19 ± 0.06	1.22 ± 0.06	2.10 ± 0.90	5.10 ± 0.30	174
WASP-167	7043 ⁺⁸⁹ ₋₆₈	1.59 ± 0.08	1.79 ± 0.05	1.54 ± 0.40	49.94 ± 0.04	175
WASP-174	6400 ± 100	1.24 ± 0.04	1.35 ± 0.02	1.65 ± 0.85	16.50 ± 0.50	176
WASP-180	6600 ± 200	1.30 ± 0.10	1.19 ± 0.06	1.22 ± 0.99	19.60 ± 0.60	177
WASP-189	8000 ± 80	2.03 ± 0.07	2.36 ± 0.03	0.73 ± 0.13	100.00 ± 5.00	178
WASP-190	6400 ± 100	1.35 ± 0.05	1.60 ± 0.10	2.80 ± 0.40	13.30 ± 0.60	179
XO-2	5332 ± 57	0.96 ± 0.05	1.00 ^{+0.03} _{-0.03}	7.80 ^{+1.20} _{-1.30}	1.07 ± 0.09	9,180
XO-3	6429 ± 75	1.21 ± 0.06	1.41 ± 0.06	2.82 ^{+0.58} _{-0.82}	18.40 ± 0.80	9,181
XO-4	6397 ± 70	1.29 ^{+0.03} _{-0.03}	1.55 ^{+0.04} _{-0.03}	2.10 ± 0.60	8.90 ± 0.50	182,183
XO-6	6720 ± 100	1.47 ± 0.06	1.93 ± 0.18	1.88 ^{+0.90} _{-0.20}	48.00 ± 3.00	184
pi Men	5998 ± 62	1.07 ± 0.04	1.17 ± 0.02	2.98 ^{+1.40} _{-0.30}	3.16 ± 0.27	185,186

NOTE— All data is taken from TEPCat (Southworth 2011) or the following references: 1 (Plavchan et al. 2020), 2 (Hirano et al. 2020a), 3 (Kervella et al. 2004), 4 (Lacour et al. 2021), 5 (Zuckerman et al. 2001), 6 (Royer et al. 2007), 7 (Maxted et al. 2015), 8 (Czesla et al. 2012), 9 (Bonomo et al. 2017), 10 (Triaud et al. 2009), 11 (Gandolfi et al. 2010), 12 (Gandolfi et al. 2012), 13 (Hébrard et al. 2011b), 14 (Newton et al. 2019), 15 (Zhou et al. 2020), 16 (Yu et al. 2018), 17 (Bailer-Jones et al. 2018), 18 (Stefansson et al. 2022), 19 (Bonfils et al.

Note— All data is taken from TEPCat (Southworth 2011) or the following references: 1 (Plavchan et al. 2020), 2 (Hirano et al. 2020a), 3 (Kervella et al. 2004), 4 (Lacour et al. 2021), 5 (Zuckerman et al.

2012), 20 (Bourrier et al. 2018), 21 (Bonfanti et al. 2015), 22 (Johnson et al. 2008), 23 (Pál et al. 2010), 24 (Loeillet et al. 2008), 25 (Mancini et al. 2018), 26 (Kovács et al. 2007), 27 (Winn et al. 2011), 28 (Noyes et al. 2008), 29 (Albrecht et al. 2012b), 30 (Lund et al. 2014), 31 (Latham et al. 2009), 32 (Moutou et al. 2011), 33 (Shporer et al. 2009), 34 (Bakos et al. 2010), 35 (Winn et al. 2010b), 36 (Hartman et al. 2009), 37 (Bakos et al. 2009), 38 (Winn et al. 2010c), 39 (Torres et al. 2010), 40 (Buchhave et al. 2010), 41 (Howard et al. 2012), 42 (Fulton et al. 2013), 43 (Hartman et al. 2011), 44 (Esposito et al. 2014), 45 (Bakos et al. 2011), 46 (Esposito et al. 2017), 47 (Kipping et al. 2010), 48 (Johnson et al. 2011), 49 (Mancini et al. 2015), 50 (Johnson et al. 2017), 51 (Zhou et al. 2016a), 52 (Zhou et al. 2019a), 53 (Mohler-Fischer et al. 2013), 54 (Addison et al. 2014), 55 (Zhou et al. 2019b), 56 (Dalba et al. 2020), 57 (Knudstrup & Albrecht 2022), 58 (Christiansen et al. 2017), 59 (Dalaal et al. 2019), 60 (Nutzman et al. 2011), 61 (Narita et al. 2009b), 62 (Mann et al. 2020), 63 (Liu et al. 2018), 64 (Hébrard et al. 2010), 65 (Crossfield et al. 2017), 66 (Zhou et al. 2018), 67 (Cegla et al. 2016), 68 (Santos et al. 2020), 69 (Rizzuto et al. 2020), 70 (Heitzmann et al. 2021), 71 (Mann et al. 2016), 72 (Stefansson et al. 2020), 73 (Santerne et al. 2016), 74 (Hirano et al. 2016), 75 (Korth et al. 2019), 76 (Rice et al. 2021), 77 (Brahm et al. 2018), 78 (Wang et al. 2021), 79 (Hjorth et al. 2019a), 80 (Siverd et al. 2012), 81 (Damasso et al. 2015a), 82 (Bieryla et al. 2015), 83 (Gaudi et al. 2017), 84 (Wyttenbach et al. 2020), 85 (Zhou et al. 2016b), 86 (Siverd et al. 2018), 87 (Johnson et al. 2018), 88 (Rodríguez Martínez et al. 2020), 89 (Holman et al. 2010), 90 (Wang et al. 2018), 91 (Szabó et al. 2011), 92 (Howarth & Morello 2017), 93 (Désert et al. 2011), 94 (Benomar et al. 2014), 95 (Albrecht et al. 2013), 96 (Sanchis-Ojeda et al. 2012), 97 (Fabrycky et al. 2012), 98 (Chaplin et al. 2013), 99 (Huber et al. 2013), 100 (Sanchis-Ojeda et al. 2013), 101 (Hirano et al. 2012), 102 (Kamiaka et al. 2019), 103 (Van Eylen et al. 2014), 104 (Santerne et al. 2014), 105 (Bourrier et al. 2015), 106 (Talens

et al. 2017), 107 (Lund et al. 2017), 108 (Rodríguez et al. 2019), 109 (Dorval et al. 2020), 110 (Anderson et al. 2018b), 111 (Covino et al. 2013), 112 (Močnik et al. 2017), 113 (Bryan et al. 2012), 114 (Dong et al. 2022), 115 (Rodríguez et al. 2021), 116 (Cabot et al. 2021), 117 (Wong et al. 2021), 118 (Zhou et al. 2021), 119 (Newton et al. 2021), 120 (Carmichael et al. 2021), 121 (Burgasser & Mamajek 2017), 122 (Hirano et al. 2020b), 123 (Narita et al. 2007), 124 (Winn et al. 2008), 125 (Narita et al. 2010b), 126 (David et al. 2019b), 127 (Johnson et al. 2022), 128 (David et al. 2019a), 129 (Miller et al. 2010), 130 (Sanchis-Ojeda et al. 2011), 131 (Triaud et al. 2010), 132 (Gillon et al. 2009), 133 (Southworth et al. 2011), 134 (Albrecht et al. 2012a), 135 (Queloz et al. 2010), 136 (Bourrier et al. 2017), 137 (Brothwell et al. 2014), 138 (Johnson et al. 2009), 139 (Southworth et al. 2013), 140 (Anderson et al. 2015a), 141 (Chen et al. 2020), 142 (Anderson et al. 2011a), 143 (Simpson et al. 2011), 144 (Enoch et al. 2011), 145 (Brown et al. 2012a), 146 (Triaud et al. 2013), 147 (Brown et al. 2012b), 148 (Moya et al. 2011), 149 (Johnson et al. 2015), 150 (Southworth et al. 2016), 151 (Vanderburg et al. 2017), 152 (Sanchis-Ojeda et al. 2015), 153 (Triaud et al. 2017), 154 (Brown et al. 2017), 155 (Addison et al. 2016), 156 (Casasayas-Barris et al. 2017), 157 (Gillon et al. 2013), 158 (Addison et al. 2018), 159 (Luque et al. 2020), 160 (Ehrenreich et al. 2020), 161 (Triaud et al. 2015), 162 (Anderson et al. 2015b), 163 (Brown 2014), 164 (Močnik et al. 2016), 165 (Anderson et al. 2014), 166 (Neveu-VanMalle et al. 2014), 167 (Piaulet et al. 2021), 168 (Anderson et al. 2017), 169 (Carone et al. 2021), 170 (Bourrier et al. 2020), 171 (Allart et al. 2020), 172 (Anderson et al. 2018a), 173 (Wang et al. 2022), 174 (Hellier et al. 2019), 175 (Temple et al. 2017), 176 (Temple et al. 2018), 177 (Temple et al. 2019a), 178 (Anderson et al. 2018c), 179 (Temple et al. 2019b), 180 (Damasso et al. 2015b), 181 (Hirano et al. 2011a), 182 (McCullough et al. 2008), 183 (Narita et al. 2010a), 184 (Crouzet et al. 2017), 185 (Huang et al. 2018), 186 (Kunovac Hodžić et al. 2021)

Table 5. Key properties of planets for which λ , i , or both angles were determined. In the reference column, the boldface number refers to the work from which we drew the λ measurement. The other numbers refer to works reporting additional measurements of λ or other system parameters not taken from [TEPCat](#) (Southworth 2011). Stellar parameters are given in Table 4. For a few systems, obliquities have been measured with respect to more than one planetary orbit, but in this table we display only a single measurement. The multi-planetary systems are separately listed in Table § 2.

Planet	a/R	m	r	e	λ	i	ψ	References
		(M_Jupiter)	(R_Jupiter)		(°)	(°)	(°)	
(1)	(2)	(3)	(4)	(5)	(6)	(7)	(8)	(9)
AU Mich	$18.92^{+2.15}_{-2.42}$	0.05 ± 0.01	0.38 ± 0.02	$0.100^{+0.170}_{-0.090}$	$4.7^{+6.4}_{-6.8}$	$90.0^{+0.0}_{-19.5}$	$12.1^{+11.3}_{-7.5}$	1,2,3,4,5
Beta PICb	1141.92 ± 3.47	$11.90^{+2.93}_{-3.04}$	1.46 ± 0.01	0.103 ± 0.030	3.0 ± 5.0	—	—	6,7,8
CoRoT-2b	6.77 ± 0.18	3.57 ± 0.15	1.46 ± 0.03	$0.000^{+0.024}_{-0.000}$	$1.0^{+7.7}_{-6.0}$	$90.0^{+0.0}_{-10.8}$	$8.9^{+6.7}_{-5.1}$	9,10,2,11,12,13
CoRoT-3b	$7.90^{+0.49}_{-0.48}$	21.96 ± 0.70	1.04 ± 0.07	$0.000^{+0.016}_{-0.000}$	$37.6^{+10.0}_{-22.3}$	—	—	9,14
CoRoT-11b	6.89 ± 0.40	2.34 ± 0.39	1.43 ± 0.06	$0.000^{+0.360}_{-0.000}$	0.1 ± 2.6	—	—	9,15
CoRoT-18b	$7.01^{+0.28}_{-0.31}$	3.30 ± 0.19	$1.15^{+0.04}_{-0.05}$	$0.000^{+0.025}_{-0.000}$	10.0 ± 20.0	$90.0^{+0.0}_{-23.2}$	$25.4^{+13.6}_{-13.1}$	9,16,2
DS Tucb	$16.08^{+0.32}_{-0.28}$	$0.09^{+0.11}_{-0.04}$	0.50 ± 0.02	0	$2.9^{+0.9}_{-0.9}$	$90.0^{+0.0}_{-7.3}$	$4.0^{+4.6}_{-1.6}$	17,18,2,19
EPIC 246851721b	$9.59^{+0.23}_{-0.23}$	$3.00^{+1.10}_{-1.20}$	$1.00^{+0.05}_{-0.05}$	0	1.5 ± 0.9	$90.0^{+0.0}_{-12.4}$	$2.9^{+10.8}_{-1.6}$	20,2
GJ 3470 b	$13.84^{+0.51}_{-0.46}$	0.04 ± 0.01	0.35 ± 0.03	$0.126^{+0.042}_{-0.041}$	$101.0^{+29.0}_{-14.0}$	$51.0^{+25.0}_{-21.0}$	$97.0^{+16.0}_{-11.0}$	21,22
GJ 436b	$14.56^{+0.84}_{-0.81}$	$0.08^{+0.01}_{-0.01}$	0.37 ± 0.01	$0.162^{+0.004}_{-0.003}$	$72.0^{+33.0}_{-24.0}$	$37.3^{+16.2}_{-12.5}$	$80.0^{+21.0}_{-18.0}$	23
HAT-P-1b	$10.19^{+0.27}_{-0.28}$	0.53 ± 0.02	1.32 ± 0.02	$0.000^{+0.011}_{-0.000}$	3.7 ± 2.1	—	—	9,24
HAT-P-2b	8.63 ± 0.78	8.74 ± 0.27	1.19 ± 0.12	$0.508^{+0.001}_{-0.001}$	$0.2^{+12.2}_{-12.5}$	—	—	9,25,26,27
HAT-P-3b	9.81 ± 0.31	0.59 ± 0.02	0.91 ± 0.03	$0.000^{+0.010}_{-0.000}$	21.2 ± 8.7	—	—	9,28
HAT-P-4b	$6.00^{+0.47}_{-0.19}$	$0.68^{+0.05}_{-0.03}$	$1.34^{+0.08}_{-0.04}$	$0.000^{+0.007}_{-0.000}$	4.9 ± 11.9	—	—	9,29
HAT-P-6b	7.43 ± 0.37	1.06 ± 0.06	1.40 ± 0.08	$0.000^{+0.044}_{-0.000}$	165.0 ± 6.0	—	—	9,27,30
HAT-P-7b	4.05 ± 0.04	1.87 ± 0.03	1.53 ± 0.01	$0.000^{+0.004}_{-0.000}$	$142.0^{+12.0}_{-16.0}$	$0.0^{+36.0}_{-0.0}$	97.0 ± 14.0	9,31,32,33,27,34
HAT-P-8b	6.40 ± 0.20	1.27 ± 0.05	1.32 ± 0.04	$0.000^{+0.006}_{-0.000}$	$17.0^{+11.5}_{-9.2}$	—	—	9,35,36

Table 5 continued

Table 5 (continued)

Planet	a/R	m	r	e	λ	i	ψ	References
		(M _{Jupiter})	(R _{Jupiter})		(°)	(°)	(°)	
(1)	(2)	(3)	(4)	(5)	(6)	(7)	(8)	(9)
WASP-18b	3.52 ± 0.09	10.52 ± 0.32	1.20 ± 0.03	0.008 ± 0.001	13.0 ± 7.0	—	—	9,27
WASP-19b	3.45 ± 0.07	1.14 ± 0.04	1.41 ± 0.02	0.000 ^{+0.006} _{-0.000}	1.0 ± 1.2	90.0 ^{+0.0} _{-29.2}	3.7 ^{+28.0} _{-2.3}	9,167,2,27,168,169
WASP-20b	10.13 ± 0.38	0.40 ± 0.05	1.38 ± 0.06	0.000 ^{+0.039} _{-0.000}	12.7 ± 4.2	—	—	9,170
WASP-21b	9.45 ± 0.51	0.28 ± 0.02	1.16 ± 0.05	0.000 ^{+0.048} _{-0.000}	8.0 ^{+26.0} _{-27.0}	—	—	9,171
WASP-22b	8.38 ± 0.26	0.62 ^{+0.03} _{-0.02}	1.20 ^{+0.05} _{-0.03}	0.000 ^{+0.021} _{-0.000}	22.0 ± 16.0	—	—	9,172
WASP-24b	5.94 ± 0.22	1.11 ± 0.05	1.30 ± 0.05	0.000 ^{+0.005} _{-0.000}	4.7 ± 4.0	—	—	9,36
WASP-25b	11.22 ± 0.26	0.60 ± 0.05	1.25 ± 0.03	0.000 ^{+0.083} _{-0.000}	14.6 ± 6.7	—	—	9,163
WASP-26b	6.64 ± 0.21	1.02 ± 0.03	1.22 ± 0.05	0.000 ^{+0.004} _{-0.000}	34.0 ^{+26.0} _{-36.0}	—	—	9,27
WASP-28b	8.78 ± 0.28	0.89 ± 0.06	1.22 ± 0.03	0.000 ^{+0.058} _{-0.000}	8.0 ± 18.0	—	—	9,170,173
WASP-30b	8.57 ^{+0.22} _{-0.17}	62.50 ± 1.20	0.95 ^{+0.03} _{-0.02}	0.000 ^{+0.004} _{-0.000}	7.0 ^{+19.0} _{-27.0}	—	—	174
WASP-31b	8.00 ± 0.22	0.48 ± 0.03	1.55 ± 0.05	0.000 ^{+0.047} _{-0.000}	2.8 ± 3.1	—	—	9,163,27
WASP-32b	7.63 ± 0.35	3.60 ± 0.07	1.18 ± 0.07	0.000 ^{+0.004} _{-0.000}	10.5 ^{+6.4} _{-6.5}	54.5 ^{+17.9} _{-11.0}	35.8 ^{+10.2} _{-17.2}	9,175,2,160
WASP-33b	3.69 ^{+0.05} _{-0.10}	2.16 ± 0.20	1.68 ^{+0.02} _{-0.03}	0	112.9 ^{+0.2} _{-0.2}	37.5 ^{+6.8} _{-5.7}	104.1 ^{+2.8} _{-2.8}	176,2,95,177,178
WASP-38b	12.15 ^{+0.30} _{-0.26}	2.69 ± 0.06	1.09 ^{+0.03} _{-0.03}	0.028 ^{+0.003} _{-0.003}	7.5 ^{+4.7} _{-6.1}	—	—	9,175,36
WASP-39b	11.06 ± 0.32	0.28 ± 0.03	1.28 ± 0.04	0.000 ^{+0.048} _{-0.000}	0.0 ± 11.0	—	—	9,28
WASP-41b	9.95 ± 0.18	0.98 ± 0.03	1.18 ± 0.02	0.000 ^{+0.120} _{-0.000}	6.0 ± 11.0	62.0 ^{+28.0} _{-16.5}	22.6 ^{+28.9} _{-11.9}	9,179,2,180
WASP-43b	4.92 ^{+0.09} _{-0.10}	2.03 ^{+0.05} _{-0.05}	1.04 ± 0.02	0.000 ^{+0.006} _{-0.000}	3.5 ± 6.8	90.0 ^{+0.0} _{-27.8}	12.7 ^{+19.7} _{-7.7}	9,46,2
WASP-47b	9.67 ± 0.15	1.14 ± 0.02	1.12 ± 0.01	0.028 ^{+0.004} _{-0.002}	0.0 ± 24.0	—	—	181
WASP-52b	7.23 ± 0.21	0.43 ± 0.02	1.25 ± 0.03	0.000 ^{+0.092} _{-0.000}	1.1 ± 1.1	90.0 ^{+0.0} _{-11.1}	2.8 ^{+9.8} _{-1.8}	9,171,2,182,183
WASP-53b	11.05 ^{+0.39} _{-0.40}	2.13 ^{+0.09} _{-0.09}	1.07 ± 0.04	0.000 ^{+0.030} _{-0.000}	1.0 ± 12.0	—	—	184
WASP-60b	8.51 ± 0.41	0.56 ± 0.04	1.23 ± 0.07	0.000 ^{+0.064} _{-0.000}	129.0 ± 17.0	—	—	9,28
WASP-61b	8.06 ± 0.21	2.06 ± 0.16	1.22 ± 0.03	0.000 ^{+0.074} _{-0.000}	4.0 ^{+17.1} _{-18.4}	—	—	9,185
WASP-62b	9.53 ± 0.39	0.57 ± 0.04	1.39 ± 0.06	0.006 ± 0.001	19.4 ^{+5.1} _{-4.9}	73.0 ^{+12.2} _{-6.4}	25.0 ^{+6.6} _{-6.2}	186,185,2
WASP-66b	6.71 ± 0.36	2.32 ± 0.13	1.39 ± 0.09	0.000 ^{+0.046} _{-0.000}	4.0 ± 22.0	—	—	9,187
WASP-69b	11.97 ± 0.44	0.26 ± 0.02	1.06 ± 0.05	0.000 ^{+0.110} _{-0.000}	0.4 ^{+2.0} _{-1.9}	90.0 ^{+0.0} _{-21.5}	3.8 ^{+18.5} _{-2.7}	9,188,2
WASP-71b	4.40 ± 0.34	2.24 ± 0.08	1.46 ± 0.13	0.000 ^{+0.019} _{-0.000}	1.9 ^{+7.5} _{-7.1}	—	—	9,185,189
WASP-72b	4.03 ± 0.49	1.46 ^{+0.06} _{-0.06}	1.27 ± 0.20	0.000 ^{+0.017} _{-0.000}	7.0 ^{+12.0} _{-11.0}	—	—	9,190
WASP-74b	4.82 ± 0.09	0.83 ± 0.02	1.40 ± 0.02	0.000 ^{+0.030} _{-0.000}	0.8 ± 1.0	—	—	9,191
WASP-76b	4.02 ± 0.16	0.89 ^{+0.02} _{-0.01}	1.85 ^{+0.08} _{-0.08}	0.000 ^{+0.050} _{-0.000}	61.3 ^{+7.6} _{-5.1}	9.1 ^{+2.4} _{-2.1}	85.7 ^{+2.5} _{-2.4}	192,2,185
WASP-78b	3.36 ^{+0.16} _{-0.15}	0.86 ± 0.08	2.06 ± 0.10	0.000 ^{+0.092} _{-0.000}	6.4 ± 5.9	—	—	9,185
WASP-79b	7.39 ^{+0.23} _{-0.19}	0.86 ± 0.08	1.53 ± 0.04	0.000 ^{+0.066} _{-0.000}	99.1 ^{+3.9} _{-4.1}	—	—	9,49,185,193
WASP-80b	12.62 ± 0.35	0.56 ± 0.03	0.99 ± 0.02	0.000 ^{+0.020} _{-0.000}	14.0 ± 14.0	—	—	9,194
WASP-84b	21.70 ± 0.72	0.69 ± 0.03	0.98 ± 0.03	0.000 ^{+0.077} _{-0.000}	0.3 ± 1.7	71.4 ^{+13.7} _{-7.1}	18.6 ^{+4.4} _{-15.7}	9,195,2
WASP-85b	8.97 ± 0.32	1.26 ± 0.07	1.24 ± 0.03	0	0.0 ± 14.0	90.0 ^{+0.0} _{-31.3}	22.1 ^{+17.4} _{-12.1}	196,2
WASP-87b	3.89 ± 0.18	2.18 ± 0.15	1.39 ± 0.06	0.000 ^{+0.099} _{-0.000}	8.0 ± 11.0	—	—	187
WASP-94Ab	7.30 ^{+0.26} _{-0.22}	0.45 ^{+0.04} _{-0.03}	1.72 ^{+0.06} _{-0.05}	0.000 ^{+0.130} _{-0.000}	151.0 ^{+16.0} _{-23.0}	33.1 ^{+8.8} _{-7.1}	116.6 ^{+9.9} _{-9.1}	197,2
WASP-100b	5.54 ^{+0.88} _{-0.53}	2.03 ± 0.12	1.40 ^{+0.20} _{-0.30}	0.000 ^{+0.044} _{-0.000}	79.0 ^{+19.0} _{-10.0}	—	—	9,190
WASP-103b	3.01 ^{+0.12} _{-0.14}	1.47 ^{+0.11} _{-0.13}	1.65 ^{+0.05} _{-0.06}	0.000 ^{+0.150} _{-0.000}	3.0 ± 33.0	—	—	9,187
WASP-107b	17.75 ± 0.67	0.10 ± 0.01	0.92 ± 0.02	0.060 ± 0.040	112.6 ^{+24.9} _{-20.6}	28.2 ^{+40.4} _{-20.0}	92.6 ^{+30.7} _{-18.8}	198,199,200
WASP-109b	7.40 ± 0.30	0.91 ± 0.13	1.44 ± 0.05	0.000 ^{+0.320} _{-0.000}	99.0 ^{+10.0} _{-9.0}	—	—	190
WASP-111b	4.55 ± 0.27	1.83 ± 0.15	1.44 ± 0.09	0.000 ^{+0.100} _{-0.000}	5.0 ± 16.0	—	—	201
WASP-117b	17.39 ^{+1.01} _{-0.89}	0.28 ± 0.01	1.02 ^{+0.08} _{-0.07}	0.300 ± 0.026	46.9 ^{+4.8} _{-5.5}	—	—	9,202,203
WASP-121b	3.80 ^{+0.11} _{-0.11}	1.18 ^{+0.06} _{-0.06}	1.86 ± 0.04	0.000 ^{+0.070} _{-0.000}	87.2 ^{+0.4} _{-0.4}	39.8 ^{+7.4} _{-6.3}	88.1 ± 0.2	204,205,206
WASP-127b	8.39 ± 0.19	0.17 ^{+0.02} _{-0.02}	1.31 ^{+0.03} _{-0.03}	0	128.4 ^{+5.5} _{-5.6}	—	—	207,208
WASP-134b	17.50 ± 0.85	1.41 ± 0.07	0.99 ± 0.06	0.145 ± 0.009	43.7 ± 9.9	—	—	209
WASP-148b	19.80 ± 1.50	0.35 ^{+0.05} _{-0.05}	0.80 ^{+0.02} _{-0.02}	0.351 ^{+0.060} _{-0.064}	8.2 ^{+9.7} _{-8.7}	—	—	210,211
WASP-166b	11.32 ± 0.56	0.10 ± 0.00	0.63 ± 0.03	0.000 ^{+0.070} _{-0.000}	3.0 ± 5.0	90.0 ^{+0.0} _{-23.8}	10.1 ^{+16.7} _{-5.9}	212,2
WASP-167b	4.38 ± 0.14	0.00 ^{+8.00} _{-0.00}	1.56 ± 0.05	0	165.0 ± 5.0	35.0 ^{+5.2} _{-4.6}	123.8 ^{+11.6} _{-10.6}	213,2
WASP-174b	8.79 ± 0.15	0.33 ± 0.09	1.44 ± 0.05	0	31.0 ± 1.0	—	—	214

Table 5 continued

Table 5 (*continued*)

Planet	a/R	m	r	e	λ	i	ψ	References
		(M _{Jupiter})	(R _{Jupiter})		(°)	(°)	(°)	
(1)	(2)	(3)	(4)	(5)	(6)	(7)	(8)	(9)
WASP-180b	8.67 ± 0.47	0.80 ± 0.10	1.29 ± 0.07	0	162.0 ± 5.0	—	—	215
WASP-189b	4.60 ± 0.11	1.99 ^{+0.16} _{-0.14}	1.62 ± 0.02	0	89.3 ± 1.4	75.5 ^{+3.1} _{-2.2}	87.4 ^{+5.0} _{-4.0}	216,217,2,218
WASP-190b	8.91 ± 0.57	1.00 ± 0.10	1.15 ± 0.09	0	21.0 ± 6.0	—	—	219
XO-2b	7.79 ^{+0.36} _{-0.59}	0.60 ± 0.02	1.02 ± 0.03	0.000 ^{+0.006} _{-0.000}	7.0 ± 11.0	64.6 ^{+19.2} _{-9.6}	26.5 ^{+11.8} _{-13.7}	9,220,2,221
XO-3b	6.91 ± 0.30	11.83 ± 0.38	1.25 ± 0.05	0.276 ^{+0.001} _{-0.001}	37.3 ± 3.0	—	—	9,222,223,224
XO-4b	7.68 ± 0.11	1.61 ± 0.10	1.32 ^{+0.04} _{-0.03}	0.000 ^{+0.004} _{-0.000}	46.7 ^{+6.1} _{-8.1}	—	—	225,9
XO-6b	8.08 ± 1.03	2.01 ± 0.71	2.08 ± 0.18	0	20.7 ± 2.3	62.3 ^{+17.4} _{-9.3}	23.3 ^{+14.3} _{-2.9}	226,2
pi Men b	12.50 ± 0.26	0.04 ± 0.00	0.19 ± 0.00	0	24.0 ± 4.1	79.7 ^{+10.3} _{-11.4}	26.9 ^{+5.8} _{-4.7}	227,228

NOTE—All data is taken from TEPCat (Southworth 2011) or the following references: 1 (Hirano et al. 2020a), 2 (Albrecht et al. 2021), 3 (Martoli et al. 2020), 4 (Palle et al. 2020), 5 (Addison et al. 2021), 6 (Lacour et al. 2021), 7 (Chilcote et al. 2017), 8 (Kraus et al. 2020), 9 (Bonomo et al. 2017), 10 (Czesla et al. 2012), 11 (Bouchy et al. 2008), 12 (Nutzman et al. 2011), 13 (Gillon et al. 2010), 14 (Triaud et al. 2009), 15 (Gandolfi et al. 2012), 16 (Hébrard et al. 2011b), 17 (Zhou et al. 2020), 18 (Chen & Kipping 2017), 19 (Benatti et al. 2021), 20 (Yu et al. 2018), 21 (Stefansson et al. 2022), 22 (Biddle et al. 2014), 23 (Bourrier et al. 2018), 24 (Johnson et al. 2008), 25 (Loeillet et al. 2008), 26 (Winn et al. 2007), 27 (Albrecht et al. 2012b), 28 (Mancini et al. 2018), 29 (Winn et al. 2011), 30 (Hébrard et al. 2011a), 31 (Masuda 2015), 32 (Lund et al. 2014), 33 (Winn et al. 2009a), 34 (Narita et al. 2009a), 35 (Moutou et al. 2011), 36 (Simpson et al. 2011), 37 (Winn et al. 2010b), 38 (Sanchis-Ojeda & Winn 2011), 39 (Hirano et al. 2011b), 40 (Sanchis-Ojeda et al. 2011), 41 (Deming et al. 2011), 42 (Hardy et al. 2017), 43 (Winn et al. 2010c), 44 (Fulton et al. 2013), 45 (Esposito et al. 2014), 46 (Esposito et al. 2017), 47 (Johnson et al. 2011), 48 (Mancini et al. 2015), 49 (Johnson et al. 2017), 50 (Zhou et al. 2016a), 51 (Zhou et al. 2019a), 52 (Mohler-Fischer et al. 2013), 53 (Addison et al. 2014), 54 (Zhou et al. 2019b), 55 (Bello-Arufe et al. 2022), 56 (Dalba et al. 2020), 57 (Knudstrup & Albrecht 2022), 58 (Sedaghati et al. 2022), 59 (Dalaal et al. 2019), 60 (Narita et al. 2009b), 61 (Narita et al. 2008), 62 (Cochran et al. 2008), 63 (Barbieri et al. 2009), 64 (Dai et al. 2020), 65 (Mann et al. 2020), 66 (Hébrard et al. 2010), 67 (Moutou et al. 2009), 68 (Pont et al. 2009), 69 (Winn et al. 2009c), 70 (Zhou et al. 2018), 71 (Wolf et al. 2007), 72 (Cegla et al. 2016), 73 (Collier Cameron et al. 2010a), 74 (Winn et al. 2006), 75 (Santos et al. 2020), 76 (Queloz et al. 2000), 77 (Winn et al. 2005), 78 (Heitzmann et al. 2021), 79 (Rizzuto et al. 2020), 80 (Stefansson et al. 2020), 81 (Gaidos et al. 2020), 82 (Santerne et al. 2016), 83 (Hirano et al. 2016), 84 (Rice et al. 2021), 85 (Korth et al. 2019), 86 (Brahm et al. 2018), 87 (Wang et al. 2021), 88 (Hjorth et al. 2019a), 89 (Hjorth et al. 2021), 90 (Siverd et al. 2012), 91 (Damasso et al. 2015a), 92 (Bieryla et al. 2015), 93 (Wyttensbach et al. 2020), 94 (Ahlers et al. 2020b), 95 (Stephan et al. 2022), 96 (Borsa et al. 2019), 97 (Zhou et al. 2016b), 98 (Siverd et al. 2018), 99 (Johnson et al. 2018), 100 (Rodríguez Martínez et al. 2020), 101 (Jenkins et al. 2010), 102 (Wang et al. 2018), 103 (Howarth & Morello 2017), 104 (Barnes et al. 2011), 105 (Johnson et al. 2014), 106 (Herman et al. 2018), 107 (Désert et al. 2011), 108 (Albrecht et al. 2013), 109 (Campante et al. 2016), 110 (Benomar et al. 2014), 111 (Sanchis-Ojeda et al. 2012), 112 (Chaplin et al. 2013), 113 (Huber et al. 2013),

114 (Sanchis-Ojeda et al. 2013), 115 (Hirano et al. 2012), 116 (Marcy et al. 2014), 117 (Kamiaka et al. 2019), 118 (Van Eylen et al. 2014), 119 (Santerne et al. 2014), 120 (Quinn et al. 2015), 121 (Masuda 2017), 122 (Bourrier et al. 2015), 123 (Talens et al. 2017), 124 (Hooton et al. 2022), 125 (Lund et al. 2017), 126 (Talens et al. 2018), 127 (Rodriguez et al. 2019), 128 (Hjorth et al. 2019b), 129 (Dorval et al. 2020), 130 (Ahlers et al. 2020a), 131 (Anderson et al. 2018b), 132 (Covino et al. 2013), 133 (Močnik et al. 2017), 134 (Dong et al. 2022), 135 (Šubjak et al. 2022), 136 (Rodriguez et al. 2021), 137 (Cabot et al. 2021), 138 (Wong et al. 2021), 139 (Zhou et al. 2021), 140 (Newton et al. 2021), 141 (Carmichael et al. 2021), 142 (Wirth et al. 2021), 143 (Hirano et al. 2020b), 144 (Narita et al. 2007), 145 (Winn et al. 2008), 146 (Narita et al. 2010b), 147 (Johnson et al. 2022), 148 (David et al. 2019a), 149 (Gaidos et al. 2022), 150 (Miller et al. 2010), 151 (Simpson et al. 2010), 152 (Tripathi et al. 2010), 153 (Oshagh et al. 2013), 154 (Triaud et al. 2010), 155 (Tregloan-Reed et al. 2015), 156 (Gillon et al. 2009), 157 (Albrecht et al. 2012a), 158 (Bourrier et al. 2017), 159 (Queloz et al. 2010), 160 (Brothwell et al. 2014), 161 (Johnson et al. 2009), 162 (Joshi et al. 2009), 163 (Brown et al. 2012a), 164 (Anderson et al. 2011b), 165 (Bayliss et al. 2010), 166 (Anderson et al. 2010), 167 (Tregloan-Reed et al. 2013), 168 (Hellier et al. 2011), 169 (Sedaghati et al. 2021), 170 (Anderson et al. 2015a), 171 (Chen et al. 2020), 172 (Anderson et al. 2011a), 173 (Močnik et al. 2020), 174 (Triaud et al. 2013), 175 (Brown et al. 2012b), 176 (Johnson et al. 2015), 177 (Collier Cameron et al. 2010b), 178 (Watanabe et al. 2022), 179 (Southworth et al. 2016), 180 (Neveu-VanMalle et al. 2016), 181 (Sanchis-Ojeda et al. 2015), 182 (Hébrard et al. 2013), 183 (Mancini et al. 2017), 184 (Triaud et al. 2017), 185 (Brown et al. 2017), 186 (Garhart et al. 2020), 187 (Addison et al. 2016), 188 (Casasayas-Barris et al. 2017), 189 (Smith et al. 2013), 190 (Addison et al. 2018), 191 (Luque et al. 2020), 192 (Ehrenreich et al. 2020), 193 (Addison et al. 2013), 194 (Triaud et al. 2015), 195 (Anderson et al. 2015b), 196 (Močnik et al. 2016), 197 (Neveu-VanMalle et al. 2014), 198 (Piaulet et al. 2021), 199 (Rubenzahl et al. 2021), 200 (Dai & Winn 2017), 201 (Anderson et al. 2014), 202 (Carone et al. 2021), 203 (Lendl et al. 2014), 204 (Bourrier et al. 2020), 205 (Delrez et al. 2016), 206 (Borsa et al. 2021), 207 (Allart et al. 2020), 208 (Cristó et al. 2022), 209 (Anderson et al. 2018a), 210 (Hébrard et al. 2020), 211 (Wang et al. 2022), 212 (Hellier et al. 2019), 213 (Temple et al. 2017), 214 (Temple et al. 2018), 215 (Temple et al. 2019a), 216 (Anderson et al. 2018c), 217 (Lendl et al. 2020), 218 (Deline et al. 2022), 219 (Temple et al. 2019b), 220 (Damasso et al. 2015b), 221 (Narita et al. 2011), 222 (Hirano et al. 2011a), 223 (Hébrard et al. 2008), 224 (Winn et al. 2009b), 225 (Narita et al. 2010a), 226 (Crouzet et al. 2017), 227 (Hatzes et al. 2022), 228 (Kunovac Hodžić et al. 2021)

REFERENCES

- Addison, B. C., Tinney, C. G., Wright, D. J., & Bayliss, D. 2014, *ApJ*, 792, 112, doi: 10.1088/0004-637X/792/2/112
—. 2016, *ApJ*, 823, 29, doi: 10.3847/0004-637X/823/1/29
Addison, B. C., Tinney, C. G., Wright, D. J., et al. 2013, *ApJL*, 774, L9, doi: 10.1088/2041-8205/774/1/L9
Addison, B. C., Wang, S., Johnson, M. C., et al. 2018, *AJ*, 156, 197, doi: 10.3847/1538-3881/aade91
Addison, B. C., Horner, J., Wittenmyer, R. A., et al. 2021, *AJ*, 162, 137, doi: 10.3847/1538-3881/ac1685
Agol, E., Dorn, C., Grimm, S. L., et al. 2021, *PSJ*, 2, 1, doi: 10.3847/PSJ/ab022

- Ahlers, J. P., Barnes, J. W., & Barnes, R. 2015, *ApJ*, **814**, 67, doi: [10.1088/0004-637X/814/1/67](https://doi.org/10.1088/0004-637X/814/1/67)
- Ahlers, J. P., Seubert, S. A., & Barnes, J. W. 2014, *ApJ*, **786**, 131, doi: [10.1088/0004-637X/786/2/131](https://doi.org/10.1088/0004-637X/786/2/131)
- Ahlers, J. P., Kruse, E., Colón, K. D., et al. 2020a, *ApJ*, **888**, 63, doi: [10.3847/1538-4357/ab59d0](https://doi.org/10.3847/1538-4357/ab59d0)
- Ahlers, J. P., Johnson, M. C., Stassun, K. G., et al. 2020b, *AJ*, **160**, 4, doi: [10.3847/1538-3881/ab8fa3](https://doi.org/10.3847/1538-3881/ab8fa3)
- Albrecht, S., Quirrenbach, A., Tubbs, R. N., & Vink, R. 2010, *Experimental Astronomy*, **27**, 157, doi: [10.1007/s10686-009-9181-6](https://doi.org/10.1007/s10686-009-9181-6)
- Albrecht, S., Reffert, S., Snellen, I., Quirrenbach, A., & Mitchell, D. S. 2007, *A&A*, **474**, 565, doi: [10.1051/0004-6361:20077953](https://doi.org/10.1051/0004-6361:20077953)
- Albrecht, S., Reffert, S., Snellen, I. A. G., & Winn, J. N. 2009, *Nature*, **461**, 373, doi: [10.1038/nature08408](https://doi.org/10.1038/nature08408)
- Albrecht, S., Winn, J. N., Butler, R. P., et al. 2012a, *ApJ*, **744**, 189, doi: [10.1088/0004-637X/744/2/189](https://doi.org/10.1088/0004-637X/744/2/189)
- Albrecht, S., Winn, J. N., Marcy, G. W., et al. 2013, *ApJ*, **771**, 11, doi: [10.1088/0004-637X/771/1/11](https://doi.org/10.1088/0004-637X/771/1/11)
- Albrecht, S., Winn, J. N., Johnson, J. A., et al. 2011, *ApJ*, **738**, 50, doi: [10.1088/0004-637X/738/1/50](https://doi.org/10.1088/0004-637X/738/1/50)
- . 2012b, *ApJ*, **757**, 18, doi: [10.1088/0004-637X/757/1/18](https://doi.org/10.1088/0004-637X/757/1/18)
- Albrecht, S., Winn, J. N., Torres, G., et al. 2014, *ApJ*, **785**, 83, doi: [10.1088/0004-637X/785/2/83](https://doi.org/10.1088/0004-637X/785/2/83)
- Albrecht, S. H., Marcussen, M. L., Winn, J. N., Dawson, R. I., & Knudstrup, E. 2021, *ApJL*, **916**, L1, doi: [10.3847/2041-8213/ac0f03](https://doi.org/10.3847/2041-8213/ac0f03)
- Allart, R., Pino, L., Lovis, C., et al. 2020, *A&A*, **644**, A155, doi: [10.1051/0004-6361/202039234](https://doi.org/10.1051/0004-6361/202039234)
- Anderson, D. R., Hellier, C., Gillon, M., et al. 2010, *ApJ*, **709**, 159, doi: [10.1088/0004-637X/709/1/159](https://doi.org/10.1088/0004-637X/709/1/159)
- Anderson, D. R., Collier Cameron, A., Gillon, M., et al. 2011a, *A&A*, **534**, A16, doi: [10.1051/0004-6361/201117597](https://doi.org/10.1051/0004-6361/201117597)
- Anderson, D. R., Smith, A. M. S., Lanotte, A. A., et al. 2011b, *MNRAS*, **416**, 2108, doi: [10.1111/j.1365-2966.2011.19182.x](https://doi.org/10.1111/j.1365-2966.2011.19182.x)
- Anderson, D. R., Brown, D. J. A., Collier Cameron, A., et al. 2014, arXiv e-prints, arXiv:1410.3449. <https://arxiv.org/abs/1410.3449>
- Anderson, D. R., Collier Cameron, A., Hellier, C., et al. 2015a, *A&A*, **575**, A61, doi: [10.1051/0004-6361/201423591](https://doi.org/10.1051/0004-6361/201423591)
- Anderson, D. R., Triaud, A. H. M. J., Turner, O. D., et al. 2015b, *ApJL*, **800**, L9, doi: [10.1088/2041-8205/800/1/L9](https://doi.org/10.1088/2041-8205/800/1/L9)
- Anderson, D. R., Collier Cameron, A., Delrez, L., et al. 2017, *A&A*, **604**, A110, doi: [10.1051/0004-6361/201730439](https://doi.org/10.1051/0004-6361/201730439)
- Anderson, D. R., Bouchy, F., Brown, D. J. A., et al. 2018a, arXiv e-prints, arXiv:1812.09264. <https://arxiv.org/abs/1812.09264>
- . 2018b, arXiv e-prints, arXiv:1809.07709. <https://arxiv.org/abs/1809.07709>
- Anderson, D. R., Temple, L. Y., Nielsen, L. D., et al. 2018c, arXiv e-prints, arXiv:1809.04897. <https://arxiv.org/abs/1809.04897>
- Anderson, K. R., & Lai, D. 2018, *MNRAS*, **480**, 1402, doi: [10.1093/mnras/sty1937](https://doi.org/10.1093/mnras/sty1937)
- Anderson, K. R., Storch, N. I., & Lai, D. 2016, *MNRAS*, **456**, 3671, doi: [10.1093/mnras/stv2906](https://doi.org/10.1093/mnras/stv2906)
- Anderson, K. R., Winn, J. N., & Penev, K. 2021, *ApJ*, **914**, 56, doi: [10.3847/1538-4357/abf8af](https://doi.org/10.3847/1538-4357/abf8af)
- Atobe, K., & Ida, S. 2007, *Icarus*, **188**, 1, doi: [10.1016/j.icarus.2006.11.022](https://doi.org/10.1016/j.icarus.2006.11.022)
- Bailer-Jones, C. A. L., Rybizki, J., Fouesneau, M., Mantelet, G., & Andrae, R. 2018, *AJ*, **156**, 58, doi: [10.3847/1538-3881/aacb21](https://doi.org/10.3847/1538-3881/aacb21)
- Bailey, E., Batygin, K., & Brown, M. E. 2016, *AJ*, **152**, 126, doi: [10.3847/0004-6256/152/5/126](https://doi.org/10.3847/0004-6256/152/5/126)
- Bakos, G. Á., Howard, A. W., Noyes, R. W., et al. 2009, *ApJ*, **707**, 446, doi: [10.1088/0004-637X/707/1/446](https://doi.org/10.1088/0004-637X/707/1/446)
- Bakos, G. Á., Torres, G., Pál, A., et al. 2010, *ApJ*, **710**, 1724, doi: [10.1088/0004-637X/710/2/1724](https://doi.org/10.1088/0004-637X/710/2/1724)
- Bakos, G. Á., Hartman, J., Torres, G., et al. 2011, *ApJ*, **742**, 116, doi: [10.1088/0004-637X/742/2/116](https://doi.org/10.1088/0004-637X/742/2/116)
- Ballot, J., Appourchaux, T., Toutain, T., & Guittet, M. 2008, *A&A*, **486**, 867, doi: [10.1051/0004-6361:20079343](https://doi.org/10.1051/0004-6361:20079343)
- Ballot, J., García, R. A., & Lambert, P. 2006, *MNRAS*, **369**, 1281, doi: [10.1111/j.1365-2966.2006.10375.x](https://doi.org/10.1111/j.1365-2966.2006.10375.x)
- Barbieri, M., Alonso, R., Desidera, S., et al. 2009, *A&A*, **503**, 601, doi: [10.1051/0004-6361/200811466](https://doi.org/10.1051/0004-6361/200811466)
- Barker, A. J. 2016, *MNRAS*, **459**, 939, doi: [10.1093/mnras/stw702](https://doi.org/10.1093/mnras/stw702)
- Barker, A. J., & Ogilvie, G. I. 2009, *MNRAS*, **395**, 2268, doi: [10.1111/j.1365-2966.2009.14694.x](https://doi.org/10.1111/j.1365-2966.2009.14694.x)
- . 2010, *MNRAS*, **404**, 1849, doi: [10.1111/j.1365-2966.2010.16400.x](https://doi.org/10.1111/j.1365-2966.2010.16400.x)
- Barnes, J. W. 2009, *ApJ*, **705**, 683, doi: [10.1088/0004-637X/705/1/683](https://doi.org/10.1088/0004-637X/705/1/683)
- Barnes, J. W., Ahlers, J. P., Seubert, S. A., & Relles, H. M. 2015, *ApJL*, **808**, L38, doi: [10.1088/2041-8205/808/2/L38](https://doi.org/10.1088/2041-8205/808/2/L38)
- Barnes, J. W., & Fortney, J. J. 2003, *ApJ*, **588**, 545, doi: [10.1086/373893](https://doi.org/10.1086/373893)
- Barnes, J. W., Linscott, E., & Shporer, A. 2011, *ApJS*, **197**, 10, doi: [10.1088/0067-0049/197/1/10](https://doi.org/10.1088/0067-0049/197/1/10)
- Barnes, S. A. 2010, *ApJ*, **722**, 222, doi: [10.1088/0004-637X/722/1/222](https://doi.org/10.1088/0004-637X/722/1/222)

- Bate, M. R. 2018, *MNRAS*, **475**, 5618, doi: [10.1093/mnras/sty169](https://doi.org/10.1093/mnras/sty169)
- Bate, M. R., Lodato, G., & Pringle, J. E. 2010, *MNRAS*, **401**, 1505, doi: [10.1111/j.1365-2966.2009.15773.x](https://doi.org/10.1111/j.1365-2966.2009.15773.x)
- Batygin, K. 2012, *Nature*, **491**, 418, doi: [10.1038/nature11560](https://doi.org/10.1038/nature11560)
- Batygin, K., & Adams, F. C. 2013, *ApJ*, **778**, 169, doi: [10.1088/0004-637X/778/2/169](https://doi.org/10.1088/0004-637X/778/2/169)
- Bayliss, D. D. R., Winn, J. N., Mardling, R. A., & Sackett, P. D. 2010, *ApJL*, **722**, L224, doi: [10.1088/2041-8205/722/2/L224](https://doi.org/10.1088/2041-8205/722/2/L224)
- Beaugé, C., & Nesvorný, D. 2012, *ApJ*, **751**, 119, doi: [10.1088/0004-637X/751/2/119](https://doi.org/10.1088/0004-637X/751/2/119)
- Beck, J. G., & Giles, P. 2005, *ApJL*, **621**, L153, doi: [10.1086/429224](https://doi.org/10.1086/429224)
- Becker, J. C., Vanderburg, A., Adams, F. C., Khain, T., & Bryan, M. 2017, *AJ*, **154**, 230, doi: [10.3847/1538-3881/aa9176](https://doi.org/10.3847/1538-3881/aa9176)
- Behmard, A., Dai, F., & Howard, A. W. 2022, *AJ*, **163**, 160, doi: [10.3847/1538-3881/ac53a7](https://doi.org/10.3847/1538-3881/ac53a7)
- Bello-Arufe, A., Cabot, S. H. C., Mendonça, J. M., Buchhave, L. A., & Rathcke, A. D. 2022, *AJ*, **163**, 96, doi: [10.3847/1538-3881/ac402e](https://doi.org/10.3847/1538-3881/ac402e)
- Benatti, S., Damasso, M., Borsa, F., et al. 2021, *A&A*, **650**, A66, doi: [10.1051/0004-6361/202140416](https://doi.org/10.1051/0004-6361/202140416)
- Benomar, O., Masuda, K., Shibahashi, H., & Suto, Y. 2014, *PASJ*, **66**, 94, doi: [10.1093/pasj/psu069](https://doi.org/10.1093/pasj/psu069)
- Benz, W., Broeg, C., Fortier, A., et al. 2021, *Experimental Astronomy*, **51**, 109, doi: [10.1007/s10686-020-09679-4](https://doi.org/10.1007/s10686-020-09679-4)
- Best, S., & Petrovich, C. 2022, *ApJL*, **925**, L5, doi: [10.3847/2041-8213/ac49e9](https://doi.org/10.3847/2041-8213/ac49e9)
- Biddle, L. I., Pearson, K. A., Crossfield, I. J. M., et al. 2014, *MNRAS*, **443**, 1810, doi: [10.1093/mnras/stu1199](https://doi.org/10.1093/mnras/stu1199)
- Biersteker, J., & Schlichting, H. 2017, *AJ*, **154**, 164, doi: [10.3847/1538-3881/aa88c2](https://doi.org/10.3847/1538-3881/aa88c2)
- Bieryla, A., Collins, K., Beatty, T. G., et al. 2015, *AJ*, **150**, 12, doi: [10.1088/0004-6256/150/1/12](https://doi.org/10.1088/0004-6256/150/1/12)
- Bonfanti, A., Ortolani, S., Piotto, G., & Nascimbeni, V. 2015, *A&A*, **575**, A18, doi: [10.1051/0004-6361/201424951](https://doi.org/10.1051/0004-6361/201424951)
- Bonfils, X., Gillon, M., Udry, S., et al. 2012, *A&A*, **546**, A27, doi: [10.1051/0004-6361/201219623](https://doi.org/10.1051/0004-6361/201219623)
- Bonomo, A. S., Desidera, S., Benatti, S., et al. 2017, *A&A*, **602**, A107, doi: [10.1051/0004-6361/201629882](https://doi.org/10.1051/0004-6361/201629882)
- Borderies, N., Goldreich, P., & Tremaine, S. 1984, *ApJ*, **284**, 429, doi: [10.1086/162423](https://doi.org/10.1086/162423)
- Borsa, F., Rainer, M., Bonomo, A. S., et al. 2019, *A&A*, **631**, A34, doi: [10.1051/0004-6361/201935718](https://doi.org/10.1051/0004-6361/201935718)
- Borsa, F., Allart, R., Casasayas-Barris, N., et al. 2021, *A&A*, **645**, A24, doi: [10.1051/0004-6361/202039344](https://doi.org/10.1051/0004-6361/202039344)
- Bouchy, F., Moutou, C., Queloz, D., & CoRoT Exoplanet Science Team. 2009, in *Transiting Planets*, ed. F. Pont, D. Sasselov, & M. J. Holman, Vol. 253, 129–139
- Bouchy, F., Queloz, D., Deleuil, M., et al. 2008, *A&A*, **482**, L25, doi: [10.1051/0004-6361:200809433](https://doi.org/10.1051/0004-6361:200809433)
- Boué, G., & Fabrycky, D. C. 2014, *ApJ*, **789**, 110, doi: [10.1088/0004-637X/789/2/110](https://doi.org/10.1088/0004-637X/789/2/110)
- Bourrier, V., Cegla, H. M., Lovis, C., & Wyttenbach, A. 2017, *A&A*, **599**, A33, doi: [10.1051/0004-6361/201629973](https://doi.org/10.1051/0004-6361/201629973)
- Bourrier, V., & Hébrard, G. 2014, *A&A*, **569**, A65, doi: [10.1051/0004-6361/201424266](https://doi.org/10.1051/0004-6361/201424266)
- Bourrier, V., Lecavelier des Etangs, A., Hébrard, G., et al. 2015, *A&A*, **579**, A55, doi: [10.1051/0004-6361/201525750](https://doi.org/10.1051/0004-6361/201525750)
- Bourrier, V., Lovis, C., Beust, H., et al. 2018, *Nature*, **553**, 477, doi: [10.1038/nature24677](https://doi.org/10.1038/nature24677)
- Bourrier, V., Ehrenreich, D., Lendl, M., et al. 2020, *A&A*, **635**, A205, doi: [10.1051/0004-6361/201936640](https://doi.org/10.1051/0004-6361/201936640)
- Bourrier, V., Lovis, C., Cretignier, M., et al. 2021, *A&A*, **654**, A152, doi: [10.1051/0004-6361/202141527](https://doi.org/10.1051/0004-6361/202141527)
- Brahm, R., Espinoza, N., Jordán, A., et al. 2018, *MNRAS*, **477**, 2572, doi: [10.1093/mnras/sty795](https://doi.org/10.1093/mnras/sty795)
- Brinch, C., Jørgensen, J. K., Hogerheijde, M. R., Nelson, R. P., & Gressel, O. 2016, *ApJL*, **830**, L16, doi: [10.3847/2041-8205/830/1/L16](https://doi.org/10.3847/2041-8205/830/1/L16)
- Brothwell, R. D., Watson, C. A., Hébrard, G., et al. 2014, *MNRAS*, **440**, 3392, doi: [10.1093/mnras/stu520](https://doi.org/10.1093/mnras/stu520)
- Brown, D. J. A. 2014, *MNRAS*, **442**, 1844, doi: [10.1093/mnras/stu950](https://doi.org/10.1093/mnras/stu950)
- Brown, D. J. A., Cameron, A. C., Anderson, D. R., et al. 2012a, *MNRAS*, **423**, 1503, doi: [10.1111/j.1365-2966.2012.20973.x](https://doi.org/10.1111/j.1365-2966.2012.20973.x)
- Brown, D. J. A., Collier Cameron, A., Díaz, R. F., et al. 2012b, *ApJ*, **760**, 139, doi: [10.1088/0004-637X/760/2/139](https://doi.org/10.1088/0004-637X/760/2/139)
- Brown, D. J. A., Triaud, A. H. M. J., Doyle, A. P., et al. 2017, *MNRAS*, **464**, 810, doi: [10.1093/mnras/stw2316](https://doi.org/10.1093/mnras/stw2316)
- Bryan, M. L., Chiang, E., Morley, C. V., Mace, G. N., & Bowler, B. P. 2021, *AJ*, **162**, 217, doi: [10.3847/1538-3881/ac1bb1](https://doi.org/10.3847/1538-3881/ac1bb1)
- Bryan, M. L., Alsubai, K. A., Latham, D. W., et al. 2012, *ApJ*, **750**, 84, doi: [10.1088/0004-637X/750/1/84](https://doi.org/10.1088/0004-637X/750/1/84)
- Bryan, M. L., Knutson, H. A., Howard, A. W., et al. 2016, *ApJ*, **821**, 89, doi: [10.3847/0004-637X/821/2/89](https://doi.org/10.3847/0004-637X/821/2/89)
- Bryan, M. L., Chiang, E., Bowler, B. P., et al. 2020, *AJ*, **159**, 181, doi: [10.3847/1538-3881/ab76c6](https://doi.org/10.3847/1538-3881/ab76c6)
- Buchhave, L. A., Bakos, G. Á., Hartman, J. D., et al. 2010, *ApJ*, **720**, 1118, doi: [10.1088/0004-637X/720/2/1118](https://doi.org/10.1088/0004-637X/720/2/1118)
- Burgasser, A. J., & Mamajek, E. E. 2017, *ApJ*, **845**, 110, doi: [10.3847/1538-4357/aa7fea](https://doi.org/10.3847/1538-4357/aa7fea)
- Cabot, S. H. C., Bello-Arufe, A., Mendonça, J. M., et al. 2021, *AJ*, **162**, 218, doi: [10.3847/1538-3881/ac1ba3](https://doi.org/10.3847/1538-3881/ac1ba3)

- Campante, T. L., Lund, M. N., Kuszlewicz, J. S., et al. 2016, *ApJ*, **819**, 85, doi: [10.3847/0004-637X/819/1/85](https://doi.org/10.3847/0004-637X/819/1/85)
- Carmichael, T. W., Quinn, S. N., Mustill, A. J., et al. 2020, *AJ*, **160**, 53, doi: [10.3847/1538-3881/ab9b84](https://doi.org/10.3847/1538-3881/ab9b84)
- Carmichael, T. W., Quinn, S. N., Zhou, G., et al. 2021, *AJ*, **161**, 97, doi: [10.3847/1538-3881/abd4e1](https://doi.org/10.3847/1538-3881/abd4e1)
- Carone, L., Mollière, P., Zhou, Y., et al. 2021, *A&A*, **646**, A168, doi: [10.1051/0004-6361/202038620](https://doi.org/10.1051/0004-6361/202038620)
- Carter, J. A., & Winn, J. N. 2010a, *ApJ*, **709**, 1219, doi: [10.1088/0004-637X/709/2/1219](https://doi.org/10.1088/0004-637X/709/2/1219)
- . 2010b, *ApJ*, **716**, 850, doi: [10.1088/0004-637X/716/1/850](https://doi.org/10.1088/0004-637X/716/1/850)
- Casanovas, J. 1997, in Astronomical Society of the Pacific Conference Series, Vol. 118, 1st Advances in Solar Physics Euroconference. Advances in Physics of Sunspots, ed. B. Schmieder, J. C. del Toro Iniesta, & M. Vazquez, 3
- Casasayas-Barris, N., Palle, E., Nowak, G., et al. 2017, *A&A*, **608**, A135, doi: [10.1051/0004-6361/201731956](https://doi.org/10.1051/0004-6361/201731956)
- Casassus, S. 2016, *Publications of the Astronomical Society of Australia*, **33**, e013, doi: [10.1017/pasa.2016.7](https://doi.org/10.1017/pasa.2016.7)
- Cébron, D., Le Bars, M., Le Gal, P., et al. 2013, *Icarus*, **226**, 1642, doi: [10.1016/j.icarus.2012.12.017](https://doi.org/10.1016/j.icarus.2012.12.017)
- Cegla, H. M., Lovis, C., Bourrier, V., et al. 2016, *A&A*, **588**, A127, doi: [10.1051/0004-6361/201527794](https://doi.org/10.1051/0004-6361/201527794)
- Chaplin, W. J., & Miglio, A. 2013, *ARA&A*, **51**, 353, doi: [10.1146/annurev-astro-082812-140938](https://doi.org/10.1146/annurev-astro-082812-140938)
- Chaplin, W. J., Sanchis-Ojeda, R., Campante, T. L., et al. 2013, *ApJ*, **766**, 101, doi: [10.1088/0004-637X/766/2/101](https://doi.org/10.1088/0004-637X/766/2/101)
- Chatterjee, S., Ford, E. B., Matsumura, S., & Rasio, F. A. 2008, *ApJ*, **686**, 580, doi: [10.1086/590227](https://doi.org/10.1086/590227)
- Chelli, A., & Petrov, R. G. 1995, *A&AS*, **109**, 401
- Chen, G., Casasayas-Barris, N., Pallé, E., et al. 2020, *A&A*, **635**, A171, doi: [10.1051/0004-6361/201936986](https://doi.org/10.1051/0004-6361/201936986)
- Chen, J., & Kipping, D. 2017, *ApJ*, **834**, 17, doi: [10.3847/1538-4357/834/1/17](https://doi.org/10.3847/1538-4357/834/1/17)
- Chiang, E. I., & Murray-Clay, R. A. 2004, *ApJ*, **607**, 913, doi: [10.1086/383522](https://doi.org/10.1086/383522)
- Chilcote, J., Pueyo, L., De Rosa, R. J., et al. 2017, *AJ*, **153**, 182, doi: [10.3847/1538-3881/aa63e9](https://doi.org/10.3847/1538-3881/aa63e9)
- Christensen-Dalsgaard, J., & Thompson, M. J. 2011, in Astrophysical Dynamics: From Stars to Galaxies, ed. N. H. Brummell, A. S. Brun, M. S. Miesch, & Y. Ponty, Vol. 271, 32–61. <http://dx.doi.org/10.1017/S1743921311017443>
- Christian, S., Vanderburg, A., Becker, J., et al. 2022, *AJ*, **163**, 207, doi: [10.3847/1538-3881/ac517f](https://doi.org/10.3847/1538-3881/ac517f)
- Christiansen, J. L., Vanderburg, A., Burt, J., et al. 2017, *AJ*, **154**, 122, doi: [10.3847/1538-3881/aa832d](https://doi.org/10.3847/1538-3881/aa832d)
- Cochran, W. D., Redfield, S., Endl, M., & Cochran, A. L. 2008, *ApJL*, **683**, L59, doi: [10.1086/591317](https://doi.org/10.1086/591317)
- Collier Cameron, A., Bruce, V. A., Miller, G. R. M., Triaud, A. H. M. J., & Queloz, D. 2010a, *MNRAS*, **403**, 151, doi: [10.1111/j.1365-2966.2009.16131.x](https://doi.org/10.1111/j.1365-2966.2009.16131.x)
- Collier Cameron, A., Guenther, E., Smalley, B., et al. 2010b, *MNRAS*, **407**, 507, doi: [10.1111/j.1365-2966.2010.16922.x](https://doi.org/10.1111/j.1365-2966.2010.16922.x)
- Correia, A. C. M. 2015, *A&A*, **582**, A69, doi: [10.1051/0004-6361/201525939](https://doi.org/10.1051/0004-6361/201525939)
- Covino, E., Esposito, M., Barbieri, M., et al. 2013, *A&A*, **554**, A28, doi: [10.1051/0004-6361/201321298](https://doi.org/10.1051/0004-6361/201321298)
- Cristo, E., Santos, N. C., Demangeon, O., et al. 2022, *A&A*, **660**, A52, doi: [10.1051/0004-6361/202142353](https://doi.org/10.1051/0004-6361/202142353)
- Crossfield, I. J. M., Ciardi, D. R., Isaacson, H., et al. 2017, *AJ*, **153**, 255, doi: [10.3847/1538-3881/aa6e01](https://doi.org/10.3847/1538-3881/aa6e01)
- Crouzet, N., McCullough, P. R., Long, D., et al. 2017, *AJ*, **153**, 94, doi: [10.3847/1538-3881/153/3/94](https://doi.org/10.3847/1538-3881/153/3/94)
- Czesla, S., Schröter, S., Wolter, U., et al. 2012, *A&A*, **539**, A150, doi: [10.1051/0004-6361/201118042](https://doi.org/10.1051/0004-6361/201118042)
- Dai, F., Masuda, K., & Winn, J. N. 2018a, *ApJL*, **864**, L38, doi: [10.3847/2041-8213/aadd4f](https://doi.org/10.3847/2041-8213/aadd4f)
- Dai, F., & Winn, J. N. 2017, *AJ*, **153**, 205, doi: [10.3847/1538-3881/aa65d1](https://doi.org/10.3847/1538-3881/aa65d1)
- Dai, F., Winn, J. N., Berta-Thompson, Z., Sanchis-Ojeda, R., & Albrecht, S. 2018b, *AJ*, **155**, 177, doi: [10.3847/1538-3881/aab618](https://doi.org/10.3847/1538-3881/aab618)
- Dai, F., Roy, A., Fulton, B., et al. 2020, *AJ*, **160**, 193, doi: [10.3847/1538-3881/abb3bd](https://doi.org/10.3847/1538-3881/abb3bd)
- Dalal, S., Hébrard, G., Lecavelier des Étangs, A., et al. 2019, *A&A*, **631**, A28, doi: [10.1051/0004-6361/201935944](https://doi.org/10.1051/0004-6361/201935944)
- Dalba, P. A., Gupta, A. F., Rodriguez, J. E., et al. 2020, *AJ*, **159**, 241, doi: [10.3847/1538-3881/ab84e3](https://doi.org/10.3847/1538-3881/ab84e3)
- Damasso, M., Esposito, M., Nascimbeni, V., et al. 2015a, *A&A*, **581**, L6, doi: [10.1051/0004-6361/201526995](https://doi.org/10.1051/0004-6361/201526995)
- Damasso, M., Biazzo, K., Bonomo, A. S., et al. 2015b, *A&A*, **575**, A111, doi: [10.1051/0004-6361/201425332](https://doi.org/10.1051/0004-6361/201425332)
- Damiani, C., & Lanza, A. F. 2015, *A&A*, **574**, A39, doi: [10.1051/0004-6361/201424318](https://doi.org/10.1051/0004-6361/201424318)
- Damiani, C., & Mathis, S. 2018, *A&A*, **618**, A90, doi: [10.1051/0004-6361/201732538](https://doi.org/10.1051/0004-6361/201732538)
- David, T. J., Petigura, E. A., Luger, R., et al. 2019a, *ApJL*, **885**, L12, doi: [10.3847/2041-8213/ab4c99](https://doi.org/10.3847/2041-8213/ab4c99)
- David, T. J., Cody, A. M., Hedges, C. L., et al. 2019b, *AJ*, **158**, 79, doi: [10.3847/1538-3881/ab290f](https://doi.org/10.3847/1538-3881/ab290f)
- Davies, C. L. 2019, *MNRAS*, **484**, 1926, doi: [10.1093/mnras/stz086](https://doi.org/10.1093/mnras/stz086)
- Dawson, R. I. 2014, *ApJL*, **790**, L31, doi: [10.1088/2041-8205/790/2/L31](https://doi.org/10.1088/2041-8205/790/2/L31)
- Dawson, R. I., & Johnson, J. A. 2018, *ARA&A*, **56**, 175, doi: [10.1146/annurev-astro-081817-051853](https://doi.org/10.1146/annurev-astro-081817-051853)

- Deitrick, R., Barnes, R., Quinn, T. R., et al. 2018, *AJ*, **155**, 60, doi: [10.3847/1538-3881/aaa301](https://doi.org/10.3847/1538-3881/aaa301)
- Deline, A., Hooton, M. J., Lendl, M., et al. 2022, *A&A*, **659**, A74, doi: [10.1051/0004-6361/202142400](https://doi.org/10.1051/0004-6361/202142400)
- Delrez, L., Santerne, A., Almenara, J. M., et al. 2016, *MNRAS*, **458**, 4025, doi: [10.1093/mnras/stw522](https://doi.org/10.1093/mnras/stw522)
- Deming, D., Sada, P. V., Jackson, B., et al. 2011, *ApJ*, **740**, 33, doi: [10.1088/0004-637X/740/1/33](https://doi.org/10.1088/0004-637X/740/1/33)
- Désert, J.-M., Charbonneau, D., Demory, B.-O., et al. 2011, *ApJS*, **197**, 14, doi: [10.1088/0067-0049/197/1/14](https://doi.org/10.1088/0067-0049/197/1/14)
- Dobbs-Dixon, I., Lin, D. N. C., & Mardling, R. A. 2004, *ApJ*, **610**, 464, doi: [10.1086/421510](https://doi.org/10.1086/421510)
- Domiciano de Souza, A., Kervella, P., Jankov, S., et al. 2003, *A&A*, **407**, L47, doi: [10.1051/0004-6361:20030786](https://doi.org/10.1051/0004-6361:20030786)
- Domiciano de Souza, A., Zorec, J., Jankov, S., et al. 2004, *A&A*, **418**, 781, doi: [10.1051/0004-6361:20040051](https://doi.org/10.1051/0004-6361:20040051)
- Dones, L., & Tremaine, S. 1993, *Science*, **259**, 350, doi: [10.1126/science.259.5093.350](https://doi.org/10.1126/science.259.5093.350)
- Dong, J., Huang, C. X., Zhou, G., et al. 2022, *ApJL*, **926**, L7, doi: [10.3847/2041-8213/ac4da0](https://doi.org/10.3847/2041-8213/ac4da0)
- Dorval, P., Talens, G. J. J., Otten, G. P. P. L., et al. 2020, *A&A*, **635**, A60, doi: [10.1051/0004-6361/201935611](https://doi.org/10.1051/0004-6361/201935611)
- Dupuy, T. J., Kraus, A. L., Kratter, K. M., et al. 2022, *MNRAS*, **512**, 648, doi: [10.1093/mnras/stac306](https://doi.org/10.1093/mnras/stac306)
- Ehrenreich, D., Lovis, C., Allart, R., et al. 2020, *Nature*, **580**, 597, doi: [10.1038/s41586-020-2107-1](https://doi.org/10.1038/s41586-020-2107-1)
- Enoch, B., Cameron, A. C., Anderson, D. R., et al. 2011, *MNRAS*, **410**, 1631, doi: [10.1111/j.1365-2966.2010.17550.x](https://doi.org/10.1111/j.1365-2966.2010.17550.x)
- Epstein, C. R., & Pinsonneault, M. H. 2014, *ApJ*, **780**, 159, doi: [10.1088/0004-637X/780/2/159](https://doi.org/10.1088/0004-637X/780/2/159)
- Esposito, M., Covino, E., Mancini, L., et al. 2014, *A&A*, **564**, L13, doi: [10.1051/0004-6361/201423735](https://doi.org/10.1051/0004-6361/201423735)
- Esposito, M., Covino, E., Desidera, S., et al. 2017, *A&A*, **601**, A53, doi: [10.1051/0004-6361/201629720](https://doi.org/10.1051/0004-6361/201629720)
- Fabrycky, D., & Tremaine, S. 2007, *ApJ*, **669**, 1298, doi: [10.1086/521702](https://doi.org/10.1086/521702)
- Fabrycky, D. C., Johnson, E. T., & Goodman, J. 2007, *ApJ*, **665**, 754, doi: [10.1086/519075](https://doi.org/10.1086/519075)
- Fabrycky, D. C., & Winn, J. N. 2009, *ApJ*, **696**, 1230, doi: [10.1088/0004-637X/696/2/1230](https://doi.org/10.1088/0004-637X/696/2/1230)
- Fabrycky, D. C., Ford, E. B., Steffen, J. H., et al. 2012, *ApJ*, **750**, 114, doi: [10.1088/0004-637X/750/2/114](https://doi.org/10.1088/0004-637X/750/2/114)
- Fabrycky, D. C., Lissauer, J. J., Ragozzine, D., et al. 2014, *ApJ*, **790**, 146, doi: [10.1088/0004-637X/790/2/146](https://doi.org/10.1088/0004-637X/790/2/146)
- Feinstein, A. D., Montet, B. T., Johnson, M. C., et al. 2021, *AJ*, **162**, 213, doi: [10.3847/1538-3881/ac1f24](https://doi.org/10.3847/1538-3881/ac1f24)
- Fielding, D. B., McKee, C. F., Socrates, A., Cunningham, A. J., & Klein, R. I. 2015, *MNRAS*, **450**, 3306, doi: [10.1093/mnras/stv836](https://doi.org/10.1093/mnras/stv836)
- Foucart, F., & Lai, D. 2011, *MNRAS*, **412**, 2799, doi: [10.1111/j.1365-2966.2010.18176.x](https://doi.org/10.1111/j.1365-2966.2010.18176.x)
- Franchini, A., Martin, R. G., & Lubow, S. H. 2020, *MNRAS*, **491**, 5351, doi: [10.1093/mnras/stz3175](https://doi.org/10.1093/mnras/stz3175)
- Fulton, B. J., Howard, A. W., Winn, J. N., et al. 2013, *ApJ*, **772**, 80, doi: [10.1088/0004-637X/772/2/80](https://doi.org/10.1088/0004-637X/772/2/80)
- Gaidos, E., Hirano, T., Wilson, D. J., et al. 2020, *MNRAS*, **498**, L119, doi: [10.1093/mnrasl/slaa136](https://doi.org/10.1093/mnrasl/slaa136)
- Gaidos, E., Hirano, T., Beichman, C., et al. 2022, *MNRAS*, **509**, 2969, doi: [10.1093/mnras/stab3107](https://doi.org/10.1093/mnras/stab3107)
- Gandolfi, D., Hébrard, G., Alonso, R., et al. 2010, *A&A*, **524**, A55, doi: [10.1051/0004-6361/201015132](https://doi.org/10.1051/0004-6361/201015132)
- Gandolfi, D., Collier Cameron, A., Endl, M., et al. 2012, *A&A*, **543**, L5, doi: [10.1051/0004-6361/201219533](https://doi.org/10.1051/0004-6361/201219533)
- Garhart, E., Deming, D., Mandell, A., et al. 2020, *AJ*, **159**, 137, doi: [10.3847/1538-3881/ab6cff](https://doi.org/10.3847/1538-3881/ab6cff)
- Gaudi, B. S., & Winn, J. N. 2007, *ApJ*, **655**, 550, doi: [10.1086/509910](https://doi.org/10.1086/509910)
- Gaudi, B. S., Stassun, K. G., Collins, K. A., et al. 2017, *Nature*, **546**, 514, doi: [10.1038/nature22392](https://doi.org/10.1038/nature22392)
- Gilliland, R. L., Brown, T. M., Guhathakurta, P., et al. 2000, *ApJL*, **545**, L47, doi: [10.1086/317334](https://doi.org/10.1086/317334)
- Gillon, M., Anderson, D. R., Triaud, A. H. M. J., et al. 2009, *A&A*, **501**, 785, doi: [10.1051/0004-6361/200911749](https://doi.org/10.1051/0004-6361/200911749)
- Gillon, M., Lanotte, A. A., Barman, T., et al. 2010, *A&A*, **511**, A3, doi: [10.1051/0004-6361/200913507](https://doi.org/10.1051/0004-6361/200913507)
- Gillon, M., Anderson, D. R., Collier-Cameron, A., et al. 2013, *A&A*, **552**, A82, doi: [10.1051/0004-6361/201220561](https://doi.org/10.1051/0004-6361/201220561)
- Giménez, A. 2006, *ApJ*, **650**, 408, doi: [10.1086/507021](https://doi.org/10.1086/507021)
- Ginski, C., Facchini, S., Huang, J., et al. 2021, *ApJL*, **908**, L25, doi: [10.3847/2041-8213/abdf57](https://doi.org/10.3847/2041-8213/abdf57)
- Gizon, L., & Solanki, S. K. 2003, *ApJ*, **589**, 1009, doi: [10.1086/374715](https://doi.org/10.1086/374715)
- Glebocki, R., & Stawikowski, A. 1997, *A&A*, **328**, 579
- Goldreich, P., Lithwick, Y., & Sari, R. 2004, *ARA&A*, **42**, 549, doi: [10.1146/annurev.astro.42.053102.134004](https://doi.org/10.1146/annurev.astro.42.053102.134004)
- Gomes, R., Deienno, R., & Morbidelli, A. 2017, *AJ*, **153**, 27, doi: [10.3847/1538-3881/153/1/27](https://doi.org/10.3847/1538-3881/153/1/27)
- Gough, D. O., & Kosovichev, A. G. 1993, in Astronomical Society of the Pacific Conference Series, Vol. 40, IAU Colloq. 137: Inside the Stars, ed. W. W. Weiss & A. Baglin, 566.
- <https://ui.adsabs.harvard.edu/abs/1993ASPC...40..566G>
- Gratia, P., & Fabrycky, D. 2017, *MNRAS*, **464**, 1709, doi: [10.1093/mnras/stw2180](https://doi.org/10.1093/mnras/stw2180)
- Gray, D. F. 2005, The Observation and Analysis of Stellar Photospheres, 3rd Ed. (ISBN 0521851866, Cambridge University Press)
- Greaves, J. S., Kennedy, G. M., Thureau, N., et al. 2014, *MNRAS*, **438**, L31, doi: [10.1093/mnras/slt153](https://doi.org/10.1093/mnras/slt153)

- Grishin, E., Lai, D., & Perets, H. B. 2018, *MNRAS*, **474**, 3547, doi: [10.1093/mnras/stx3005](https://doi.org/10.1093/mnras/stx3005)
- Groot, P. J. 2012, *ApJ*, **745**, 55, doi: [10.1088/0004-637X/745/1/55](https://doi.org/10.1088/0004-637X/745/1/55)
- Grundahl, F., Fredslund Andersen, M., Christensen-Dalsgaard, J., et al. 2017, *ApJ*, **836**, 142, doi: [10.3847/1538-4357/836/1/142](https://doi.org/10.3847/1538-4357/836/1/142)
- Guenther, E. W., Díaz, R. F., Gazzano, J.-C., et al. 2012, *A&A*, **537**, A136, doi: [10.1051/0004-6361/201117706](https://doi.org/10.1051/0004-6361/201117706)
- Hale, A. 1994, *AJ*, **107**, 306, doi: [10.1086/116855](https://doi.org/10.1086/116855)
- Hamers, A. S. 2017, *MNRAS*, **466**, 4107, doi: [10.1093/mnras/stx035](https://doi.org/10.1093/mnras/stx035)
- Hamers, A. S., Antonini, F., Lithwick, Y., Perets, H. B., & Portegies Zwart, S. F. 2017, *MNRAS*, **464**, 688, doi: [10.1093/mnras/stw2370](https://doi.org/10.1093/mnras/stw2370)
- Hamers, A. S., & Tremaine, S. 2017, *AJ*, **154**, 272, doi: [10.3847/1538-3881/aa9926](https://doi.org/10.3847/1538-3881/aa9926)
- Hansen, B. M. S. 2012, *ApJ*, **757**, 6, doi: [10.1088/0004-637X/757/1/6](https://doi.org/10.1088/0004-637X/757/1/6)
- Hao, W., Kouwenhoven, M. B. N., & Spurzem, R. 2013, *MNRAS*, **433**, 867, doi: [10.1093/mnras/stt771](https://doi.org/10.1093/mnras/stt771)
- Hardy, R. A., Harrington, J., Hardin, M. R., et al. 2017, *ApJ*, **836**, 143, doi: [10.3847/1538-4357/836/1/143](https://doi.org/10.3847/1538-4357/836/1/143)
- Hartman, J. D., Bakos, G. Á., Torres, G., et al. 2009, *ApJ*, **706**, 785, doi: [10.1088/0004-637X/706/1/785](https://doi.org/10.1088/0004-637X/706/1/785)
- Hartman, J. D., Bakos, G. Á., Sato, B., et al. 2011, *ApJ*, **726**, 52, doi: [10.1088/0004-637X/726/1/52](https://doi.org/10.1088/0004-637X/726/1/52)
- Hatzes, A. P., Gandolfi, D., Korth, J., et al. 2022, *AJ*, **163**, 223, doi: [10.3847/1538-3881/ac5dc9](https://doi.org/10.3847/1538-3881/ac5dc9)
- Hébrard, G., Bouchy, F., Pont, F., et al. 2008, *A&A*, **488**, 763, doi: [10.1051/0004-6361:200810056](https://doi.org/10.1051/0004-6361:200810056)
- Hébrard, G., Désert, J.-M., Díaz, R. F., et al. 2010, *A&A*, **516**, A95, doi: [10.1051/0004-6361/201014327](https://doi.org/10.1051/0004-6361/201014327)
- Hébrard, G., Ehrenreich, D., Bouchy, F., et al. 2011a, *A&A*, **527**, L11, doi: [10.1051/0004-6361/201016331](https://doi.org/10.1051/0004-6361/201016331)
- Hébrard, G., Evans, T. M., Alonso, R., et al. 2011b, *A&A*, **533**, A130, doi: [10.1051/0004-6361/201117192](https://doi.org/10.1051/0004-6361/201117192)
- Hébrard, G., Collier Cameron, A., Brown, D. J. A., et al. 2013, *A&A*, **549**, A134, doi: [10.1051/0004-6361/201220363](https://doi.org/10.1051/0004-6361/201220363)
- Hébrard, G., Díaz, R. F., Correia, A. C. M., et al. 2020, *A&A*, **640**, A32, doi: [10.1051/0004-6361/202038296](https://doi.org/10.1051/0004-6361/202038296)
- Heitzmann, A., Zhou, G., Quinn, S. N., et al. 2021, *ApJL*, **922**, L1, doi: [10.3847/2041-8213/ac3485](https://doi.org/10.3847/2041-8213/ac3485)
- Heller, C. H. 1993, *ApJ*, **408**, 337, doi: [10.1086/172591](https://doi.org/10.1086/172591)
- Heller, R., & Albrecht, S. 2014, *ApJL*, **796**, L1, doi: [10.1088/2041-8205/796/1/L1](https://doi.org/10.1088/2041-8205/796/1/L1)
- Heller, R., Leconte, J., & Barnes, R. 2011, *A&A*, **528**, A27, doi: [10.1051/0004-6361/201015809](https://doi.org/10.1051/0004-6361/201015809)
- Hellier, C., Anderson, D. R., Collier-Cameron, A., et al. 2011, *ApJL*, **730**, L31, doi: [10.1088/2041-8205/730/2/L31](https://doi.org/10.1088/2041-8205/730/2/L31)
- Hellier, C., Anderson, D. R., Triaud, A. H. M. J., et al. 2019, *MNRAS*, **488**, 3067, doi: [10.1093/mnras/stz1903](https://doi.org/10.1093/mnras/stz1903)
- Herman, M. K., de Mooij, E. J. W., Huang, C. X., & Jayawardhana, R. 2018, *AJ*, **155**, 13, doi: [10.3847/1538-3881/aa991f](https://doi.org/10.3847/1538-3881/aa991f)
- Herman, M. K., Zhu, W., & Wu, Y. 2019, *AJ*, **157**, 248, doi: [10.3847/1538-3881/ab1f70](https://doi.org/10.3847/1538-3881/ab1f70)
- Hirano, T., Narita, N., Sato, B., et al. 2011a, *PASJ*, **63**, L57. <https://arxiv.org/abs/1108.4493>
- Hirano, T., Narita, N., Shporer, A., et al. 2011b, *PASJ*, **63**, 531. <https://arxiv.org/abs/1009.5677>
- Hirano, T., Sanchis-Ojeda, R., Takeda, Y., et al. 2014, *ApJ*, **783**, 9, doi: [10.1088/0004-637X/783/1/9](https://doi.org/10.1088/0004-637X/783/1/9)
- Hirano, T., Suto, Y., Winn, J. N., et al. 2011c, *ApJ*, **742**, 69, doi: [10.1088/0004-637X/742/2/69](https://doi.org/10.1088/0004-637X/742/2/69)
- Hirano, T., Narita, N., Sato, B., et al. 2012, *ApJL*, **759**, L36, doi: [10.1088/2041-8205/759/2/L36](https://doi.org/10.1088/2041-8205/759/2/L36)
- Hirano, T., Nowak, G., Kuzuhara, M., et al. 2016, *ApJ*, **825**, 53, doi: [10.3847/0004-637X/825/1/53](https://doi.org/10.3847/0004-637X/825/1/53)
- Hirano, T., Krishnamurthy, V., Gaidos, E., et al. 2020a, *ApJL*, **899**, L13, doi: [10.3847/2041-8213/aba6eb](https://doi.org/10.3847/2041-8213/aba6eb)
- Hirano, T., Gaidos, E., Winn, J. N., et al. 2020b, *ApJL*, **890**, L27, doi: [10.3847/2041-8213/ab74dc](https://doi.org/10.3847/2041-8213/ab74dc)
- Hjorth, M., Albrecht, S., Hirano, T., et al. 2021, *Proceedings of the National Academy of Science*, **118**, 2017418118, doi: [10.1073/pnas.2017418118](https://doi.org/10.1073/pnas.2017418118)
- Hjorth, M., Justesen, A. B., Hirano, T., et al. 2019a, *MNRAS*, **484**, 3522, doi: [10.1093/mnras/stz139](https://doi.org/10.1093/mnras/stz139)
- Hjorth, M., Albrecht, S., Talens, G. J. J., et al. 2019b, *A&A*, **631**, A76, doi: [10.1051/0004-6361/201936082](https://doi.org/10.1051/0004-6361/201936082)
- Hoeijmakers, H. J., Cabot, S. H. C., Zhao, L., et al. 2020, *A&A*, **641**, A120, doi: [10.1051/0004-6361/202037437](https://doi.org/10.1051/0004-6361/202037437)
- Holczer, T., Shporer, A., Mazeh, T., et al. 2015, *ApJ*, **807**, 170, doi: [10.1088/0004-637X/807/2/170](https://doi.org/10.1088/0004-637X/807/2/170)
- Holman, M. J., Fabrycky, D. C., Ragozzine, D., et al. 2010, *Science*, **330**, 51, doi: [10.1126/science.1195778](https://doi.org/10.1126/science.1195778)
- Holt, J. R. 1893, *Astronomy and Astro-Physics (formerly The Sidereal Messenger)*, **12**, 646
- Hooton, M. J., Hoyer, S., Kitzmann, D., et al. 2022, *A&A*, **658**, A75, doi: [10.1051/0004-6361/202141645](https://doi.org/10.1051/0004-6361/202141645)
- Hosokawa, Y. 1953, *PASJ*, **5**, 88
- Howard, A. W., Bakos, G. Á., Hartman, J., et al. 2012, *ApJ*, **749**, 134, doi: [10.1088/0004-637X/749/2/134](https://doi.org/10.1088/0004-637X/749/2/134)
- Howarth, I. D., & Morello, G. 2017, *MNRAS*, **470**, 932, doi: [10.1093/mnras/stx1260](https://doi.org/10.1093/mnras/stx1260)
- Howe, K. S., & Clarke, C. J. 2009, *MNRAS*, **392**, 448, doi: [10.1111/j.1365-2966.2008.14073.x](https://doi.org/10.1111/j.1365-2966.2008.14073.x)

- Huang, C. X., Burt, J., Vanderburg, A., et al. 2018, *ApJL*, **868**, L39, doi: [10.3847/2041-8213/aaef91](https://doi.org/10.3847/2041-8213/aaef91)
- Huber, D., Carter, J. A., Barbieri, M., et al. 2013, *Science*, **342**, 331, doi: [10.1126/science.1242066](https://doi.org/10.1126/science.1242066)
- Hut, P. 1980, *A&A*, **92**, 167
- . 1981, *A&A*, **99**, 126
- Innanen, K. A., Zheng, J. Q., Mikkola, S., & Valtonen, M. J. 1997, *AJ*, **113**, 1915, doi: [10.1086/118405](https://doi.org/10.1086/118405)
- Jenkins, J. M., Borucki, W. J., Koch, D. G., et al. 2010, *ApJ*, **724**, 1108, doi: [10.1088/0004-637X/724/2/1108](https://doi.org/10.1088/0004-637X/724/2/1108)
- Jennings, R. M., & Chiang, E. 2021, *MNRAS*, **507**, 5187, doi: [10.1093/mnras/stab2429](https://doi.org/10.1093/mnras/stab2429)
- Jensen, E. L. N., & Akeson, R. 2014, *Nature*, **511**, 567, doi: [10.1038/nature13521](https://doi.org/10.1038/nature13521)
- Johnson, J. A., Winn, J. N., Albrecht, S., et al. 2009, *PASP*, **121**, 1104, doi: [10.1086/644604](https://doi.org/10.1086/644604)
- Johnson, J. A., Winn, J. N., Narita, N., et al. 2008, *ApJ*, **686**, 649, doi: [10.1086/591078](https://doi.org/10.1086/591078)
- Johnson, J. A., Winn, J. N., Bakos, G. Á., et al. 2011, *ApJ*, **735**, 24, doi: [10.1088/0004-637X/735/1/24](https://doi.org/10.1088/0004-637X/735/1/24)
- Johnson, M. C., Cochran, W. D., Addison, B. C., Tinney, C. G., & Wright, D. J. 2017, *AJ*, **154**, 137, doi: [10.3847/1538-3881/aa8462](https://doi.org/10.3847/1538-3881/aa8462)
- Johnson, M. C., Cochran, W. D., Albrecht, S., et al. 2014, *ApJ*, **790**, 30, doi: [10.1088/0004-637X/790/1/30](https://doi.org/10.1088/0004-637X/790/1/30)
- Johnson, M. C., Cochran, W. D., Collier Cameron, A., & Bayliss, D. 2015, *ApJL*, **810**, L23, doi: [10.1088/2041-8205/810/2/L23](https://doi.org/10.1088/2041-8205/810/2/L23)
- Johnson, M. C., Rodriguez, J. E., Zhou, G., et al. 2018, *AJ*, **155**, 100, doi: [10.3847/1538-3881/aaa5af](https://doi.org/10.3847/1538-3881/aaa5af)
- Johnson, M. C., David, T. J., Petigura, E. A., et al. 2022, *AJ*, **163**, 247, doi: [10.3847/1538-3881/ac6271](https://doi.org/10.3847/1538-3881/ac6271)
- Jones, J., White, R. J., Boyajian, T., et al. 2015, *ApJ*, **813**, 58, doi: [10.1088/0004-637X/813/1/58](https://doi.org/10.1088/0004-637X/813/1/58)
- Joshi, Y. C., Pollacco, D., Collier Cameron, A., et al. 2009, *MNRAS*, **392**, 1532, doi: [10.1111/j.1365-2966.2008.14178.x](https://doi.org/10.1111/j.1365-2966.2008.14178.x)
- Justesen, A. B., & Albrecht, S. 2020, *A&A*, **642**, A212, doi: [10.1051/0004-6361/202039138](https://doi.org/10.1051/0004-6361/202039138)
- Kaib, N. A., Raymond, S. N., & Duncan, M. J. 2011, *ApJL*, **742**, L24, doi: [10.1088/2041-8205/742/2/L24](https://doi.org/10.1088/2041-8205/742/2/L24)
- Kamiaka, S., Benomar, O., Suto, Y., et al. 2019, *AJ*, **157**, 137, doi: [10.3847/1538-3881/ab04a9](https://doi.org/10.3847/1538-3881/ab04a9)
- Kervella, P., Thévenin, F., Morel, P., et al. 2004, in Stars as Suns : Activity, Evolution and Planets, ed. A. K. Dupree & A. O. Benz, Vol. 219, 80. <https://ui.adsabs.harvard.edu/abs/2004IAUS..219...80K>
- Kippenhahn, R., Weigert, A., & Weiss, A. 2012, Stellar Structure and Evolution (Springer-Verlag Berlin Heidelberg), doi: [10.1007/978-3-642-30304-3](https://doi.org/10.1007/978-3-642-30304-3)
- Kipping, D. M., Bakos, G. Á., Hartman, J., et al. 2010, *ApJ*, **725**, 2017, doi: [10.1088/0004-637X/725/2/2017](https://doi.org/10.1088/0004-637X/725/2/2017)
- Knudstrup, E., & Albrecht, S. H. 2022, *A&A*, **660**, A99, doi: [10.1051/0004-6361/202142726](https://doi.org/10.1051/0004-6361/202142726)
- Knutson, H. A., Fulton, B. J., Montet, B. T., et al. 2014, *ApJ*, **785**, 126, doi: [10.1088/0004-637X/785/2/126](https://doi.org/10.1088/0004-637X/785/2/126)
- Kopal, Z. 1959, Close binary systems (The International Astrophysics Series, London: Chapman & Hall, 1959)
- Korth, J., Csizmadia, S., Gandolfi, D., et al. 2019, *MNRAS*, **482**, 1807, doi: [10.1093/mnras/sty2760](https://doi.org/10.1093/mnras/sty2760)
- Kovács, G., Bakos, G. Á., Torres, G., et al. 2007, *ApJL*, **670**, L41, doi: [10.1086/524058](https://doi.org/10.1086/524058)
- Kozai, Y. 1962, *AJ*, **67**, 591, doi: [10.1086/108790](https://doi.org/10.1086/108790)
- Kraus, S. 2019, in The Very Large Telescope in 2030, 36. <http://dx.doi.org/10.5281/zenodo.3356286>
- Kraus, S., Le Bouquin, J.-B., Kreplin, A., et al. 2020, *ApJL*, **897**, L8, doi: [10.3847/2041-8213/ab9d27](https://doi.org/10.3847/2041-8213/ab9d27)
- Kuffmeier, M., Dullemond, C. P., Reissl, S., & Goicovic, F. G. 2021, *A&A*, **656**, A161, doi: [10.1051/0004-6361/202039614](https://doi.org/10.1051/0004-6361/202039614)
- Kunovac Hodžić, V., Triaud, A. H. M. J., Cegla, H. M., Chaplin, W. J., & Davies, G. R. 2021, *MNRAS*, **502**, 2893, doi: [10.1093/mnras/stab237](https://doi.org/10.1093/mnras/stab237)
- Kurtz, D. 2022, arXiv e-prints, arXiv:2201.11629. <https://arxiv.org/abs/2201.11629>
- Kuszlewicz, J. S., Chaplin, W. J., North, T. S. H., et al. 2019, *MNRAS*, **488**, 572, doi: [10.1093/mnras/stz1689](https://doi.org/10.1093/mnras/stz1689)
- Lachaume, R. 2003, *A&A*, **400**, 795, doi: [10.1051/0004-6361:20030072](https://doi.org/10.1051/0004-6361:20030072)
- Lacour, S., Wang, J. J., Rodet, L., et al. 2021, *A&A*, **654**, L2, doi: [10.1051/0004-6361/202141889](https://doi.org/10.1051/0004-6361/202141889)
- Lai, D. 2012, *MNRAS*, **423**, 486, doi: [10.1111/j.1365-2966.2012.20893.x](https://doi.org/10.1111/j.1365-2966.2012.20893.x)
- . 2014, *MNRAS*, **440**, 3532, doi: [10.1093/mnras/stu485](https://doi.org/10.1093/mnras/stu485)
- . 2016, *AJ*, **152**, 215, doi: [10.3847/0004-6256/152/6/215](https://doi.org/10.3847/0004-6256/152/6/215)
- Lai, D., Anderson, K. R., & Pu, B. 2018, *MNRAS*, **475**, 5231, doi: [10.1093/mnras/sty133](https://doi.org/10.1093/mnras/sty133)
- Lai, D., Foucart, F., & Lin, D. N. C. 2011, *MNRAS*, **412**, 2790, doi: [10.1111/j.1365-2966.2010.18127.x](https://doi.org/10.1111/j.1365-2966.2010.18127.x)
- Laskar, J. 2008, *Icarus*, **196**, 1, doi: [10.1016/j.icarus.2008.02.017](https://doi.org/10.1016/j.icarus.2008.02.017)
- Laskar, J., Joutel, F., & Robutel, P. 1993, *Nature*, **361**, 615, doi: [10.1038/361615a0](https://doi.org/10.1038/361615a0)
- Laskar, J., & Robutel, P. 1993, *Nature*, **361**, 608, doi: [10.1038/361608a0](https://doi.org/10.1038/361608a0)
- Latham, D. W., Mazeh, T., Stefanik, R. P., Mayor, M., & Burki, G. 1989, *Nature*, **339**, 38, doi: [10.1038/339038a0](https://doi.org/10.1038/339038a0)
- Latham, D. W., Bakos, G. Á., Torres, G., et al. 2009, *ApJ*, **704**, 1107, doi: [10.1088/0004-637X/704/2/1107](https://doi.org/10.1088/0004-637X/704/2/1107)

- Le Bouquin, J., Absil, O., Benisty, M., et al. 2009, *A&A*, **498**, L41, doi: [10.1051/0004-6361/200911854](https://doi.org/10.1051/0004-6361/200911854)
- Lendl, M., Triaud, A. H. M. J., Anderson, D. R., et al. 2014, *A&A*, **568**, A81, doi: [10.1051/0004-6361/201424481](https://doi.org/10.1051/0004-6361/201424481)
- Lendl, M., Csizmadia, S., Deline, A., et al. 2020, *A&A*, **643**, A94, doi: [10.1051/0004-6361/202038677](https://doi.org/10.1051/0004-6361/202038677)
- Li, G., Naoz, S., Holman, M., & Loeb, A. 2014a, *ApJ*, **791**, 86, doi: [10.1088/0004-637X/791/2/86](https://doi.org/10.1088/0004-637X/791/2/86)
- Li, G., Naoz, S., Kocsis, B., & Loeb, A. 2014b, *ApJ*, **785**, 116, doi: [10.1088/0004-637X/785/2/116](https://doi.org/10.1088/0004-637X/785/2/116)
- Li, G., Naoz, S., Valsecchi, F., Johnson, J. A., & Rasio, F. A. 2014c, *ApJ*, **794**, 131, doi: [10.1088/0004-637X/794/2/131](https://doi.org/10.1088/0004-637X/794/2/131)
- Li, G., & Winn, J. N. 2016, *ApJ*, **818**, 5, doi: [10.3847/0004-637X/818/1/5](https://doi.org/10.3847/0004-637X/818/1/5)
- Li, J., & Lai, D. 2020, *ApJL*, **898**, L20, doi: [10.3847/2041-8213/aba2c4](https://doi.org/10.3847/2041-8213/aba2c4)
- Liang, Y., Winn, J. N., & Albrecht, S. H. 2022, *ApJ*, **927**, 114, doi: [10.3847/1538-4357/ac4f65](https://doi.org/10.3847/1538-4357/ac4f65)
- Lidov, M. L. 1962, *Planet. Space Sci.*, **9**, 719, doi: [10.1016/0032-0633\(62\)90129-0](https://doi.org/10.1016/0032-0633(62)90129-0)
- Lin, Y., & Ogilvie, G. I. 2017, *MNRAS*, **468**, 1387, doi: [10.1093/mnras/stx540](https://doi.org/10.1093/mnras/stx540)
- Lissauer, J. J., Fabrycky, D. C., Ford, E. B., et al. 2011, *Nature*, **470**, 53, doi: [10.1038/nature09760](https://doi.org/10.1038/nature09760)
- Lithwick, Y., & Wu, Y. 2014, *Proceedings of the National Academy of Science*, **111**, 12610, doi: [10.1073/pnas.1308261110](https://doi.org/10.1073/pnas.1308261110)
- Liu, F., Yong, D., Asplund, M., et al. 2018, *A&A*, **614**, A138, doi: [10.1051/0004-6361/201832701](https://doi.org/10.1051/0004-6361/201832701)
- Loeillet, B., Shporer, A., Bouchy, F., et al. 2008, *A&A*, **481**, 529, doi: [10.1051/0004-6361:20078167](https://doi.org/10.1051/0004-6361:20078167)
- López-Morales, M., Triaud, A. H. M. J., Rodler, F., et al. 2014, *ApJL*, **792**, L31, doi: [10.1088/2041-8205/792/2/L31](https://doi.org/10.1088/2041-8205/792/2/L31)
- Louden, E. M., Winn, J. N., Petigura, E. A., et al. 2021, *AJ*, **161**, 68, doi: [10.3847/1538-3881/abcebd](https://doi.org/10.3847/1538-3881/abcebd)
- Lubow, S. H., & Martin, R. G. 2016, *ApJ*, **817**, 30, doi: [10.3847/0004-637X/817/1/30](https://doi.org/10.3847/0004-637X/817/1/30)
- Lubow, S. H., & Ogilvie, G. I. 2000, *ApJ*, **538**, 326, doi: [10.1086/309101](https://doi.org/10.1086/309101)
- Lund, M. B., Rodriguez, J. E., Zhou, G., et al. 2017, *AJ*, **154**, 194, doi: [10.3847/1538-3881/aa8f95](https://doi.org/10.3847/1538-3881/aa8f95)
- Lund, M. N., Lundkvist, M., Silva Aguirre, V., et al. 2014, *A&A*, **570**, A54, doi: [10.1051/0004-6361/201424326](https://doi.org/10.1051/0004-6361/201424326)
- Luque, R., Casasayas-Barris, N., Parviainen, H., et al. 2020, *A&A*, **642**, A50, doi: [10.1051/0004-6361/202038703](https://doi.org/10.1051/0004-6361/202038703)
- Ma, L., & Fuller, J. 2021, *ApJ*, **918**, 16, doi: [10.3847/1538-4357/ac088e](https://doi.org/10.3847/1538-4357/ac088e)
- Malmberg, D., Davies, M. B., & Heggie, D. C. 2011, *MNRAS*, **411**, 859, doi: [10.1111/j.1365-2966.2010.17730.x](https://doi.org/10.1111/j.1365-2966.2010.17730.x)
- Mancini, L., Esposito, M., Covino, E., et al. 2015, *A&A*, **579**, A136, doi: [10.1051/0004-6361/201526030](https://doi.org/10.1051/0004-6361/201526030)
- Mancini, L., Southworth, J., Raia, G., et al. 2017, *MNRAS*, **465**, 843, doi: [10.1093/mnras/stw1987](https://doi.org/10.1093/mnras/stw1987)
- Mancini, L., Esposito, M., Covino, E., et al. 2018, *A&A*, **613**, A41, doi: [10.1051/0004-6361/201732234](https://doi.org/10.1051/0004-6361/201732234)
- Mann, A. W., Gaidos, E., Mace, G. N., et al. 2016, *ApJ*, **818**, 46, doi: [10.3847/0004-637X/818/1/46](https://doi.org/10.3847/0004-637X/818/1/46)
- Mann, A. W., Johnson, M. C., Vanderburg, A., et al. 2020, *AJ*, **160**, 179, doi: [10.3847/1538-3881/abaef64](https://doi.org/10.3847/1538-3881/abaef64)
- Marcussen, M. L., & Albrecht, S. H. 2021, arXiv e-prints, arXiv:2112.00824. <https://arxiv.org/abs/2112.00824>
- Marcy, G. W., & Butler, R. P. 1996, *ApJL*, **464**, L147, doi: [10.1086/310096](https://doi.org/10.1086/310096)
- Marcy, G. W., Isaacson, H., Howard, A. W., et al. 2014, *ApJS*, **210**, 20, doi: [10.1088/0067-0049/210/2/20](https://doi.org/10.1088/0067-0049/210/2/20)
- Marino, S., Perez, S., & Casassus, S. 2015, *ApJ*, **798**, L44, doi: [10.1088/2041-8205/798/2/L44](https://doi.org/10.1088/2041-8205/798/2/L44)
- Martioli, E., Hébrard, G., Moutou, C., et al. 2020, *A&A*, **641**, L1, doi: [10.1051/0004-6361/202038695](https://doi.org/10.1051/0004-6361/202038695)
- Masuda, K. 2015, *ApJ*, **805**, 28, doi: [10.1088/0004-637X/805/1/28](https://doi.org/10.1088/0004-637X/805/1/28)
- . 2017, *AJ*, **154**, 64, doi: [10.3847/1538-3881/aa7aeb](https://doi.org/10.3847/1538-3881/aa7aeb)
- Masuda, K., & Tamayo, D. 2020, *AJ*, **160**, 224, doi: [10.3847/1538-3881/abb8cd](https://doi.org/10.3847/1538-3881/abb8cd)
- Masuda, K., & Winn, J. N. 2017, *AJ*, **153**, 187, doi: [10.3847/1538-3881/aa647c](https://doi.org/10.3847/1538-3881/aa647c)
- . 2020, *AJ*, **159**, 81, doi: [10.3847/1538-3881/ab65be](https://doi.org/10.3847/1538-3881/ab65be)
- Matsakos, T., & Königl, A. 2017, *AJ*, **153**, 60, doi: [10.3847/1538-3881/153/2/60](https://doi.org/10.3847/1538-3881/153/2/60)
- Maxted, P. F. L. 2018, *Rotation of Planet-Hosting Stars* (Springer, Cham), 18
- Maxted, P. F. L., Serenelli, A. M., & Southworth, J. 2015, *A&A*, **577**, A90, doi: [10.1051/0004-6361/201525774](https://doi.org/10.1051/0004-6361/201525774)
- Mayor, M., & Queloz, D. 1995, *Nature*, **378**, 355, doi: [10.1038/378355a0](https://doi.org/10.1038/378355a0)
- Mazeh, T. 2008, in *EAS Publications Series*, Vol. 29, *EAS Publications Series*, ed. M.-J. Goupil & J.-P. Zahn, 1–65. <http://adsabs.harvard.edu/abs/2008EAS....29....1M>
- Mazeh, T., Holczer, T., & Shporer, A. 2015a, *ApJ*, **800**, 142, doi: [10.1088/0004-637X/800/2/142](https://doi.org/10.1088/0004-637X/800/2/142)
- Mazeh, T., Perets, H. B., McQuillan, A., & Goldstein, E. S. 2015b, *ApJ*, **801**, 3, doi: [10.1088/0004-637X/801/1/3](https://doi.org/10.1088/0004-637X/801/1/3)
- McCullough, P. R., Burke, C. J., Valenti, J. A., et al. 2008, arXiv e-prints, arXiv:0805.2921. <https://arxiv.org/abs/0805.2921>
- McLaughlin, D. B. 1924, *ApJ*, **60**, 22, doi: [10.1086/142826](https://doi.org/10.1086/142826)
- McQuillan, A., Mazeh, T., & Aigrain, S. 2013, *ApJL*, **775**, L11, doi: [10.1088/2041-8205/775/1/L11](https://doi.org/10.1088/2041-8205/775/1/L11)

- Meibom, S., Barnes, S. A., Platais, I., et al. 2015, *Nature*, **517**, 589, doi: 10.1038/nature14118
- Miller, G. R. M., Collier Cameron, A., Simpson, E. K., et al. 2010, *A&A*, **523**, A52, doi: 10.1051/0004-6361/201015052
- Millholland, S., & Laughlin, G. 2018, *ApJL*, **869**, L15, doi: 10.3847/2041-8213/aaedb1
- . 2019, *Nature Astronomy*, **3**, 424, doi: 10.1038/s41550-019-0701-7
- Millholland, S. C., He, M. Y., Ford, E. B., et al. 2021, *AJ*, **162**, 166, doi: 10.3847/1538-3881/ac0f7a
- Mohler-Fischer, M., Mancini, L., Hartman, J. D., et al. 2013, *A&A*, **558**, A55, doi: 10.1051/0004-6361/201321663
- Monin, J. L., Clarke, C. J., Prato, L., & McCabe, C. 2007, 395. <https://arxiv.org/abs/astro-ph/0604031>
- Morton, T. D., & Johnson, J. A. 2011, *ApJ*, **729**, 138, doi: 10.1088/0004-637X/729/2/138
- Morton, T. D., & Winn, J. N. 2014, *ApJ*, **796**, 47, doi: 10.1088/0004-637X/796/1/47
- Mourard, D., Nardetto, N., ten Brummelaar, T., et al. 2018, in Society of Photo-Optical Instrumentation Engineers (SPIE) Conference Series, Vol. 10701, Optical and Infrared Interferometry and Imaging VI, ed. M. J. Creech-Eakman, P. G. Tuthill, & A. Mérand, 1070120
- Moutou, C., Hébrard, G., Bouchy, F., et al. 2009, *A&A*, **498**, L5, doi: 10.1051/0004-6361/200911954
- Moutou, C., Díaz, R. F., Udry, S., et al. 2011, *A&A*, **533**, A113, doi: 10.1051/0004-6361/201116760
- Močnik, T., Clark, B. J. M., Anderson, D. R., Hellier, C., & Brown, D. J. A. 2016, *AJ*, **151**, 150, doi: 10.3847/0004-6256/151/6/150
- Močnik, T., Hellier, C., & Anderson, D. R. 2020, *PASP*, **132**, 014401, doi: 10.1088/1538-3873/ab5598
- Močnik, T., Southworth, J., & Hellier, C. 2017, *MNRAS*, **471**, 394, doi: 10.1093/mnras/stx1557
- Moya, A., Bouy, H., Marchis, F., Vicente, B., & Barrado, D. 2011, *A&A*, **535**, A110, doi: 10.1051/0004-6361/201116889
- Muñoz, D. J., & Perets, H. B. 2018, *AJ*, **156**, 253, doi: 10.3847/1538-3881/aae7d0
- Naef, D., Latham, D. W., Mayor, M., et al. 2001, *A&A*, **375**, L27, doi: 10.1051/0004-6361:20010853
- Nagasawa, M., & Ida, S. 2011, *ApJ*, **742**, 72, doi: 10.1088/0004-637X/742/2/72
- Nagasawa, M., Ida, S., & Bessho, T. 2008, *ApJ*, **678**, 498, doi: 10.1086/529369
- Naoz, S. 2016, *ARA&A*, **54**, 441, doi: 10.1146/annurev-astro-081915-023315
- Naoz, S., Farr, W. M., Lithwick, Y., Rasio, F. A., & Teyssandier, J. 2011, *Nature*, **473**, 187, doi: 10.1038/nature10076
- Naoz, S., Farr, W. M., & Rasio, F. A. 2012, *ApJL*, **754**, L36, doi: 10.1088/2041-8205/754/2/L36
- Narita, N., Hirano, T., Sanchis-Ojeda, R., et al. 2010a, *PASJ*, **62**, L61, doi: 10.1093/pasj/62.6.L61
- Narita, N., Hirano, T., Sato, B., et al. 2011, *PASJ*, **63**, L67, doi: 10.1093/pasj/63.6.L67
- Narita, N., Sato, B., Hirano, T., & Tamura, M. 2009a, *PASJ*, **61**, L35. <https://arxiv.org/abs/0908.1673>
- Narita, N., Sato, B., Hirano, T., et al. 2010b, *PASJ*, **62**, 653. <https://arxiv.org/abs/1003.2268>
- Narita, N., Sato, B., Ohshima, O., & Winn, J. N. 2008, *PASJ*, **60**, L1, doi: 10.1093/pasj/60.2.L1
- Narita, N., Enya, K., Sato, B., et al. 2007, *PASJ*, **59**, 763
- Narita, N., Hirano, T., Sato, B., et al. 2009b, *PASJ*, **61**, 991. <https://arxiv.org/abs/0905.4727>
- Neveu-VanMalle, M., Queloz, D., Anderson, D. R., et al. 2014, *A&A*, **572**, A49, doi: 10.1051/0004-6361/201424744
- . 2016, *A&A*, **586**, A93, doi: 10.1051/0004-6361/201526965
- Newton, E. R., Mann, A. W., Toftlemire, B. M., et al. 2019, *ApJL*, **880**, L17, doi: 10.3847/2041-8213/ab2988
- Newton, E. R., Mann, A. W., Kraus, A. L., et al. 2021, *AJ*, **161**, 65, doi: 10.3847/1538-3881/abccc6
- Ngo, H., Knutson, H. A., Hinkley, S., et al. 2015, *ApJ*, **800**, 138, doi: 10.1088/0004-637X/800/2/138
- . 2016, *ApJ*, **827**, 8, doi: 10.3847/0004-637X/827/1/8
- Noyes, R. W., Bakos, G. Á., Torres, G., et al. 2008, *ApJL*, **673**, L79, doi: 10.1086/527358
- Nutzman, P. A., Fabrycky, D. C., & Fortney, J. J. 2011, *ApJL*, **740**, L10, doi: 10.1088/2041-8205/740/1/L10
- Ogilvie, G. I. 2014, *ARA&A*, **52**, 171, doi: 10.1146/annurev-astro-081913-035941
- Ohta, Y., Taruya, A., & Suto, Y. 2005, *ApJ*, **622**, 1118, doi: 10.1086/428344
- Oshagh, M., Boisse, I., Boué, G., et al. 2013, *A&A*, **549**, A35, doi: 10.1051/0004-6361/201220173
- Pál, A., Bakos, G. Á., Torres, G., et al. 2010, *MNRAS*, **401**, 2665, doi: 10.1111/j.1365-2966.2009.15849.x
- Palle, E., Oshagh, M., Casasayas-Barris, N., et al. 2020, *A&A*, **643**, A25, doi: 10.1051/0004-6361/202038583
- Penev, K., Bouma, L. G., Winn, J. N., & Hartman, J. D. 2018, *AJ*, **155**, 165, doi: 10.3847/1538-3881/aaaf71
- Perryman, M., Hartman, J., Bakos, G. Á., & Lindegren, L. 2014, *ApJ*, **797**, 14, doi: 10.1088/0004-637X/797/1/14
- Petigura, E. A., Howard, A. W., Marcy, G. W., et al. 2017, *AJ*, **154**, 107, doi: 10.3847/1538-3881/aa80de

- Petrov, R. G. 1989, in NATO ASIC Proc. 274: Diffraction-Limited Imaging with Very Large Telescopes, ed. D. M. Alloin & J.-M. Mariotti, 249
- Petrovich, C. 2015, *ApJ*, **799**, 27, doi: 10.1088/0004-637X/799/1/27
- Petrovich, C., Muñoz, D. J., Kratter, K. M., & Malhotra, R. 2020, *ApJL*, **902**, L5, doi: 10.3847/2041-8213/abb952
- Petrovich, C., & Tremaine, S. 2016, *ApJ*, **829**, 132, doi: 10.3847/0004-637X/829/2/132
- Philippov, A. A., & Rafikov, R. R. 2013, *ApJ*, **768**, 112, doi: 10.1088/0004-637X/768/2/112
- Piaulet, C., Benneke, B., Rubenzahl, R. A., et al. 2021, *AJ*, **161**, 70, doi: 10.3847/1538-3881/abcd3c
- Picogna, G., & Marzari, F. 2015, *A&A*, **583**, A133, doi: 10.1051/0004-6361/201526162
- Piskorz, D., Knutson, H. A., Ngo, H., et al. 2015, *ApJ*, **814**, 148, doi: 10.1088/0004-637X/814/2/148
- Plavchan, P., Barclay, T., Gagné, J., et al. 2020, *Nature*, **582**, 497, doi: 10.1038/s41586-020-2400-z
- Pont, F., Hébrard, G., Irwin, J. M., et al. 2009, *A&A*, **502**, 695, doi: 10.1051/0004-6361/200912463
- Pont, F., Endl, M., Cochran, W. D., et al. 2010, *MNRAS*, **402**, L1, doi: 10.1111/j.1745-3933.2009.00785.x
- Poon, M., Zanazzi, J. J., & Zhu, W. 2021, *MNRAS*, **503**, 1599, doi: 10.1093/mnras/stab575
- Poppenhaeger, K., & Wolk, S. J. 2014, *A&A*, **565**, L1, doi: 10.1051/0004-6361/201423454
- Portegies Zwart, S., Pelupessy, I., van Elteren, A., Wijnen, T. P. G., & Lugaro, M. 2018, *A&A*, **616**, A85, doi: 10.1051/0004-6361/201732060
- Queloz, D., Eggenberger, A., Mayor, M., et al. 2000, *A&A*, **359**, L13. <https://arxiv.org/abs/astro-ph/0006213>
- Queloz, D., Anderson, D., Collier Cameron, A., et al. 2010, *A&A*, **517**, L1, doi: 10.1051/0004-6361/201014768
- Quinn, S. N., White, T. R., Latham, D. W., et al. 2015, *ApJ*, **803**, 49, doi: 10.1088/0004-637X/803/2/49
- Rauer, H., Catala, C., Aerts, C., et al. 2014, *Experimental Astronomy*, **38**, 249, doi: 10.1007/s10686-014-9383-4
- Reisenberger, M. P., & Guinan, E. F. 1989, *AJ*, **97**, 216, doi: 10.1086/114972
- Rice, M., Wang, S., & Laughlin, G. 2022, *ApJL*, **926**, L17, doi: 10.3847/2041-8213/ac502d
- Rice, M., Wang, S., Howard, A. W., et al. 2021, *AJ*, **162**, 182, doi: 10.3847/1538-3881/ac1f8f
- Ricker, G. R., Winn, J. N., Vanderspek, R., et al. 2015, *Journal of Astronomical Telescopes, Instruments, and Systems*, **1**, 014003, doi: 10.1117/1.JATIS.1.1.014003
- Rizzuto, A. C., Newton, E. R., Mann, A. W., et al. 2020, *AJ*, **160**, 33, doi: 10.3847/1538-3881/ab94b7
- Rodriguez, J. E., Eastman, J. D., Zhou, G., et al. 2019, *AJ*, **158**, 197, doi: 10.3847/1538-3881/ab4136
- Rodriguez, J. E., Quinn, S. N., Zhou, G., et al. 2021, *AJ*, **161**, 194, doi: 10.3847/1538-3881/abe38a
- Rodríguez Martínez, R., Gaudi, B. S., Rodriguez, J. E., et al. 2020, *AJ*, **160**, 111, doi: 10.3847/1538-3881/ab9f2d
- Rogers, T. M., Lin, D. N. C., & Lau, H. H. B. 2012, *ApJL*, **758**, L6, doi: 10.1088/2041-8205/758/1/L6
- Rogers, T. M., Lin, D. N. C., McElwaine, J. N., & Lau, H. H. B. 2013, *ApJ*, **772**, 21, doi: 10.1088/0004-637X/772/1/21
- Romanova, M. M., Koldoba, A. V., Ustyugova, G. V., et al. 2021, *MNRAS*, **506**, 372, doi: 10.1093/mnras/stab1724
- Romanova, M. M., Ustyugova, G. V., Koldoba, A. V., & Lovelace, R. V. E. 2013, *MNRAS*, **430**, 699, doi: 10.1093/mnras/sts670
- Rossiter, R. A. 1924, *ApJ*, **60**, 15, doi: 10.1086/142825
- Royer, F., Zorec, J., & Gómez, A. E. 2007, *A&A*, **463**, 671, doi: 10.1051/0004-6361:20065224
- Rubenzahl, R. A., Dai, F., Howard, A. W., et al. 2021, *AJ*, **161**, 119, doi: 10.3847/1538-3881/abd177
- Safsten, E. D., Dawson, R. I., & Wolfgang, A. 2020, *AJ*, **160**, 214, doi: 10.3847/1538-3881/abb536
- Sailhenfest, M., Lari, G., & Boué, G. 2021, *Nature Astronomy*, **5**, 345, doi: 10.1038/s41550-020-01284-x
- Sakai, N., Hanawa, T., Zhang, Y., et al. 2019, *Nature*, **565**, 206, doi: 10.1038/s41586-018-0819-2
- Sanchis-Ojeda, R., & Winn, J. N. 2011, *ApJ*, **743**, 61, doi: 10.1088/0004-637X/743/1/61
- Sanchis-Ojeda, R., Winn, J. N., Holman, M. J., et al. 2011, *ApJ*, **733**, 127, doi: 10.1088/0004-637X/733/2/127
- Sanchis-Ojeda, R., Fabrycky, D. C., Winn, J. N., et al. 2012, *Nature*, **487**, 449, doi: 10.1038/nature11301
- Sanchis-Ojeda, R., Winn, J. N., Marcy, G. W., et al. 2013, *ApJ*, **775**, 54, doi: 10.1088/0004-637X/775/1/54
- Sanchis-Ojeda, R., Winn, J. N., Dai, F., et al. 2015, *ApJL*, **812**, L11, doi: 10.1088/2041-8205/812/1/L11
- Santerne, A., Hébrard, G., Deleuil, M., et al. 2014, *A&A*, **571**, A37, doi: 10.1051/0004-6361/201424158
- Santerne, A., Hébrard, G., Lillo-Box, J., et al. 2016, *ApJ*, **824**, 55, doi: 10.3847/0004-637X/824/1/55
- Santos, N. C., Cristo, E., Demangeon, O., et al. 2020, *A&A*, **644**, A51, doi: 10.1051/0004-6361/202039454
- Sato, K. 1974, *PASJ*, **26**, 65
- Schlafzman, K. C. 2010, *ApJ*, **719**, 602, doi: 10.1088/0004-637X/719/1/602
- Schlafzman, K. C., & Winn, J. N. 2013, *ApJ*, **772**, 143, doi: 10.1088/0004-637X/772/2/143
- Schlesinger, F. 1910, *Publications of the Allegheny Observatory of the University of Pittsburgh*, **1**, 123

- Seager, S., & Hui, L. 2002, *ApJ*, **574**, 1004, doi: [10.1086/340994](https://doi.org/10.1086/340994)
- Sedaghati, E., MacDonald, R. J., Casasayas-Barris, N., et al. 2021, *MNRAS*, **505**, 435, doi: [10.1093/mnras/stab1164](https://doi.org/10.1093/mnras/stab1164)
- Sedaghati, E., Sánchez-López, A., Czesla, S., et al. 2022, *A&A*, **659**, A44, doi: [10.1051/0004-6361/202142471](https://doi.org/10.1051/0004-6361/202142471)
- Shporer, A., & Brown, T. 2011, *ApJ*, **733**, 30, doi: [10.1088/0004-637X/733/1/30](https://doi.org/10.1088/0004-637X/733/1/30)
- Shporer, A., Brown, T., Mazeh, T., & Zucker, S. 2012, *New Astronomy*, **17**, 309, doi: [10.1016/j.newast.2011.08.006](https://doi.org/10.1016/j.newast.2011.08.006)
- Shporer, A., Bakos, G. Á., Bouchy, F., et al. 2009, *ApJ*, **690**, 1393, doi: [10.1088/0004-637X/690/2/1393](https://doi.org/10.1088/0004-637X/690/2/1393)
- Simpson, E. K., Pollacco, D., Hébrard, G., et al. 2010, *MNRAS*, **405**, 1867, doi: [10.1111/j.1365-2966.2010.16576.x](https://doi.org/10.1111/j.1365-2966.2010.16576.x)
- Simpson, E. K., Pollacco, D., Cameron, A. C., et al. 2011, *MNRAS*, **414**, 3023, doi: [10.1111/j.1365-2966.2011.18603.x](https://doi.org/10.1111/j.1365-2966.2011.18603.x)
- Siverd, R. J., Beatty, T. G., Pepper, J., et al. 2012, *ApJ*, **761**, 123, doi: [10.1088/0004-637X/761/2/123](https://doi.org/10.1088/0004-637X/761/2/123)
- Siverd, R. J., Collins, K. A., Zhou, G., et al. 2018, *AJ*, **155**, 35, doi: [10.3847/1538-3881/aa9e4d](https://doi.org/10.3847/1538-3881/aa9e4d)
- Skumanich, A. 1972, *ApJ*, **171**, 565, doi: [10.1086/151310](https://doi.org/10.1086/151310)
- Smith, A. M. S., Anderson, D. R., Bouchy, F., et al. 2013, *A&A*, **552**, A120, doi: [10.1051/0004-6361/201220727](https://doi.org/10.1051/0004-6361/201220727)
- Snellen, I. A. G., Brandl, B. R., de Kok, R. J., et al. 2014, *Nature*, **509**, 63, doi: [10.1038/nature13253](https://doi.org/10.1038/nature13253)
- Southworth, J. 2011, *MNRAS*, **417**, 2166, doi: [10.1111/j.1365-2966.2011.19399.x](https://doi.org/10.1111/j.1365-2966.2011.19399.x)
- Southworth, J., Dominik, M., Jørgensen, U. G., et al. 2011, *A&A*, **527**, A8, doi: [10.1051/0004-6361/201016183](https://doi.org/10.1051/0004-6361/201016183)
- Southworth, J., Mancini, L., Browne, P., et al. 2013, *MNRAS*, **434**, 1300, doi: [10.1093/mnras/stt1089](https://doi.org/10.1093/mnras/stt1089)
- Southworth, J., Tregloan-Reed, J., Andersen, M. I., et al. 2016, *MNRAS*, **457**, 4205, doi: [10.1093/mnras/stw279](https://doi.org/10.1093/mnras/stw279)
- Spalding, C. 2019, *ApJ*, **879**, 12, doi: [10.3847/1538-4357/ab23f5](https://doi.org/10.3847/1538-4357/ab23f5)
- Spalding, C., & Batygin, K. 2015, *ApJ*, **811**, 82, doi: [10.1088/0004-637X/811/2/82](https://doi.org/10.1088/0004-637X/811/2/82)
- . 2016, *ApJ*, **830**, 5, doi: [10.3847/0004-637X/830/1/5](https://doi.org/10.3847/0004-637X/830/1/5)
- Spalding, C., Batygin, K., & Adams, F. C. 2014, *ApJL*, **797**, L29, doi: [10.1088/2041-8205/797/2/L29](https://doi.org/10.1088/2041-8205/797/2/L29)
- Spalding, C., & Winn, J. N. 2022, *ApJ*, **927**, 22, doi: [10.3847/1538-4357/ac4993](https://doi.org/10.3847/1538-4357/ac4993)
- Stefansson, G., Mahadevan, S., Maney, M., et al. 2020, *AJ*, **160**, 192, doi: [10.3847/1538-3881/abb13a](https://doi.org/10.3847/1538-3881/abb13a)
- Stefansson, G., Mahadevan, S., Petrovich, C., et al. 2022, *ApJL*, **931**, L15, doi: [10.3847/2041-8213/ac6e3c](https://doi.org/10.3847/2041-8213/ac6e3c)
- Stephan, A. P., Wang, J., Cauley, P. W., et al. 2022, *ApJ*, **931**, 111, doi: [10.3847/1538-4357/ac6b9a](https://doi.org/10.3847/1538-4357/ac6b9a)
- Storch, N. I., Anderson, K. R., & Lai, D. 2014, *Science*, **345**, 1317, doi: [10.1126/science.1254358](https://doi.org/10.1126/science.1254358)
- Struve, O., & Elvey, C. T. 1931, *MNRAS*, **91**, 663
- Su, Y., & Lai, D. 2022, *MNRAS*, **513**, 3302, doi: [10.1093/mnras/stac1096](https://doi.org/10.1093/mnras/stac1096)
- Szabó, G. M., Pál, A., Derekas, A., et al. 2012, *MNRAS*, **421**, L122, doi: [10.1111/j.1745-3933.2012.01219.x](https://doi.org/10.1111/j.1745-3933.2012.01219.x)
- Szabó, G. M., Szabó, R., Benkő, J. M., et al. 2011, *ApJL*, **736**, L4, doi: [10.1088/2041-8205/736/1/L4](https://doi.org/10.1088/2041-8205/736/1/L4)
- Takaishi, D., Tsukamoto, Y., & Suto, Y. 2020, *MNRAS*, **492**, 5641, doi: [10.1093/mnras/staa179](https://doi.org/10.1093/mnras/staa179)
- Takeda, G., Kita, R., & Rasio, F. A. 2008, *ApJ*, **683**, 1063, doi: [10.1086/589852](https://doi.org/10.1086/589852)
- Talens, G. J. J., Albrecht, S., Spronck, J. F. P., et al. 2017, *A&A*, **606**, A73, doi: [10.1051/0004-6361/201731282](https://doi.org/10.1051/0004-6361/201731282)
- Talens, G. J. J., Justesen, A. B., Albrecht, S., et al. 2018, *A&A*, **612**, A57, doi: [10.1051/0004-6361/201731512](https://doi.org/10.1051/0004-6361/201731512)
- Tejada Arevalo, R. A., Winn, J. N., & Anderson, K. R. 2021, *ApJ*, **919**, 138, doi: [10.3847/1538-4357/ac1429](https://doi.org/10.3847/1538-4357/ac1429)
- Temple, L. Y., Hellier, C., Albrow, M. D., et al. 2017, *MNRAS*, **471**, 2743, doi: [10.1093/mnras/stx1729](https://doi.org/10.1093/mnras/stx1729)
- Temple, L. Y., Hellier, C., Almleaky, Y., et al. 2018, *MNRAS*, **480**, 5307, doi: [10.1093/mnras/sty2197](https://doi.org/10.1093/mnras/sty2197)
- Temple, L. Y., Hellier, C., Anderson, D. R., et al. 2019a, *MNRAS*, **490**, 2467, doi: [10.1093/mnras/stz2632](https://doi.org/10.1093/mnras/stz2632)
- Temple, L. Y., Hellier, C., Almleaky, Y., et al. 2019b, *AJ*, **157**, 141, doi: [10.3847/1538-3881/ab095a](https://doi.org/10.3847/1538-3881/ab095a)
- Teyssandier, J., Lai, D., & Vick, M. 2019, *MNRAS*, **486**, 2265, doi: [10.1093/mnras/stz1011](https://doi.org/10.1093/mnras/stz1011)
- Teyssandier, J., Naoz, S., Lizarraga, I., & Rasio, F. A. 2013, *ApJ*, **779**, 166, doi: [10.1088/0004-637X/779/2/166](https://doi.org/10.1088/0004-637X/779/2/166)
- Thies, I., Kroupa, P., Goodwin, S. P., Stamatellos, D., & Whitworth, A. P. 2011, *MNRAS*, **417**, 1817, doi: [10.1111/j.1365-2966.2011.19390.x](https://doi.org/10.1111/j.1365-2966.2011.19390.x)
- Thompson, M. J., Toomre, J., Anderson, E. R., et al. 1996, *Science*, **272**, 1300, doi: [10.1126/science.272.5266.1300](https://doi.org/10.1126/science.272.5266.1300)
- Torres, G., Bakos, G. Á., Hartman, J., et al. 2010, *ApJ*, **715**, 458, doi: [10.1088/0004-637X/715/1/458](https://doi.org/10.1088/0004-637X/715/1/458)
- Tregloan-Reed, J., Southworth, J., & Tappert, C. 2013, *MNRAS*, **428**, 3671, doi: [10.1093/mnras/sts306](https://doi.org/10.1093/mnras/sts306)
- Tregloan-Reed, J., Southworth, J., Burgdorf, M., et al. 2015, *MNRAS*, **450**, 1760, doi: [10.1093/mnras/stv730](https://doi.org/10.1093/mnras/stv730)
- Tremaine, S. 1991, *Icarus*, **89**, 85, doi: [10.1016/0019-1035\(91\)90089-C](https://doi.org/10.1016/0019-1035(91)90089-C)
- Triaud, A. H. M. J. 2011, *A&A*, **534**, L6, doi: [10.1051/0004-6361/201117713](https://doi.org/10.1051/0004-6361/201117713)
- Triaud, A. H. M. J. 2018, The Rossiter-McLaughlin Effect in Exoplanet Research (Springer, Cham), 2

- Triaud, A. H. M. J., Queloz, D., Bouchy, F., et al. 2009, *A&A*, **506**, 377, doi: [10.1051/0004-6361/200911897](https://doi.org/10.1051/0004-6361/200911897)
- Triaud, A. H. M. J., Collier Cameron, A., Queloz, D., et al. 2010, *A&A*, **524**, A25, doi: [10.1051/0004-6361/201014525](https://doi.org/10.1051/0004-6361/201014525)
- Triaud, A. H. M. J., Queloz, D., Hellier, C., et al. 2011, *A&A*, **531**, A24, doi: [10.1051/0004-6361/201016367](https://doi.org/10.1051/0004-6361/201016367)
- Triaud, A. H. M. J., Hebb, L., Anderson, D. R., et al. 2013, *A&A*, **549**, A18, doi: [10.1051/0004-6361/201219643](https://doi.org/10.1051/0004-6361/201219643)
- Triaud, A. H. M. J., Gillon, M., Ehrenreich, D., et al. 2015, *MNRAS*, **450**, 2279, doi: [10.1093/mnras/stv706](https://doi.org/10.1093/mnras/stv706)
- Triaud, A. H. M. J., Neveu-VanMalle, M., Lendl, M., et al. 2017, *MNRAS*, **467**, 1714, doi: [10.1093/mnras/stx154](https://doi.org/10.1093/mnras/stx154)
- Tripathi, A., Winn, J. N., Johnson, J. A., et al. 2010, *ApJ*, **715**, 421, doi: [10.1088/0004-637X/715/1/421](https://doi.org/10.1088/0004-637X/715/1/421)
- Valsecchi, F., & Rasio, F. A. 2014, *ApJ*, **786**, 102, doi: [10.1088/0004-637X/786/2/102](https://doi.org/10.1088/0004-637X/786/2/102)
- Van Eylen, V., Lund, M. N., Silva Aguirre, V., et al. 2014, *ApJ*, **782**, 14, doi: [10.1088/0004-637X/782/1/14](https://doi.org/10.1088/0004-637X/782/1/14)
- van Saders, J. L., Ceillier, T., Metcalfe, T. S., et al. 2016, *Nature*, **529**, 181, doi: [10.1038/nature16168](https://doi.org/10.1038/nature16168)
- Vanderburg, A., Becker, J. C., Buchhave, L. A., et al. 2017, *AJ*, **154**, 237, doi: [10.3847/1538-3881/aa918b](https://doi.org/10.3847/1538-3881/aa918b)
- Šubjak, J., Endl, M., Chaturvedi, P., et al. 2022, arXiv e-prints, arXiv:2201.13341. <https://arxiv.org/abs/2201.13341>
- Walkowicz, L. M., & Basri, G. S. 2013, *MNRAS*, **436**, 1883, doi: [10.1093/mnras/stt1700](https://doi.org/10.1093/mnras/stt1700)
- Wang, S., Addison, B., Fischer, D. A., et al. 2018, *AJ*, **155**, 70, doi: [10.3847/1538-3881/aaa2fb](https://doi.org/10.3847/1538-3881/aaa2fb)
- Wang, S., Winn, J. N., Addison, B. C., et al. 2021, *AJ*, **162**, 50, doi: [10.3847/1538-3881/ac0626](https://doi.org/10.3847/1538-3881/ac0626)
- Wang, X.-Y., Rice, M., Wang, S., et al. 2022, *ApJL*, **926**, L8, doi: [10.3847/2041-8213/ac4f44](https://doi.org/10.3847/2041-8213/ac4f44)
- Watanabe, N., Narita, N., Palle, E., et al. 2022, *MNRAS*, **512**, 4404, doi: [10.1093/mnras/stac620](https://doi.org/10.1093/mnras/stac620)
- Watson, C. A., Littlefair, S. P., Diamond, C., et al. 2011, *MNRAS*, **413**, L71, doi: [10.1111/j.1745-3933.2011.01036.x](https://doi.org/10.1111/j.1745-3933.2011.01036.x)
- Weis, E. W. 1974, *ApJ*, **190**, 331, doi: [10.1086/152881](https://doi.org/10.1086/152881)
- Wijnen, T. P. G., Pelupessy, F. I., Pols, O. R., & Portegies Zwart, S. 2017, *A&A*, **604**, A88, doi: [10.1051/0004-6361/201730793](https://doi.org/10.1051/0004-6361/201730793)
- Winn, J. N., Fabrycky, D., Albrecht, S., & Johnson, J. A. 2010a, *ApJL*, **718**, L145, doi: [10.1088/2041-8205/718/2/L145](https://doi.org/10.1088/2041-8205/718/2/L145)
- Winn, J. N., & Fabrycky, D. C. 2015, *ARA&A*, **53**, 409, doi: [10.1146/annurev-astro-082214-122246](https://doi.org/10.1146/annurev-astro-082214-122246)
- Winn, J. N., & Holman, M. J. 2005, *ApJL*, **628**, L159, doi: [10.1086/432834](https://doi.org/10.1086/432834)
- Winn, J. N., Holman, M. J., Johnson, J. A., Stanek, K. Z., & Garnavich, P. M. 2004, *ApJL*, **603**, L45, doi: [10.1086/383089](https://doi.org/10.1086/383089)
- Winn, J. N., Johnson, J. A., Albrecht, S., et al. 2009a, *ApJL*, **703**, L99, doi: [10.1088/0004-637X/703/2/L99](https://doi.org/10.1088/0004-637X/703/2/L99)
- Winn, J. N., Noyes, R. W., Holman, M. J., et al. 2005, *ApJ*, **631**, 1215, doi: [10.1086/432571](https://doi.org/10.1086/432571)
- Winn, J. N., Johnson, J. A., Marcy, G. W., et al. 2006, *ApJL*, **653**, L69, doi: [10.1086/510528](https://doi.org/10.1086/510528)
- Winn, J. N., Johnson, J. A., Peek, K. M. G., et al. 2007, *ApJL*, **665**, L167, doi: [10.1086/521362](https://doi.org/10.1086/521362)
- Winn, J. N., Johnson, J. A., Narita, N., et al. 2008, *ApJ*, **682**, 1283, doi: [10.1086/589235](https://doi.org/10.1086/589235)
- Winn, J. N., Johnson, J. A., Fabrycky, D., et al. 2009b, *ApJ*, **700**, 302, doi: [10.1088/0004-637X/700/1/302](https://doi.org/10.1088/0004-637X/700/1/302)
- Winn, J. N., Howard, A. W., Johnson, J. A., et al. 2009c, *ApJ*, **703**, 2091, doi: [10.1088/0004-637X/703/2/2091](https://doi.org/10.1088/0004-637X/703/2/2091)
- Winn, J. N., Johnson, J. A., Howard, A. W., et al. 2010b, *ApJL*, **723**, L223, doi: [10.1088/2041-8205/723/2/L223](https://doi.org/10.1088/2041-8205/723/2/L223)
- . 2010c, *ApJ*, **718**, 575, doi: [10.1088/0004-637X/718/1/575](https://doi.org/10.1088/0004-637X/718/1/575)
- Winn, J. N., Howard, A. W., Johnson, J. A., et al. 2011, *AJ*, **141**, 63, doi: [10.1088/0004-6256/141/2/63](https://doi.org/10.1088/0004-6256/141/2/63)
- Winn, J. N., Petigura, E. A., Morton, T. D., et al. 2017, *AJ*, **154**, 270, doi: [10.3847/1538-3881/aa93e3](https://doi.org/10.3847/1538-3881/aa93e3)
- Wirth, C. P., Zhou, G., Quinn, S. N., et al. 2021, *ApJL*, **917**, L34, doi: [10.3847/2041-8213/ac13a9](https://doi.org/10.3847/2041-8213/ac13a9)
- Wolf, A. S., Laughlin, G., Henry, G. W., et al. 2007, *ApJ*, **667**, 549, doi: [10.1086/503354](https://doi.org/10.1086/503354)
- Wong, I., Shporer, A., Zhou, G., et al. 2021, *AJ*, **162**, 256, doi: [10.3847/1538-3881/ac26bd](https://doi.org/10.3847/1538-3881/ac26bd)
- Wu, Y., & Lithwick, Y. 2011, *ApJ*, **735**, 109, doi: [10.1088/0004-637X/735/2/109](https://doi.org/10.1088/0004-637X/735/2/109)
- Wu, Y., & Murray, N. 2003, *ApJ*, **589**, 605, doi: [10.1086/374598](https://doi.org/10.1086/374598)
- Wyttenbach, A., Lovis, C., Ehrenreich, D., et al. 2017, *A&A*, **602**, A36, doi: [10.1051/0004-6361/201630063](https://doi.org/10.1051/0004-6361/201630063)
- Wyttenbach, A., Mollière, P., Ehrenreich, D., et al. 2020, *A&A*, **638**, A87, doi: [10.1051/0004-6361/201937316](https://doi.org/10.1051/0004-6361/201937316)
- Xie, J.-W., Dong, S., Zhu, Z., et al. 2016, *Proceedings of the National Academy of Science*, **113**, 11431, doi: [10.1073/pnas.1604692113](https://doi.org/10.1073/pnas.1604692113)
- Xue, Y., Suto, Y., Taruya, A., et al. 2014, *ApJ*, **784**, 66, doi: [10.1088/0004-637X/784/1/66](https://doi.org/10.1088/0004-637X/784/1/66)
- Yu, L., Zhou, G., Rodriguez, J. E., et al. 2018, *AJ*, **156**, 250, doi: [10.3847/1538-3881/aae5d5](https://doi.org/10.3847/1538-3881/aae5d5)
- Zahn, J.-P. 1977, *A&A*, **57**, 383
- Zahn, J. P. 2008, in EAS Publications Series, Vol. 29, EAS Publications Series, ed. M. J. Goupil & J. P. Zahn, 67–90. <https://ui.adsabs.harvard.edu/abs/2008EAS....29...67Z>

- Zanazzi, J. J., & Lai, D. 2018, *MNRAS*, **478**, 835, doi: [10.1093/mnras/sty1075](https://doi.org/10.1093/mnras/sty1075)
- Zhang, J., Weiss, L. M., Huber, D., et al. 2021, *AJ*, **162**, 89, doi: [10.3847/1538-3881/ac0634](https://doi.org/10.3847/1538-3881/ac0634)
- Zhou, G., Latham, D. W., Bieryla, A., et al. 2016a, *MNRAS*, **460**, 3376, doi: [10.1093/mnras/stw1107](https://doi.org/10.1093/mnras/stw1107)
- Zhou, G., Bayliss, D., Hartman, J. D., et al. 2015, *ApJL*, **814**, L16, doi: [10.1088/2041-8205/814/1/L16](https://doi.org/10.1088/2041-8205/814/1/L16)
- Zhou, G., Rodriguez, J. E., Collins, K. A., et al. 2016b, *AJ*, **152**, 136, doi: [10.3847/0004-6256/152/5/136](https://doi.org/10.3847/0004-6256/152/5/136)
- Zhou, G., Rodriguez, J. E., Vanderburg, A., et al. 2018, *AJ*, **156**, 93, doi: [10.3847/1538-3881/aad085](https://doi.org/10.3847/1538-3881/aad085)
- Zhou, G., Huang, C. X., Bakos, G. Á., et al. 2019a, *AJ*, **158**, 141, doi: [10.3847/1538-3881/ab36b5](https://doi.org/10.3847/1538-3881/ab36b5)
- Zhou, G., Bakos, G. Á., Bayliss, D., et al. 2019b, *AJ*, **157**, 31, doi: [10.3847/1538-3881/aaf1bb](https://doi.org/10.3847/1538-3881/aaf1bb)
- Zhou, G., Winn, J. N., Newton, E. R., et al. 2020, *ApJL*, **892**, L21, doi: [10.3847/2041-8213/ab7d3c](https://doi.org/10.3847/2041-8213/ab7d3c)
- Zhou, G., Quinn, S. N., Irwin, J., et al. 2021, *AJ*, **161**, 2, doi: [10.3847/1538-3881/abba22](https://doi.org/10.3847/1538-3881/abba22)
- Zhu, W., & Dong, S. 2021, *ARA&A*, **59**, 291, doi: [10.1146/annurev-astro-112420-020055](https://doi.org/10.1146/annurev-astro-112420-020055)
- Zhu, W., Petrovich, C., Wu, Y., Dong, S., & Xie, J. 2018, *ApJ*, **860**, 101, doi: [10.3847/1538-4357/aac6d5](https://doi.org/10.3847/1538-4357/aac6d5)
- Zuckerman, B., Song, I., Bessell, M. S., & Webb, R. A. 2001, *ApJL*, **562**, L87, doi: [10.1086/337968](https://doi.org/10.1086/337968)
- Zwintz, K., Reese, D. R., Neiner, C., et al. 2019, *A&A*, **627**, A28, doi: [10.1051/0004-6361/201834744](https://doi.org/10.1051/0004-6361/201834744)